



NASA Robotic Mining Competition: 2018-2019

Sage Edwards

Youngstown State
University

Youngstown, OH, USA

Nicholas Borucki

Youngstown State
University

Youngstown, OH, USA

Mark Feigert

Youngstown State
University

Youngstown, OH, USA

Dr. Jason Walker

Youngstown State University

Youngstown, OH, USA

Dr. Greg Sturrus

Youngstown State University

Youngstown, OH, USA



Submitted to Youngstown State University

Mechanical Engineering Program

In partial fulfillment of Mechanical Engineering degree requirements

05/2019

NASA ROBOTIC MINING COMPETITION

Submitted by:

Team Member Date

Name: Sage Edwards

Team Member Date

Name Nicholas Borucki

Team Member Date

Name: Mark Feigert

Approved by:

Physics Dean Date

Name: Greg Sturrus

Academic Advisor Date

Name: Jason Walker

Department Chairperson Date

Dr. Hazel Marie, P.E.

ADNOWLEDGMENTS

To Aptiv, Falcon Industries, and Austintown Precision Welding, whose donations to and sponsorship of the project helped to make it a reality.

To all of the Mechanical Engineering Faculty of Youngstown State University, whose help and support on the project helped it be the best that it could be.

To Dr. Greg Sturrus, who served as the mock client and advisor for the project and provided valuable support.

And to Dr. Jason Walker, whose work as the team's lead advisor proved tremendous and wholly invaluable, and without whom the project would have floundered.

TABLE OF CONTENTS

Introduction	1
1.1. Project Background.....	1
1.2. Customer Needs Assessment and Weighting	3
1.2.1. Initial Customer Needs Assessment	3
1.2.2. Customer Needs Table	4
1.2.3. Customer Needs Weighting	6
1.2.4. Customer Needs Matrix.....	6
1.3. Project Statement	7
1.3.1. Drive Train	7
1.3.2. Mining	9
1.3.3. Autonomy	9
1.3.4. Materials.....	9
1.4. Target Specifications.....	10
1.4.1. Robot Speed.....	11
1.4.2. Trafficability.....	12
1.4.3. Slip	12
1.4.4. Weight.....	12
1.4.5. Mining Speed	13
1.4.6. Power Consumption	13
1.4.7. Operability in Dusty Conditions	13
1.4.8. Dust Produced During Operation.....	14
1.4.9. Bandwidth.....	14
1.5. Design Philosophy	14
1.5.1. Application VS Competition.....	14
1.5.2. Fail-Safe Design	15

1.6. Team Structure	15
1.7. Resources.....	16
1.8. Budget.....	17
1.9. Risk Assessment	17
1.9.1. Team Fails to Finish on Time	18
1.9.2. Team Fails to Meet Budget	18
1.9.3. Motor Failure during Competition.....	18
1.9.4. Failure of Autonomous System during Competition.....	19
1.9.5. Loss of Communication during Competition	19
1.10. Project Schedule	19
1.10.1. Fall 2018 Semester.....	20
1.10.2. Spring 2019 Semester	21
Mining Systems	22
2.1. Overview.....	22
2.1.1. Design Considerations.....	22
2.1.2. Common Designs	22
2.2. Initial Design.....	25
2.3. Design Improvements and Modifications.....	28
2.3.1. Augers	28
2.3.2. Auger Shell	31
2.3.3. Auger Frame	32
2.4. Calculations and Analysis.....	36
2.4.1. Auger Motor Sizing.....	36
2.4.2. Stepper Motor Sizing.	38
2.4.3. Linear Actuator Sizing.	39
2.5. Final Design.....	40
Non-Pneumatic Wheels	41
3.1. Design Considerations	41
3.2. Literature Review.....	41

3.2.1. Auxetic Meshes and Patent No. 8544515 B2	41
3.2.2. Terramechanics	42
3.3. Design Concepts	43
3.3.1. Inner Rings Concept based on DLR's MOVE	43
3.3.2. Auxetic Mesh.....	44
3.4. Calculations.....	46
3.5. Preliminary Analysis and Simulation	49
3.6. Final Design and Conclusions	52
Autonomous Systems	56
4.1. Overview	56
4.1.1. Design Considerations	56
4.2. Initial Design.....	56
4.2.1. Path Planning	56
Suspension and Chassis.....	59
5.1. Overview.....	59
5.2. Final Design.....	61
Assembly and Controls	63
6.1. Full Mechanical Assembly	63
6.2. Electrical Controls	64
Conclusion	66
7.1. Project Scope Review	66
7.1.1. Project Timeline	66
7.1.2. Scope Creep.....	66
7.2. Engineering Characteristic Targets	66
7.2.1. Robot Speed	67
7.2.2. Trafficability	68
7.2.3. Slip	68
7.2.4. Weight	68
7.2.5. Mining Speed	69

7.2.6. Power Consumed.....	69
7.2.7. Operability in Dusty Conditions.....	70
7.2.8. Dust Produced During Run.....	71
7.2.9. Bandwidth	71
7.2.10. Overall Performance.....	72
7.3. Suggestions / Recommendations	72
7.4. Further Considerations	73
7.4.1. External Factors.....	73
7.4.2. Team Dynamics	74
References.....	76
Appendix A: Mechanical Drawings of Machined Components.....	78
Appendix B: Gantt Chart.....	104

TABLE OF FIGURES

Figure 1.1: IR radiation map of the moon. (NASA, 2009).....	2
Figure 1.2: Water erosion on Mars. (Anderson, 2015)	3
Figure 1.3: Comparison of three different articulated suspensions. (Siewart)	8
Figure 1.4: NASA RMC team structure flowchart.....	16
Figure 2.1: Example of bucket ladder design. (University of Alabama Astrorobotics, 2015)	23
Figure 2.2: Example of an auger design. (Hustad, 2015)	24
Figure 2.3: Initial concept for central auger.	26
Figure 2.4: Initial design of auger system with cross-section cut.	27
Figure 2.5. Counterrotating auger setup.....	29
Figure 2.6. Cross-section of 4 extended auger setup with new shell.....	30
Figure 2.7. Aluminum built-up auger shell.....	32
Figure 2.8. First design of auger system frame.....	33
Figure 2.9. First design of auger system frame with augers and shell.	34
Figure 2.10. Updated design of auger system frame.....	35
Figure 2.11. Updated design of auger system frame with augers and shell.	36
Figure 2.12: Completed mining system assembly.	40
Figure 3.1: Auxetic structure from patent. (United States of America Patent No. 8544515 B2, 2013)	42
Figure 3.2: Wheel design concept based on DLR's MOVE wheel.	44
Figure 3.3: First iteration design of the auxetic wheel.....	44
Figure 3.4: First iteration print of the auxetic wheel.	45
Figure 3.5: Cracks forming at the edges of the auxetic wheel.	46
Figure 3.6: Grouser height vs. soil thrust (tractive effort) and drawbar pull.	49
Figure 3.7: Grouser height vs. max incline.....	50
Figure 3.8: Wheel width vs. drawbar pull.	50

Figure 3.9: Wheel width vs. torque.....	51
Figure 3.10: Wheel width vs. max incline.....	52
Figure 3.11: Final design iteration for the auxetic wheel, with cut away for internal geometry	54
Figure 3.12: Comparison of auxetic meshes and other wheel features.	54
Figure 4.1: Flow chart of initial path planning algorithm.	57
Figure 4.2: Binary occupancy grid.	58
Figure 4.3: Probabilistic roadmap.	58
Figure 5.1: (From top down) CRAB 1, CRAB 2, RCL-E, MER.....	60
Figure 5.2: Drive base and suspension.	61
Figure 5.3: FEA analysis of rocker.	62
Figure 6.1: Full assembly of robot.	63
Figure 6.2: Simplified diagram of the electrical and communication system to be used in the control of the robot.	64
Figure 6.3: Blynk control, graphical user interface used by the operator.	65

TABLE OF TABLES

Table 1.1. Customer needs table with revisions and engineering characteristics.	5
Table 1.2. Customer needs weighting.	6
Table 1.3. Customer needs matrix.	7
Table 1.4. Target specifications.	11
Table 1.5. Risk assessment matrix	18
Table 1.6. Monthly schedule of design project	20
Table 3.1. List of soil properties for lunar soil.	47
Table 3.2. Final wheel geometry.....	52
Table 3.3. Predicted wheel performance.	53
Table 7.1. Final engineering characteristic performance.....	67
Table 7.2. Total Power Consumption.	70

TABLE OF EQUATIONS

2.1.....	36
2.2.....	37
2.3	37
2.4.....	38
2.5.....	39
3.1.....	43
3.2	47
3.3.....	47
3.4.....	47
3.5.....	48
3.6	48
3.7.....	48
3.8.....	48
3.9.....	48
3.10.....	49

CHAPTER 1

INTRODUCTION

1.1. Project Background

Within the past 60 years, space exploration has been critical to how we understand the universe today.

In 1958, the National Aeronautics and Space Act was passed by President Dwight Eisenhower. The inception of NASA was brought about by the unique dynamics between the United States and the rest of the world powers, particularly the Soviet Union. In 1957, the Soviet Union launched the first artificial satellites, Sputnik 1 and 2, into earth's orbit. A competitive pursuit in rocketry and space flight coined as the "space race" was in full swing between the Americans and Soviets by the time NASA was created. Aerospace technology increased by leaps and bounds during this period. NASA established itself as a leader in space exploration for the sake of science. The early Mercury and Gemini missions proved that humans were capable traveling in space. In 1961, it was announced by President John F. Kennedy that NASA's latest mission, Project Apollo, would send a man to the moon. The Apollo 11 mission successfully landed Neil Armstrong and his lunar module pilot, Buzz Aldrin, on the moon. This mission was not only a victory for Americans, but a victory for mankind. For the first time in human history, man had set foot on extraterrestrial land. During the 60's, NASA began working on multiple projects that would put bases on the moon inhabited by people on the moon. However; in 1970 NASA began shifting canceling the Apollo program, and any further moon colonization programs due to huge losses in government funding during the Nixon era, and a public disinterest in moon exploration after two failed Apollo missions.

While there has not been a man on the moon since Neil Armstrong, there has been extensive lunar research conducted by space probes. NASA's Synthetic Aperture Radar (Mini-SAR) was launched aboard India's first space probe in October 2008, Chandrayaan-1. Mini-SAR detected the presence of water at the lunar poles by studying the near IR-radiation reflection from the sun, see Figure 1.1. This was

confirmed a short time later by the Lunar Crater Observation and Sensing Satellite (LCROSS).

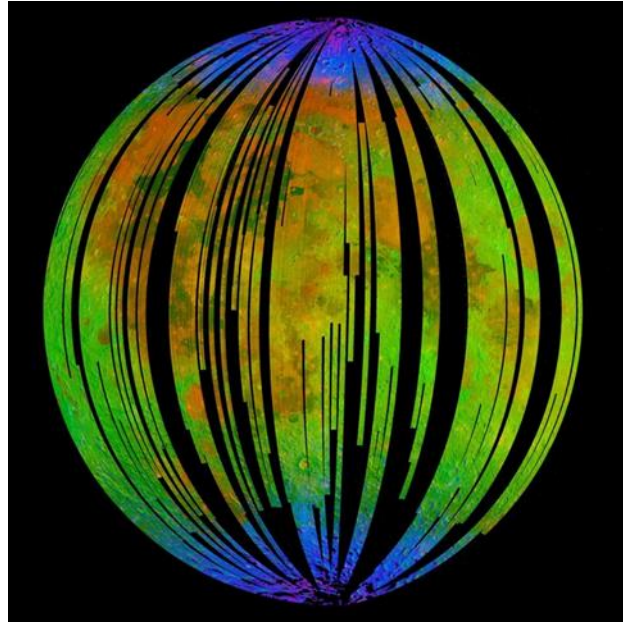


Figure 1.1: IR radiation map of the moon. (NASA, 2009)

With ever increasing climate change and overpopulation issues many scientists agree that human colonization of life supporting planets will be critical to the future of humanity.

Today, the focus has shifted from the moon to Mars, because unlike the moon, Mars has an atmosphere. It is widely agreed upon by the scientific community, that at some point in the past, Mars had conditions that would be optimal for life. For example, images from the Viking orbiters revealed what scientists believe to be surface features that could've been carved out by large bodies of water. See Figure 1.2 for a picture of sloping hills on the surface of Mars that appear to have signs of water erosion (Anderson, 2015). Even today, a small amount of water exists on the frigid planet in the form of ice crusted gravel.

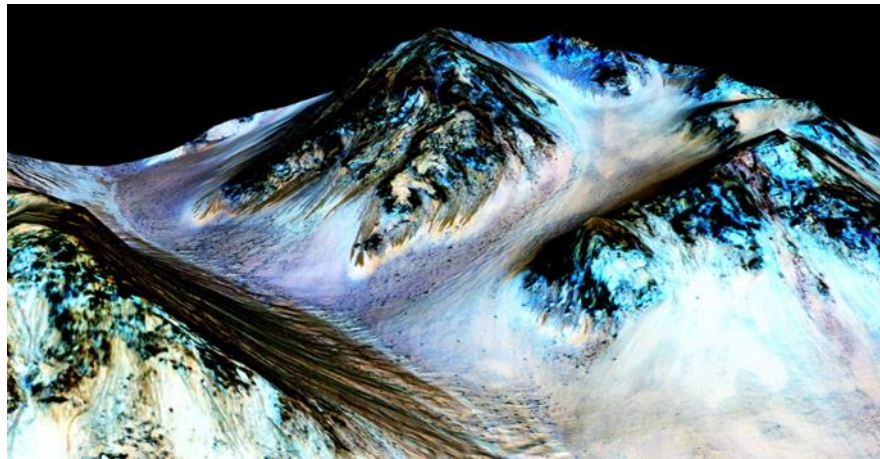


Figure 1.2: Water erosion on Mars. (Anderson, 2015)

Scientists are working to send astronauts to Mars by the year 2030. In-Situ Resource Utilization (ISRU) of the water in the icy regolith on the planet's surface will be crucial to their mission. The NASA sponsored Robotic Mining Competition (RMC) is held annually at Johnson Space Center to promote University collaboration to solve the ISRU problem. In 2019 the competition will be held for the ninth straight year; every year NASA modifies the rules to better suit the current mission scope that they are planning on executing by the year 2030.

1.2. Customer Needs Assessment and Weighting

1.2.1. Initial Customer Needs Assessment

The 2019 official rules and rubric document was published by NASA in September 2018. The Youngstown State University Robotic Mining Team met with the Kent State Robotic Club on September 30, 2018 to talk about the rules and the competition with a team who has participated in the competition for the past three years. In this competition, NASA is the customer; they are paying teams to design a robot with the intention of using the best aspects of the designs. The restrictions placed on the contesting teams are based on the real off-world restrictions engineers will face, they are as follows:

- The robot must be able to mine icy regolith efficiently.
- The robot must be able to make on-board corrections.
- The robot must not exceed 80kg; the less it weighs, the better.
- The robot must not kick up the dusty lunar surface during operation.
- The components of the robot must be able to work in a dusty environment.
- Communication bandwidth is limited.

- The robot must be capable of maneuvering the rough Martian terrain.

1.2.2. Customer Needs Table

The customer needs taken from the rule book were revised and assigned an engineering characteristic. The engineering characteristics are words or phrases that encompass the customer need. The engineering characteristics are the fundamental aspects of the design, they include things such as the following: size, efficiency, and power consumption. Table 1.1 shows the original customer needs, the revised needs, and then the corresponding engineering characteristic.

Table 1.1. Customer needs table with revisions and engineering characteristics.

Original Customer Needs	Revised Customer Needs	Engineering Characteristics
Must be able to collect icy regolith within 10 min.	Mining Capability	Mining Speed
Robot corrects itself during operation	Autonomy	Wheel Slip
Max weight limit of 80kg, the lower the better	Light-weight	Weight
Won't kick up too much dust during operation	Dust-free Operation	Amount of Dust Produced
Won't consume large amount of power	Low Power Consumption	Power Consumed
Mechanisms are sealed from dust contamination	Dust-Tolerance	Operate in Dusty Conditions
Uses as little bandwidth as possible	Low Bandwidth Used	Bandwidth Used
Able to maneuver around obstacles quickly	Drive Capability	Trafficability Robot Speed

1.2.3. Customer Needs Weighting

The customer needs were weighted based on how many points were to be gained in the competition. A ranking of 5 was given to the customer need of greatest importance, and a ranking of one was given to the least important. See Table 1.2 for the ranked needs with the corresponding characteristic.

Table 1.2. Customer needs weighting.

	Revised Customer Need	Weighting	Engineering Characteristic
1	Mining Capability	5	Mining Speed
2	Autonomy	5	Wheel Slip
3	Drive Capability	5	Trafficability, Robot Speed
4	Light-Weight	4	Weight
5	Dust-Free Mining	2	Amount of Dust Produced
6	Low Power Consumption	2	Power Consumed
7	Dust-Tolerance	1	Operate in Dusty Conditions
8	Low Bandwidth Used	1	Bandwidth Used

The mining capability is very to NASA reflected by the name of the competition. The drive capability and autonomous aspect are also weighted as a 5. The less important needs are the reduced weight below 80kg, the dust related operations, and the electronic systems bandwidth usage and power consumption.

1.2.4. Customer Needs Matrix

The revised customer needs were related to the engineering characteristics by creating a table that assigns a correlation value to the engineering characteristic based on the strength of the correlation. The scores were as follows: 9 for strong correlation, 3 for moderate correlation, and 1 for weak correlation. After the values were assigned, they were multiplied by the weighting number, and summed for each engineering characteristic. The result is a quantifiable level of importance for each

of the engineering characteristics. This tool is valuable in the design process when prioritizing design considerations. See Table 1.3 for the customer needs matrix.

Table 1.3. Customer needs matrix.

		Engineering Characteristics										
Customer Needs	Weight			Mining Speed	Robot Speed	Slip	Weight	Amount of Dust Produced	Power Consumed	Operate in Dusty Conditions	Bandwidth Used	Trafficability
	5	Mining Capability	9	3				3	3			
	5	Autonomy		1	9				1	3	3	3
	4	Light-Weight		1			9		1			1
	2	Dust-Free Mining	3	1				9				
	2	Low-Power Consumption	3	1	1	1			9			1
	1	Dust-Tolerance			1					9		
	1	Low-Bandwidth Used									9	
	5	Drive Capability		9	3	3	1	1	1	3		9
	Score	52	74	62	55	36	47	39	24	66		

1.3. Project Statement

1.3.1. Drive Train

For an autonomous mining robot to be successful in completing its mission it will first need to be able to traverse the uneven terrains of the Moon and Mars. In the NASA Robotic Mining Competition, the obstacles are defined to be either craters or rocks. The rocks will have an approximate diameter of 10-30 cm with a mass of 3-10

kg. The craters will have a depth or width no greater than 30 cm. With this being known, a drive system can be designed to traverse these obstacles.

A significant aspect of the drive train design is the reduction of slip. Slip is a very significant parameter in this design as it is an inefficiency for trafficability, time, and energy consumption. On top of this it also effects the odometry for the autonomy systems of the robot. If the robot is unable to recognize its location through perception it will need to rely on odometry to determine its location.

Three types of articulated suspensions will be investigated to determine which one is the best suited for the overall design of this robot. These systems are as follow: CRAB, RCL-E, and the Rocker Bogie. A comparison of these are seen in Figure 1.3 with different representations. (Siewart)

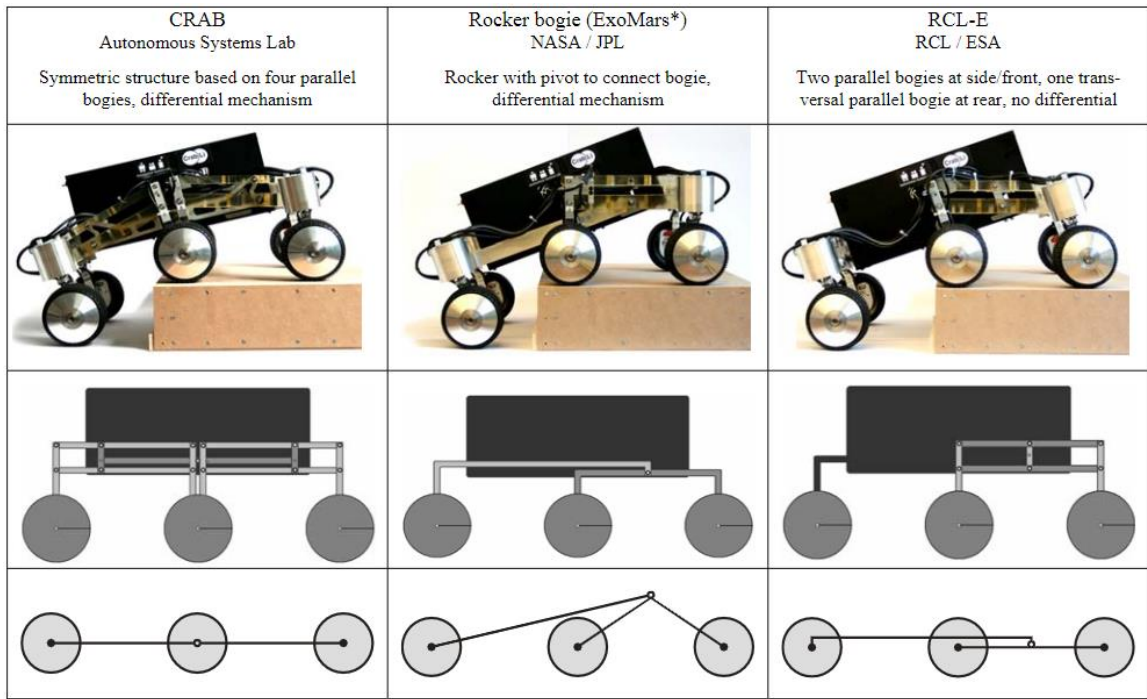


Figure 1.3: Comparison of three different articulated suspensions. (Siewart)

Along with this the team will also investigate the design of a non-pneumatic wheel, commonly referred to as a tweel. The use of auxetic meshes is a primary focus in the development of a wheel concept design due the unique properties of this type of geometry. An auxetic mesh is a geometry that gives the structure a negative Poisson's ratio that can be tuned by changing dimensions and elements of the geometry rather than the material. This will allow for a wheel design that minimizes the weight while maintaining desirable wheel characteristics.

1.3.2. Mining

With the objective of this robot being the ability to mine icy regolith this system of the robot is arguably the most important, but also the most complicated. The mining system should be able to reach a depth greater than 30.5 cm so that it can start mining the icy regolith, or in the case of the competition, gravel. There are several design aspects to consider, where the most significant ones are the constraints given by the environment. With the acceleration due to gravity on the Moon and Mars being 1.62 m/s^2 and 3.711 m/s^2 , respectively, some traditional mining methods such as front loader may not be practical due to its dependence on gravity to operate at maximum efficiency. Since one of the design goals is to minimize the mass of the robot, a gravity dependent mining system can be ruled out.

The characteristics of the soil and gravel being mined are also critical to the design of the digging mechanism. An important property to consider is the angle of repose since this will help determine the angle at which the digging mechanism mines the materials or deposits the materials.

1.3.3. Autonomy

The robot should be autonomous since direct communication and control from an operator is not feasible due to the lengthy time it takes for a signal to reach the robot from Earth. With this being said, the robot needs to be able to reliably navigate the Martian or Lunar terrain by recognizing potential obstacles. The robot will also need to be capable of decision making. It will have to be capable of determining the best path to take based on: that path's trafficability, the time it will take to travel the path, the energy required to get to the end point, and potential risks it may face on the way.

This robot will also need to be able to detect faults within its systems and recognize the kinematic positions of all acting members. This type of information will be required for the robot to analyze its situation and make logical mission plans and decisions.

1.3.4. Materials

The selection of materials is very important to the design since the robot will be operating in the harsh environments found on Mars and the Moon. The temperatures on the moon can be as cold as -173°C and -125°C . These types of extreme temperatures will have significant effects on certain plastics that may be used in the design. Along with this, radiation must be considered due to the lacking

atmosphere to shield the surface from the sun's radiation as radiation can affect the longevity of certain materials that are under stress. Another thing to consider is the low atmospheric pressures of these environments as this will make the use of composite materials very difficult due to outgassing.

These types of constraints will be used in the design of this robot but may need to be modified to accommodate the conditions found here on Earth for the competition.

1.4. Target Specifications

In order to have the ability to accurately reflect whether the customer needs and engineering characteristics were met, a set of targets were specified for each engineering characteristic. These consist of a minimum and an ideal target. The ideal targets are the desirable outcomes in the robot's design and performance, while the minimum targets are the baseline for whether the design will be considered passable. The full list of target specifications can be found in Table 1.4.

Table 1.4. Target specifications.

Engineering Characteristic	Measurement	Unit	Minimum	Ideal
Robot Speed	Time to Start Mining	s	60	20
Trafficability	Size of Obstacles Maneuvered Around/Over	cm	± 10	± 30
Slip	Difference between Distance Traveled and Expected	m	0.3	0.1
Weight	Weight	kg	80	40
Mining Speed	Amount Mined During Run	kg	1	40
Power Consumed	Power Consumed	Watt Hour	35	11
Operability in Dusty Conditions	Protection of Electrical Components	P/F*	Vital Components Protected	Components Fully Protected
Dust Produced During Run	Amount of Dust Kicked Up	P/F*	Medium Dust	Minimal Dust
Bandwidth	Bandwidth	kb/s	1000	0

*Indicates Pass/Fail Criterion. No applicable unit of measurement.

1.4.1. Robot Speed

The most important engineering characteristic to be met is the robot's speed, as it has the largest effect on the efficiency of the robot, given the 10-minute time limit. To measure success in this category, it was decided to measure the amount of time the robot took to begin its first mining session from competition start. This was chosen due to the additional need for the robot to orient itself at the start of the run, which if not optimized can quickly eat up much of the clock for the run. As a minimum target, 10% of the total time limit, or 60s, was chosen. This allows for ample time for the robot to orient and traverse the field, even if not fully optimized, while still allowing for significant mining time and the possibility of a second mining run during the time limit. The ideal target was set at one-third of the minimum, or 20s, which assumes a highly optimized orientation protocol and traversal of the field.

1.4.2. Trafficability

The next engineering characteristic to be met is the trafficability of the robot, which also has a large impact on the efficiency of the robot within the time limit. This will be measured by the robot's ability to maneuver over any potential obstacles that may be present on the field. Per competition rules, large rocks and/or craters will be placed in the surface. The obstacles are set to be no smaller than ± 10 cm, and no larger than ± 30 cm. The minimum target is set according to the minimum size of the obstacles, as the robot should be expected to handle at least the smallest obstacles. The ideal target is set at the maximum size, as ideally the robot should be able handle any obstacle present.

1.4.3. Slip

The next characteristic the slip of the robot, the difference between how far the robot has traveled and how far the robot thinks it has traveled. Large errors in slip can cause failure in the robot's ability to maneuver itself properly in the field. Distance measurements can be obtained from the robot's vision system and rotation of the wheels for actual and expected distances, respectively. In the perfectly ideal scenario, the slip will be 0, however this is not realistic as some slippage needs to occur for the wheels to function properly, so the ideal target was set at 0.1 m. As a minimum target, it was decided to limit the error to within approximately 5% of the 5.76-m field length, or 0.3 m.

1.4.4. Weight

The weight of the robot is incredibly important when considering transportation to other special bodies, as lightening the load by a few kg can save thousands of dollars. This is reflected in the competition as a heavy penalty (-8 point) for each kg of weight the robot possesses. The robot will be weighed prior to competition by officials. The minimum target was chosen to be 80 kg, as this mass is the officially recognized maximum permissible mass allowed in competition. In review of the official scores from the 2017 competition, it was found that a strong majority of robots fell within the 50-70 kg range (RMC Archive, 2017). To gain a potential edge over the competition, the ideal target for weight was set at 40 kg, which only a handful of contestants were able to meet.

1.4.5. Mining Speed

The mining speed of the robot is another important factor of overall efficiency of robot performance. Given the 10-minute time limit, it is important for the robot to be able to mine quickly and efficiently. Amount of gravel mined is also scored very favorably (+15 points per kg over 1), so maximizing this amount will prove very beneficial in competition. For a run to be considered valid and for points of any kind of points to be scored from the mining portion of the competition, at least 1 kg of gravel must be mined during the run. As such, this is set as the minimum target to be met. The ideal target was set at 40 kg of gravel. This value is set by the team as a desired target as 2017 competition data is unable to be applied here. At the time, BP-1 could also score and as such most robots were optimized to maximize BP-1 mining, and gravel scores are quite low across the board.

1.4.6. Power Consumption

The power consumed during robot operation is not a vital consideration given the limited amount of time in competition but increases in importance when considering actual operation when the robot would run for potentially much longer periods of time. Consuming power still counts negatively towards the overall score (-1 point per watt-hour) and as such should be minimized. Measurements will be taken by officials at competition for scoring. The targets are also chosen based on 2017 competition data. Runs that consumed less than 10 watt-hours were excluded as most of these robots can be assumed to have experienced critical failures and were unable to perform due to the unreasonably low amount of power consumed. From the remaining teams, a mean of approximately 23 watt-hours and a standard deviation of approximately 12 was obtained. The minimum and ideal targets were decided to ± 1 standard deviation from the mean, set at 35 and 11 watt-hours, respectively.

1.4.7. Operability in Dusty Conditions

The robot's ability to control the dust it produces is important in maintaining proper functioning of all equipment, however as this is expected to be reflected in other scoring areas, actual obtainable points for this category max out at 30. As scoring in this section is entirely left to the discretion of the judges, as it is impossible to measure, a simple pass/fail condition was set. The minimum target is chosen to be that vital components are protected. This consists of properly housing any motors, computers, or other electrical equipment, as they will be the most susceptible to

dust damage. The ideal target is set at protecting the entire robot from dust buildup, whether that be from a smooth coating that prevents particle attachment, or an electrostatic field to repel particles.

1.4.8. Dust Produced During Operation

Similar to operability in dusty conditions, dust produced during the run is considered scoring-wise a non-vital requirement, only maxing out at 70 points. Minimizing dust does however place an easier load on the systems protecting the robot from dust in the first place. Again, similar to operability in dusty conditions, scoring is left to the discretion of the judges, as it is difficult to properly measure, so a pass/fail condition was set for this target as well. The minimum target is set at what will be referred to as a medium amount of dust produced, and the ideal target is set similarly at a minimal amount of dust produced.

1.4.9. Bandwidth

The average bandwidth used over the course of the run is the final characteristic. It is also considered a non-vital statistic in scoring (-1 point per 50 kb/sec), and as such places it at the bottom. Measurement will be taken by officials during the competition. The ideal target is set at an average of 0 kb/sec, as this would mean that the robot had performed a fully autonomous run, with only the start and stop commands coming from the control center. The minimum target is set assuming some level of human control is needed during the run. This target was also chosen from 2017 competition data, this time taking the mean value, approximately 1000 kb/sec, from all competing teams.

1.5. Design Philosophy

1.5.1. Application VS Competition

With this being a design competition for the development of an autonomous mining robot that will be operating in the environmental conditions of Mars and/or the Moon. The team is committed to designing a robot that is compliant to the environmental conditions of these environments even though the competition will be hosted here, on Earth. All critical mechanisms to the operation of the robot must be compliant to these conditions. However, mechanism and material selections may be changed to accommodate for the conditions here, on Earth. These changes must

be justified in the systems engineering report to show that the fundamental mechanisms have not been altered.

1.5.2. Fail-Safe Design

The team has decided to adopt a fail-safe design philosophy in the design of this robot. The reason for this is due to the fact that there will probably not be someone there to repair these robots and a failed robot that is incapable of fulfilling its task will be considered a great economic loss, considering the cost it takes to build and deliver these robots to their destinations.

1.6. Team Structure

Two main groups provided work and support on the project. The three student team members were responsible for the design and construction of the robot. Faculty from the Mechanical Engineering and Physics Departments at Youngstown State University provided support and mentorship for the project. A full flowchart of the team organization is shown in Figure 1.4.

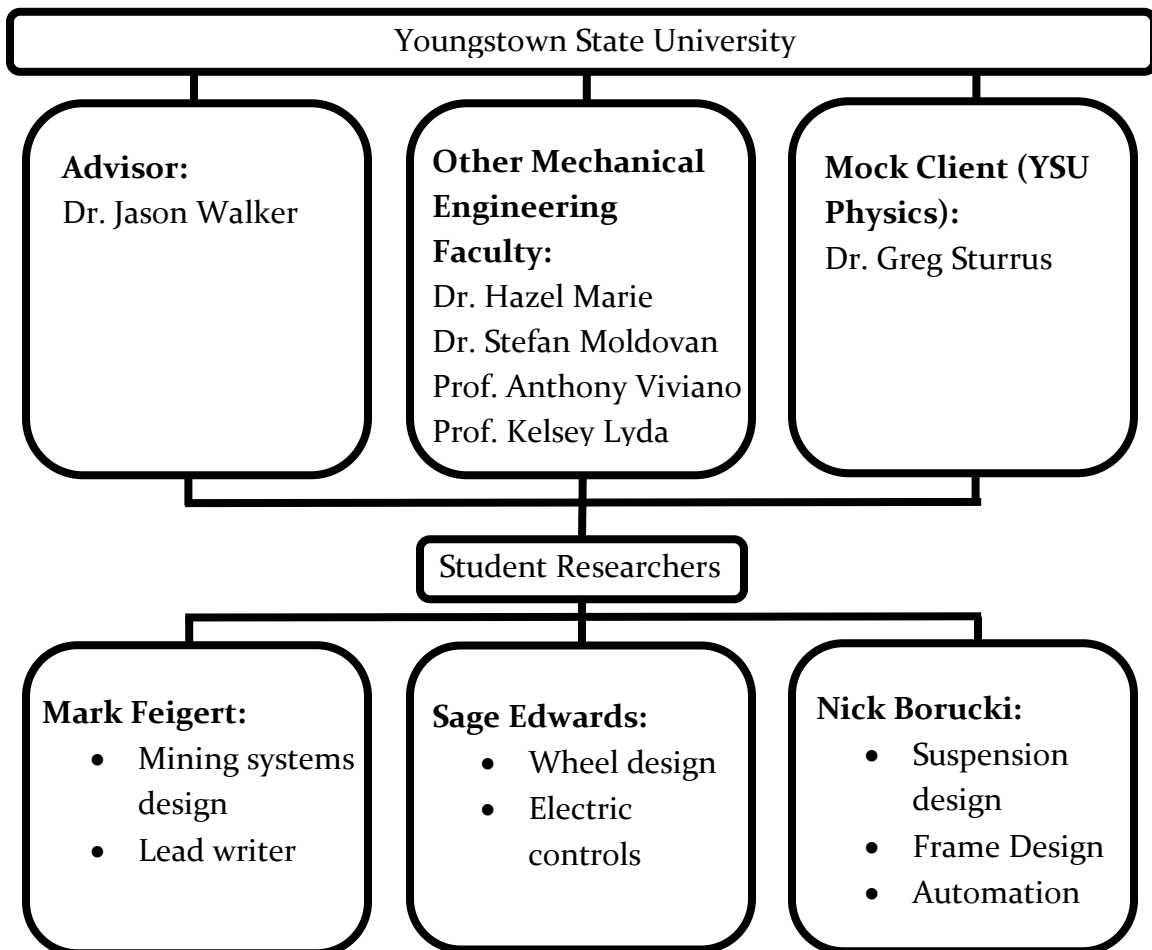


Figure 1.4: NASA RMC team structure flowchart.

Sage Edwards was responsible for the design of the wheels, from initial concepts to analysis and construction, as well as the electrical controls for the system. Mark Feigert was responsible for the design of the robot's mining and depositing capabilities and served as the team's lead writer. Nicholas Borucki led the design of the robot's frame and suspension as well as the automation program.

1.7. Resources

Resources for the project were obtained through two avenues: provided by the University or acquired from third-party private businesses, both donated and purchased. Computer design work was performed through Solidworks, Autodesk Inventor, Mathworks MATLAB, and ANSYS software on university licenses. The Physics department provided their machine shop and an empty laboratory for use in building and storing the robot. Wheel construction was performed on university-

owned 3D printers with department-provided materials. Machining and welding of components was also completed with university-owned equipment.

The remaining materials were acquired through third-party businesses. Donated parts and services included a light detection and ranging (LiDAR) system from Aptiv, a sponsorship from Falcon Industries, and weldment work by Austintown Precision Welding.

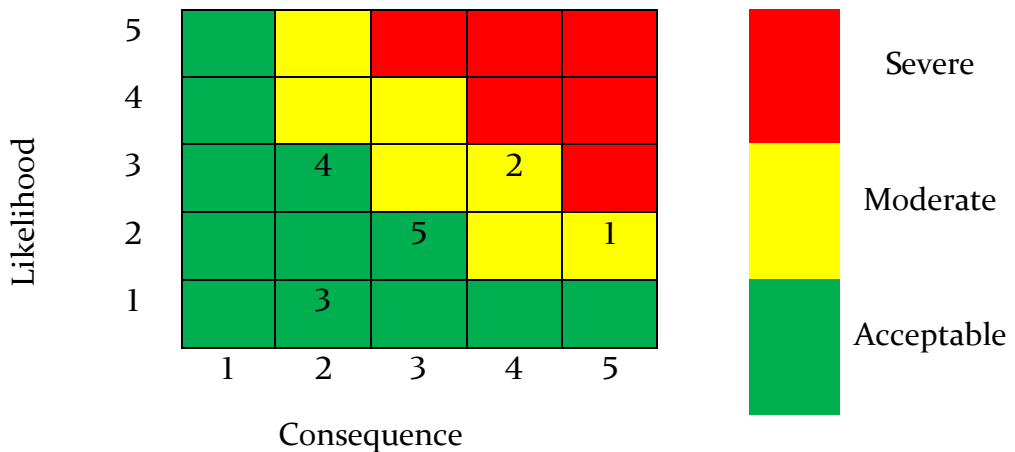
1.8. Budget

An estimated budget was developed towards the end of the design phase of the project based on the predicted cost of materials required for construction. A \$5,000 grant was obtained through the Ohio Space Grant Consortium from NASA for the project. The grant also came with a required \$5,000 cost match from the University, creating a full budget limit of \$10,000 for the project.

1.9. Risk Assessment

Any design project will be accompanied by potential risks and failure points that can and will impact the design process and performance of the final product. To help mitigate any potential problems, a risk assessment was conducted to determine key risks. Five key risks were identified. The causes and effects of each were identified, as well as potential mitigations to be implemented. Each risk was ranked on a scale of 1 to 5, 5 being the highest, in terms of both the likelihood of said risk occurring as well as the severity of the consequences on the project should said risk occur. The six risks are plotted with respect to these rankings in Table 1.5, listed according the appropriate subsequent subsection where each risk is discussed in more detail.

Table 1.5. Risk assessment matrix



1.9.1. Team Fails to Finish on Time

The first identified was failing to complete the project by the deadline. The likelihood of this occurring was considered to be fairly low but failing to meet competition deadlines would result in removal from the competition, a very serious consequence. The primary cause of this risk is time mismanagement, which was mitigated with weekly meetings and careful planning of a project schedule.

1.9.2. Team Fails to Meet Budget

The risk of going over budget on the project was also addressed. With limited funds being available from the Engineering Department, the project could end up in an unfinished or unsatisfactory state if the budget is not properly planned around. The likelihood of this occurring was considered to be somewhat possible. Causes of this risk could stem from attempting to build a design that was too ambitious and/or too robust, leading to an inflated price of components, or failing to acquire potential grant money, primarily relating to the SICHOP Grant provided by the Ohio Space Grant Consortium, upon which the budget was designed around. In order to mitigate any monetary issues, the team carefully considered price on any components that were purchased, as well as seeking discounts or sponsorships from any involved companies and donations of labor/materials from private individuals.

1.9.3. Motor Failure during Competition

A low likelihood risk that was considered was the potential of a motor failure during competition. Such a failure could stem from overstressing the motor, the invasion

of dust particles during competition, or possibly some form of electrical failure. The consequence of any single motor failing was considered to be fairly low, as the robot was designed with redundancy in mind, such that if for example one wheel motor were to fail, 5 other motors for the remaining wheels would still be active and able to carry on performance. Mitigations taken for this risk include the redundancy already mentioned, as well as careful housing to avoid dust infiltration and properly selecting any motors based on potential loads and torque requirements.

1.9.4. Failure of Autonomous System during Competition

Another identified risk is the failure of the autonomous system during competition. The risk was considered to be somewhat likely to occur as all team members have limited experience in this field, and the project timeline provides limited time to test and perfect the system. The risk was considered to be of relatively low consequence however, as manual controls were also to be built into the robot's design, such that an individual could take over should autonomous failure occur and performance could continue.

1.9.5. Loss of Communication during Competition

One moderately consequential risk that could occur during competition is the loss of communication between the robot and the command station, at which point the performance would be over, only allowing the robot to be scored based on what it had accomplished up to the point of failure. The likelihood of this occurring was considered relatively low, as only an electrical failure on the robot or the command station would cause such an issue. To mitigate this risk, computer components were ensured to be in good working condition as well as properly installed, in addition to being properly sealed from duct infiltration.

1.10. Project Schedule

The project was scheduled to run from August 29, 2018 to May 10, 2019, across both the Fall 2018 and Spring 2019 semesters. A monthly breakdown of project work is shown in Table 1.6. A Gantt chart of the full project timeline can be found in Appendix B.

Table 1.6. Monthly schedule of design project

Fall 2018				
August	September	October	November	December
- Literature review - Develop project statement	- Initial mechanical design concepts	- Mechanical component design	- Mechanical component design - Begin prototyping	- Completed mechanical design - Electrical controls - Automation algorithms
Spring 2019				
January	February	March	April	May
- Component purchasing - Electrical controls - Automation algorithms - Building	- Component purchasing - Electrical controls - Automation algorithms - Building	- Electrical controls - Automation algorithms - Building - Component testing	- Electrical controls - Automation algorithms - Robot testing - Final writeup	- Competition

1.10.1. Fall 2018 Semester

The team's primary objective during the Fall 2018 semester was to create the mechanical designs that would be used to build the robot. August and September were used for defining the project statement as well as early research and concepts on the mechanical systems. During October and November, the team worked on iterating and improving the design concepts. Also in November, the team was able to begin prototyping the wheel design. In December, the team finalized the

mechanical designs for the project so that building could begin and started work on the electrical controls and automation systems for the robot.

1.10.2. Spring 2019 Semester

As the second semester began in January, with completed mechanical designs, the team began compiling and ordering components and materials such that construction could begin. February and March saw most of the physical construction for the robot completed. In March, the team was able to start testing on individual mechanical systems. Electrical control and automation systems design work was performed across most of the semester, reaching completion in April and allowing the robot to be tested as a complete unit. The robotics competition was held May 6-10.

CHAPTER II

MINING SYSTEMS

2.1. Overview

2.1.1. Design Considerations

In order for the robot to perform its necessary function, a dedicated mining system was developed. The system needs to be capable of digging through a topsoil of BP-1 of depth 30.5 cm and pulling up icy regolith from the next layer of soil of depth 15.24 cm (NASA). The BP-1 and icy regolith then need to be transferred to a collector trough located on the side of the pit $55\text{ cm} \pm 0.5\text{ cm}$.

Other necessary considerations in the design of a mining system include the effects of reduced gravity on the system. On lunar and Martian surfaces, where the gravity is only 16.51% and 37.81% of Earth's gravity, respectively, any mining systems that significantly require the effects of gravity to achieve maximum efficiency will see limited success on alien soil compared to that seen on Earth. In addition, as gravity dependent systems require a falling mass in order to function, in an environment with lower gravity, a larger mass will be required to produce the same results, but in doing so requires a large sacrifice on the minimization of the robot's weight, a significant factor in the overall success of the robot design. Thus, any such designs are largely rejected or ignored.

2.1.2. Common Designs

Over the course of past competitions, two designs for mining systems have risen to prominence, and most well-performing robots have featured one of the two mining systems.

Bucket Ladder. The first and most popular design is what is known as the “bucket ladder” system. Pictured in Figure 2.1, the bucket ladder features two belt systems. The first contains a series of troughs that dig up the BP-1 and icy regolith as the belt is spun and lowered into the soil. The contents are then transferred into an onboard

collector trough, which holds the mined material until the robot has returned to the competition collector trough, at which point the second belt pulls the material out of the onboard collector trough and transfers it up into the competition collector trough.

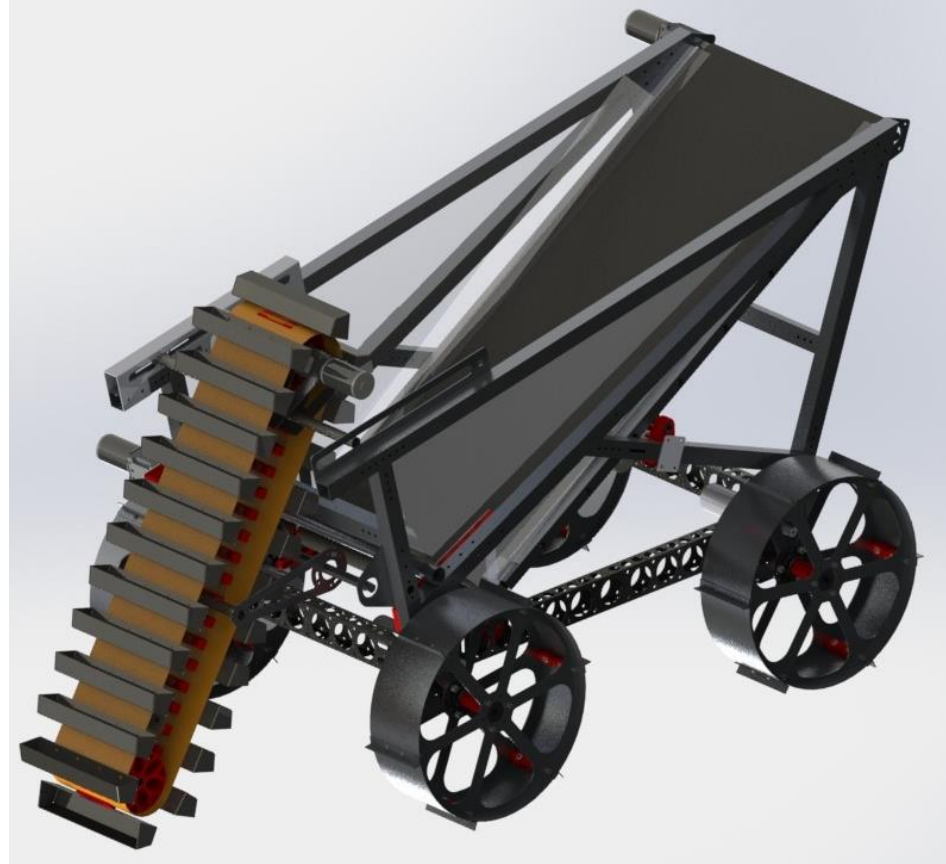


Figure 2.1: Example of bucket ladder design. (University of Alabama Astrorobotics, 2015)

Advantages of such a design include its ability to mine a large amount of material within a short time frame, as well as its storage capabilities. The onboard trough has the ability to be sufficiently large, within size constraints of the robot itself, and as such does not require constant offloading of mined material, which saves valuable time during competition.

The major disadvantage of the design lies in the amount of dust produced during operation. The amount of material mined by the bucket ladder is dependent on the speed of the belt; however, as the speed of the belt increases, the amount of dust produced by mining also increases. This requires the robot's systems and onboard electronics to be that much more protected against dust interference. As the relative

importance of dust production to that of mined material is quite low, this is often considered an acceptable sacrifice in design.

Auger. The second popular design used in the robot design is an auger system. Shown in Figure 2.2, the standard auger design utilizes a similar setup to that of the bucket ladder system, maintaining the onboard collector trough and rear belt system for offloading material, but instead of the front-mounted bucket ladder, an auger is used to mine the BP-1 and icy regolith.



Figure 2.2: Example of an auger design. (Hustad, 2015)

The auger system's main advantage over the bucket ladder system is that as most of the mining process takes place below the surface, operation produces much less dust than that of the bucket ladder, and a well-designed auger can still produce significant amounts of mined material.

The design's major drawback lies in the auger's limited ability to dig in a straight line. In doing so, augers can become stuck in the ground as the surrounding material collapses in on the small produced hole. This is especially prevalent on vertical auger designs. The consistency of loose BP-1 is similar to dry sand and so with enough force, the auger is easy enough to remove from the soil, but due to the auger's often front-mounted location, as necessitated by the inclusion of an onboard collector

trough and rear offloading belt system, such a force is unable to be applied without compromising the stability of the robot.

2.2. Initial Design

Early in the design phase of the project, the team developed an initial concept plan for the design of an auger system. Despite the systems' drawbacks, the team proposed some unique innovations to the designs to attempt to answer those concerns.

The key design change involved adapting the auger's housing, in most uses serving only as a means of holding material to the auger's flights as it travels upwards, to double as the onboard storage for the mined material. A cartoon of the auger's proposed operation can be found in Figure 2.3. Storing the material on the auger rather than using it only as a means to move the material gave this particular auger design two key advantages.

Firstly, by not offloading material into a separate onboard storage, the auger can also serve as the dumping system in addition to the mining system by being rotated and lifted to meet the collector trough. This allows for a reduction in the size of the design, as well as significant potential savings on the overall weight of the robot.

Secondly, by removing the dedicated storage and dumping system, there no longer exist any restrictions on the placement of the auger on the frame of the robot, thus the auger can freely be mounted centrally on the robot frame, giving better control over weight distribution. A more evenly distributed weight works to mitigate the auger's main drawback, that of becoming stuck in the ground due to material collapsing back onto the auger. With a centrally located load, the robot can much more effectively support the necessary loads needed to remove the auger from the ground without compromising on the stability of the robot.

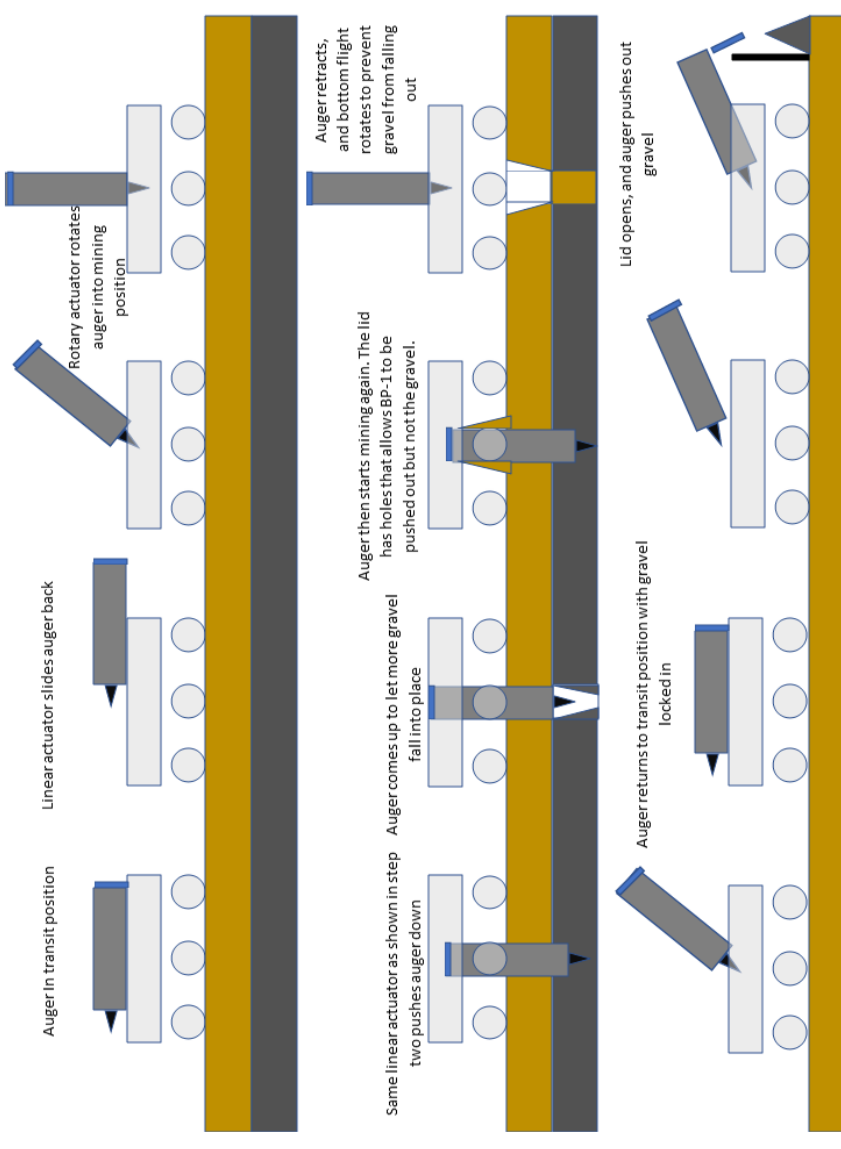


Figure 2.3: Initial concept for central auger.

With a working concept design, the team pushed forward into designing this specific auger system. The first draft of the design was very similar to the concept cartoon seen in Figure 2.3. A view of the first design iteration and a cross-section cut of the system can be found in Figure 2.4. The design consisted of a large singular auger with a 10" diameter surrounded by a thin shell of plastic or metal to house the auger and mined material. Approximately 80% of the length of the shell was perforated. The holes were intended to help sift out any BP-1 that the robot mined, as it was not the desired material to be mined, in an attempt to store as much gravel as possible. The remaining length of the shell was left whole such that a window could be cut out of the shell and remounted to serve as a hatch to empty the auger

of material into the collector trough. A small extrusion was added to the rear of the shell such that an electronic latch could be attached to the shell, keeping the hatch closed and only allowing it to be opened upon dumping the material.

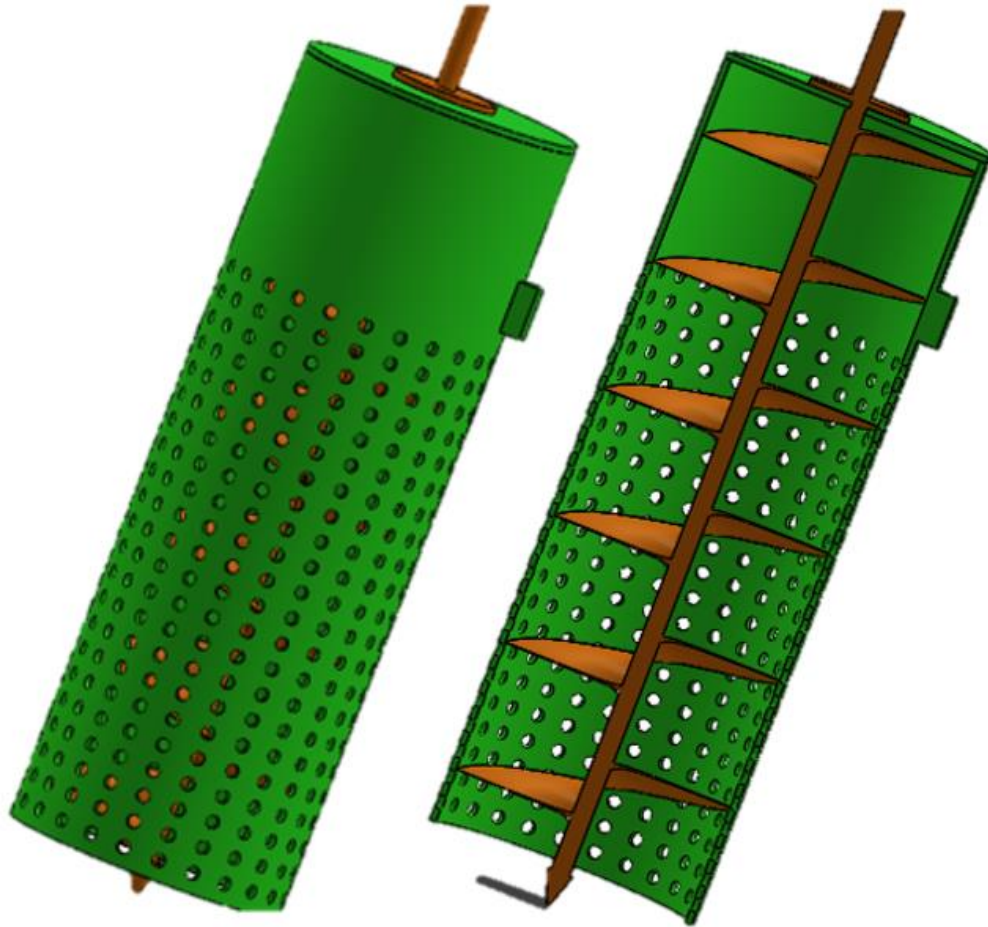


Figure 2.4: Initial design of auger system with cross-section cut.

The first design iteration contained a major drawback however. The design consisted merely of a single, large auger, a similarly large torque would need to be applied to operate said auger. In addition to requiring a significantly large and likely equally expensive motor to operate, the torque would also need to be supported by the robot's frame. The frame would potentially be subject to several large stresses throughout and would need to be designed to handle them. As well, in a case if the tires were unable to maintain traction with the soil during the auger's operation, the robot itself might begin to spin. Thus, the first major improvement to the auger design that was needed was to reduce the torque transmission outwards to the robot's frame.

2.3. Design Improvements and Modifications

2.3.1. Augers

The first major change made to the initial design of the auger system was implemented to reduce the torque transmission from the auger to the rest of the robot. In order to accomplish this, the team opted to using four 4"-diameter augers rather than one large 10"-diameter auger. By adding 3 additional augers, the augers could be set up to perform counter rotating motions. Using the setup shown in Figure 2.5, two augers, placed in opposite corners, were driven clockwise, while the remaining two were driven counterclockwise. This setup eliminates any torque transmission assuming that all augers are operating at the same torque input. In the event of an imbalance, such as an auger getting caught on the gravel or a motor failure, the net torque transmission will still be greatly reduced from the initial design due to the reduced diameter of the auger providing the imbalance.

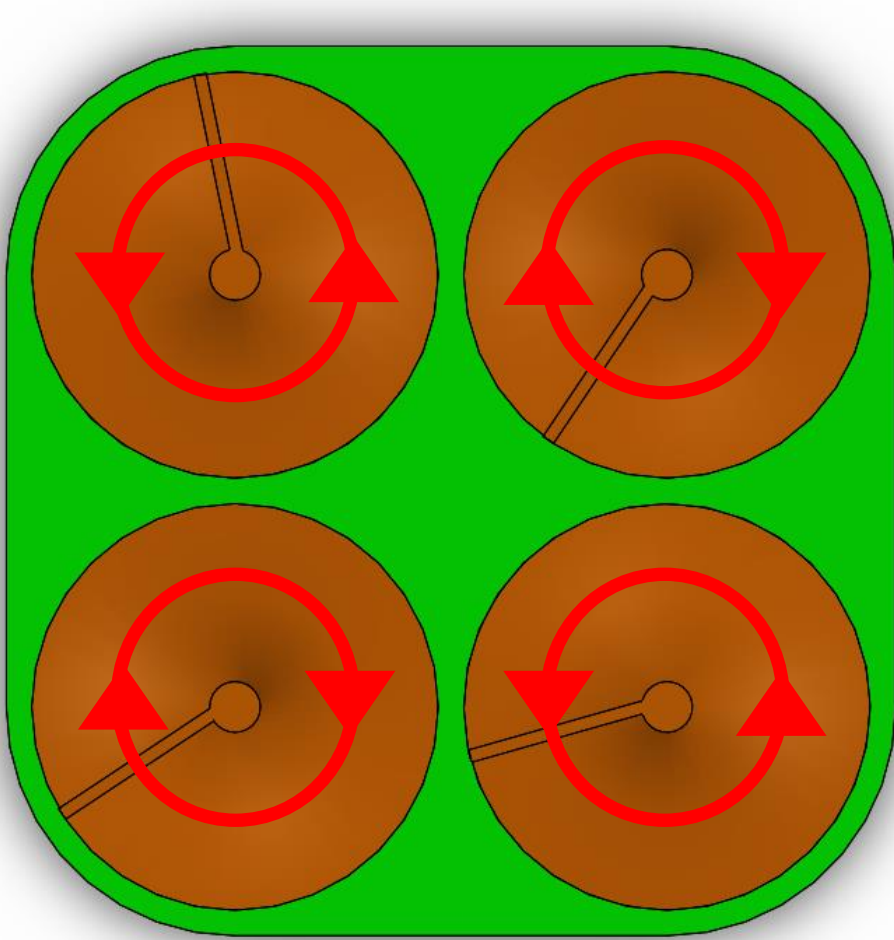


Figure 2.5. Counterrotating auger setup.

The next change made to the augers was to extend them past the length of the shell. As shown in Figure 2.4, the initial design placed the bottom of the auger and its containing shell at the same height. With concerns of the case experiencing difficulty driving into the gravel-rich section of the test soil, the augers were extended 6" past the bottom of the shell, the expected depth of the gravel-rich section of the soil as given by NASA. A cross-section of the new auger and shell setup can be seen in Figure 2.6.

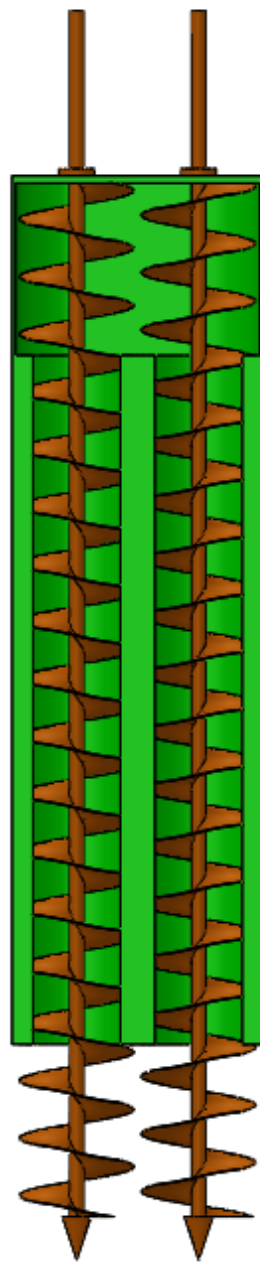


Figure 2.6. Cross-section of 4 extended auger setup with new shell.

In order to accommodate the precise lengths and diameters that the team desired for the augers, as well as being able to procure identical models in both right-hand and left-hand rotation, the team reached out to Falcon Industries, Inc. to machine custom augers for the project. As a result of ordering custom augers, the team was also able to make one final change to the auger's design. The first two flights of the augers, located below the bottom of the shell, were enlarged to a diameter of 4.5".

This change allowed the augers to dig a slightly larger hole that would be able to better accommodate the shell being driven down into the ground behind them, in addition to any mounting rails or other such external parts that would be attached to the shell.

2.3.2. Auger Shell

The shell that would contain the augers saw little directed change over the course of the design process, with most changes occurring as a result of the changes to the augers themselves. The first major change to the shell came as a result of the switch to 4 augers from 1. As shown in Figures 2.5 and 2.6, the shell completely encircled each individual auger to serve its intended function and was formed as one solid piece in order to hold the augers together. An open area was additionally created in the interior at the top of the shell. This would allow material mined by the two forward most augers to have the ability to be dumped out of the door that would be placed on the rear wall. Lastly, an additional shell was created with the same shape with the intention of mounting it on top of the original shell to provide a dust-proof housing for the motors that would be driving the augers.

Throughout the design process up to this point, the shell had been designed to be manufactured out of a plastic on a 3D printer to help save weight by using a lighter material and allowing any necessary level of detail in the design. However, due to rising concerns of cost and time of production, the team decided to make the switch to an aluminum shell. As seen in Figure 2.7, the solid plastic shell was replaced by a built-up model of aluminum tubes and sheet metal. The tubes fulfilled the shell's intended service of surrounding the augers and keeping the mined material on the flights, while the sheet metal formed the remainder of the shell. The thicker sheets held the 4 tubes in place and connected them, holding the majority of the load, while thinner sheets were used to form the top of the shell, where the dumping door and motor housing would be located.

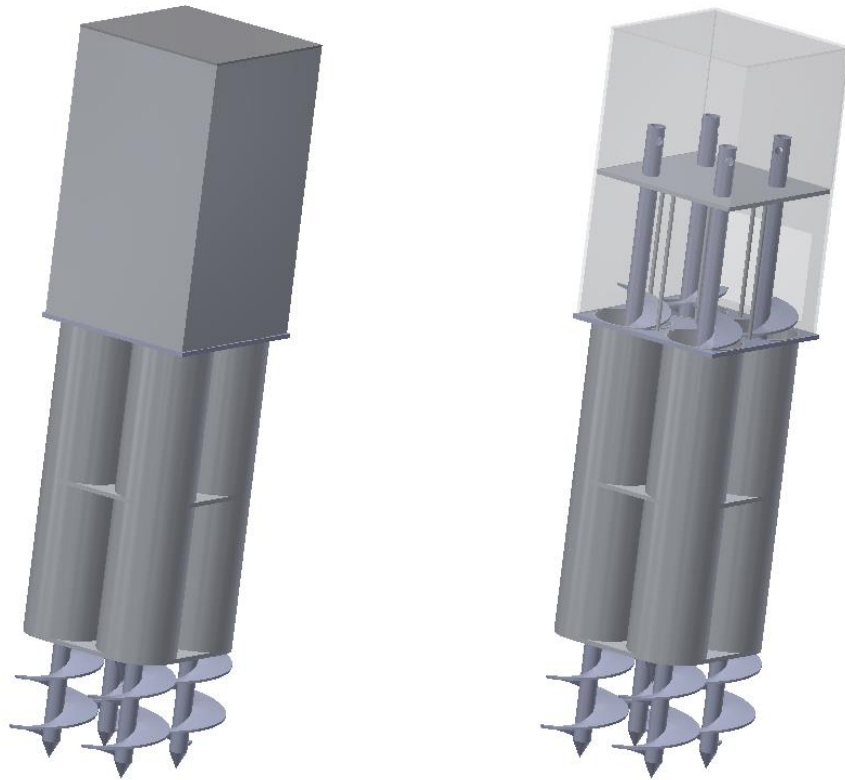


Figure 2.7. Aluminum built-up auger shell.

2.3.3. Auger Frame

The next step in the design of the mining system was to create a frame to mount the augers and auger shell onto. Such a frame would need to be able to provide the necessary translational and rotational movement to the augers' orientation, as well as serving as a connection to the larger frame of the robot itself.

The first design for this frame is shown in Figures 2.8 and 2.9. The base of the frame is a cage built up from 1" square aluminum tubing, shown in yellow. Mounted onto the sides of the frame are 4 rack and pinion gearboxes, shown in purple. These were to serve as the translational motors for the system, having one driving pinion on each side of the auger shell to raise and lower the system, as well as two free-spinning pinions to provide extra stability. The original rough sketches for the gearboxes, based on models the team had found online as potential parts, were designed such that the gearboxes fully encircled the engaged racks, preventing the racks from mounting directly onto the auger shell. This necessitated the additional mounts shown in red, which were placed at the top and bottom of the racks and connected to the auger shell. The mounting at the top needed to be a unique shape

and wrap around the auger shell as the mounting could not attach to the top of the shell housing the motors, as that section needed to remain easily removable for access to the motors. The mounts additionally needed to acknowledge the clearances necessary for the pinions to engage the racks over their full length, resulting in the shape seen.

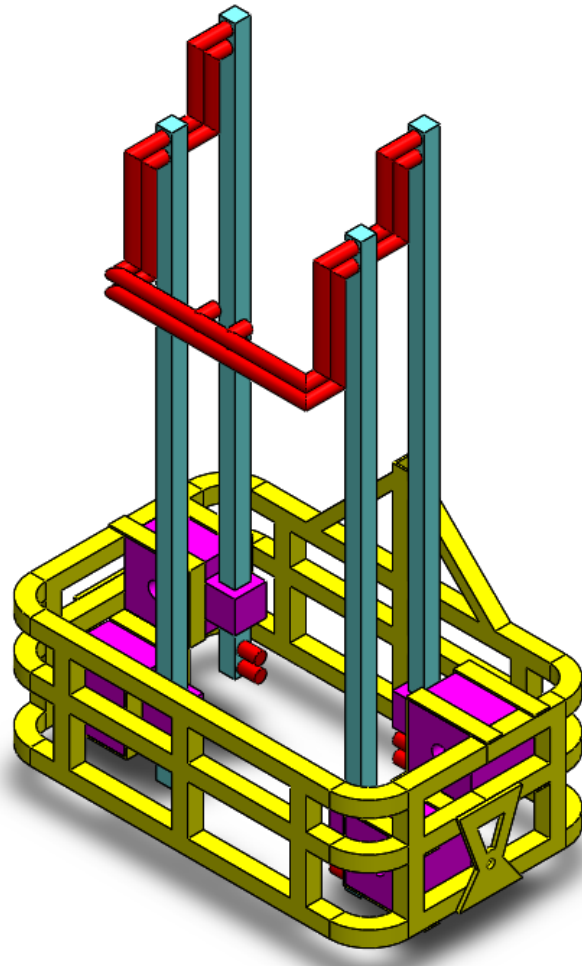


Figure 2.8. First design of auger system frame.

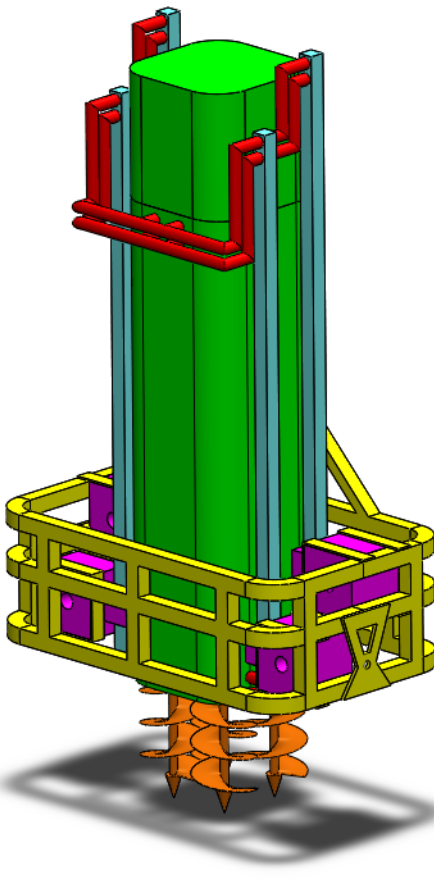


Figure 2.9. First design of auger system frame with augers and shell.

On the back of the frame, additional vertical tubing was placed that provided a location for the mounting of a linear actuator. Such an actuator, coupled with the pin mountings located on the sides of the frame would provide the necessary rotational motion for the system.

In order to reduce the weight and cost of the assembly, several adjustments were made to the frame. Firstly, the size of the aluminum cage was reduced as the additional material provided no necessary benefits to the overall strength of the assembly. The free-rotating pinions were replaced with linear slide rails, as they could serve the same function and were significantly reduced in size, weight, and cost.

The driving pinions, once parts were picked with determined maximum loading conditions, were reduced from 2 units to 1 unit. The chosen units were leanteknik gearboxes from their lifgo 5.0 series, with a maximum loading of 2000 N. The entire assembly with an estimated mass of mined material based on the available volume inside of the shell, only weighed a total of approximately 700 N. The mounting

location was also moved to the front of the assembly to maintain symmetry. Additionally, a variation of the gear box model was available that did not fully encircle the rack, allowing the rack to be mounted directly onto the shell, removing the need for the additional mounting.

The team decided that the auger system should be designed to lay flat on top of the frame of the robot when in a resting or traveling position. To accomplish this, the linear actuator needed to be moved from the rear of the frame as that would prevent the system from being able to lay fully flat without greatly enlarging the actuator so that it could be mounted far back on the robot frame and additionally increasing the size of the robot frame to accompany this. Instead, one actuator became two, and the actuators were moved to a mounting location on the sides of the frame, with similar vertical tubing sections to provide the mounting locations. A picture of the updated frame can be found in Figures 2.10 and 2.11.



Figure 2.10. Updated design of auger system frame.



Figure 2.11. Updated design of auger system frame with augers and shell.

2.4. Calculations and Analysis

2.4.1. Auger Motor Sizing

Two different calculations were performed to create an estimated maximum torque necessary for operation of augers. The first calculation utilized the power screw equation to estimate the necessary torque to rotate an auger assuming that the auger was fully loaded with mined material.

$$T = F * \mu * r \quad 2.1$$

Where T is the required torque, F is the applied force, the combined weight of the augers and material, μ is the friction coefficient, and r is the screw radius of the auger.

The downward force was calculated from the combined weight of the auger and the theoretical mined material.

$$F = W + \rho * \frac{\pi}{4} (D_{auger flights}^2 - D_{auger shaft}^2) * h \quad 2.2$$

Where F is the total applied force, W is the weight of the augers, ρ is the density of the soil, D is the diameter of the specified component, and h is the height of the auger shell.

The weight of the auger was estimated by Solidworks to be 5.45 lbf. BP-1, while differing greatly in many physical properties from regular sand, does have a very similar density, and so regular sand was used a substitute in this calculation. The density of a sand-gravel mixture that one could expect to be lifting inside the augers was estimated at 120 lbf/ft³, or 0.069444 lbf/in³. The diameter of the auger flights was 4 in, and the diameter of the shaft was 1 in. Lastly, the total height of the auger shell in which the material would be contained was 24 in. Thus the force could be found to be:

$$F = 25.08 \text{ lbf}$$

The necessary torque can now be calculated, given an estimated friction coefficient of 0.3 and a screw radius of 2 in:

$$T = 15.05 \text{ lbf} * \text{in} = 1.700 \text{ N} * \text{m}$$

The next torque calculation done estimated the necessary torque for ground penetration of the auger flights based on the shear strength of the soil:

$$T = \tau_{BP-1} * A_c * r \quad 2.3$$

Where T again is the required torque, τ is the shear strength of BP-1, A_c is the cross-sectional area of the auger flights, and r is the radius of the auger screw.

The shear strength of BP-1 could not be located from available data and so was overly estimated from similar materials to be 600,000 N/m². The cross-sectional area of the flights was found from the flight length of 3.5 in (4.5 in – 1 in) and sharpened flight thickness of 1/40 in (estimated from 20% of the full flight thickness of 1/8 in.), and calculated to be 0.4375 in², or $2.2823 * 10^{-4}$ m². The screw radius in this equation used the radius of the larger flights at the bottom of the augers of 2.25 in, or 0.05715 m. The torque required for ground penetration can then be calculated to be:

$$T = 1.565 \text{ N} * \text{m}$$

The two torque calculations were added together to provide a worst possible case that the motors would need to provide torque for, although in reality, neither case should be occurring at the same time as the other.

$$T_{max} = 1.700 + 1.565 = 3.265 \text{ N} * \text{m}$$

The motors chosen were IG42 gear motors from Shayang Ye Industrial Co., Ltd. At an available reduction ratio of 1/84, the motors are able to provide a maximum intermittently permissible torque of 5.3 N*m, as well as a nominal torque of 1.77 N*m. The nominal torque is capable of carrying the load in either worst case described above, and in an event where both should occur simultaneously, the motor is more than capable of supporting the necessary torque.

2.4.2. Stepper Motor Sizing.

The rack and pinion gear box was to be driven by a stepper motor, which would be capable of producing the large torques necessary to drive the auger system up and down, as well as having the ability to lock in place when not in use, allowing the augers to be held in any desired location. The necessary torque was calculated from the equation:

$$T = W * r \quad 2.4$$

Where T is the required torque, W is the weight of the auger assembly, and r is the radius of the pinion gear.

The mass of the auger assembly was estimated to be 70 kg, calculated from the estimated weight of an auger full of mined material in Section 2.4.1, at 25.08 lbf, or 11.38 kg for each of 4 augers, and another approximately 25 kg of mass from the rest of the auger assembly. The weight of the total assembly is 686.7 N. The radius of the pinion gear for the lifgo 5.0 gearbox chosen for the rack and pinion apparatus is 10 mm, thus the torque required for a stepper motor can be found to be:

$$T = 6.867 \text{ N} * \text{m}$$

The stepper motor chosen was a ML34HD2L4500 model hybrid stepper motor from Moons Industries. The motor is rated for a maximum torque of 9.8 N*m, which is capable of lifting the auger assembly at max capacity and allows for some additional torque to be applied, should any unexpected loads be experienced.

2.4.3. Linear Actuator Sizing.

The last mechanical part needed to be sized for the assembly was the linear actuators that would rotate the auger system. To determine this, a simple moment comparison was run comparing the moment caused by the weight of the auger assembly, and the necessary moment from the actuators to counteract it:

$$2 * F * d_{actuator} = W * d_{auger\ assembly} \quad 2.5$$

Where F is the required force of one actuator, d is the perpendicular distance from the pin connection to the specified component, and W is the weight of the auger assembly.

The weight of the auger assembly was calculated in 2.4.2 at a fully loaded scenario and found to be 686.7 N. At its traveling position, the auger system is placed such that its center of mass is located roughly above the pin connections to the robot frame. Then, when the system is ready to be engaged, the system will be retracted 6 in, or 0.1524 m, to remove the exposed auger flights from their holding shell (discussed in Section 2.5), at which the system reaches its worst loading case for the linear actuators. While the auger system is in a horizontal position, the linear actuators are mounted 35 mm above the pin connections to the frame. In this calculation, the actuators are also assumed to be horizontal themselves so as to simplify the calculation. The actuators would be only slightly below horizontal in the full assembly and as the distance between the actuator and pins also contains a horizontal offset, increasing the angle downwards would only increase the perpendicular distance between the two, and thus lower the necessary force, so this assumption was considered acceptable as it would provide an overestimate. With this assumption made, the necessary force from each actuator was calculated to be:

$$F = 1495.044\ N$$

The selected actuators for the project were PA-03-10-600 actuators from Progressive Automations Inc., with a maximum rated load of 600 lbf, or approximately 2700 N, nearly double the required force.

An analysis of the rotation of the auger system in the Autodesk Inventor modeling software provided an estimate of approximately 7 in of required stroke length. A 10 in. stroke model of the actuators was selected so as not to fully extend the actuators while in use and potentially overstress them, as well as providing a buffer on the stroke length that can be achieved in the event that any small changes made to the assembly during production changed the required stroke slightly.

2.5. Final Design

The completed design of the mining systems can be found in Figure 2.12. The completed design is largely the same as the model seen in Figure 2.11. The only difference is the addition of the stepper motor to the front of the frame. The motor was originally intended to be placed inside the frame with the driveshaft located concentrically with the pinion gear, however the gear was delivered equipped with its own shaft. The extra clearance now required no longer allowed for the motor to be placed in this location, and so the motor was moved to be mounted on top of the frame and gearbox. The parallel shafts were then connected by two sprockets linked with an ANSI 35 roller chain (not pictured). Full mechanical drawings of all machined parts for the assembly can be found in Appendix A.



Figure 2.12: Completed mining system assembly.

CHAPTER III

NON-PNEUMATIC WHEELS

3.1. Design Considerations

The operation and design of a wheel is one of the most important systems on a ground operating robot. The argument for this is obvious, if the robot cannot move it cannot perform any of its assigned tasks. Along with this, the wheel's design has direct relationships with the energy consumption, speed, maximum load, odometry, and range of terrain it can traverse. To accomplish these goals several things must be considered and analyzed during its design: wheel slip, trafficability, soil-wheel interactions, stress and deflection, and weight.

Since these will be used in low gravity and low-pressure environments certain design constraints are required. The wheel will need to be a non-pneumatic design due to functionality limits of pneumatic wheels and practicality. In addition, the wheel's materials will have to be compliant with the environmental conditions of the location the robot is deployed as described in chapter I.

3.2. Literature Review

3.2.1. Auxetic Meshes and Patent No. 8544515 B2

During the research of non-pneumatic wheel design, a US Patent titled: Ultralightweight Runflat Tires Based upon Negative Poisson Ratio (NPR) Auxetic Structures, was uncovered (United States of America Patent No. 8544515 B2, 2013).

An auxetic structure is a structure that has a negative Poisson's ratio. Some materials naturally have this property, but in most cases can be implemented by using unique geometries, such as the one proposed in the Patent as shown in Figure 3.1.

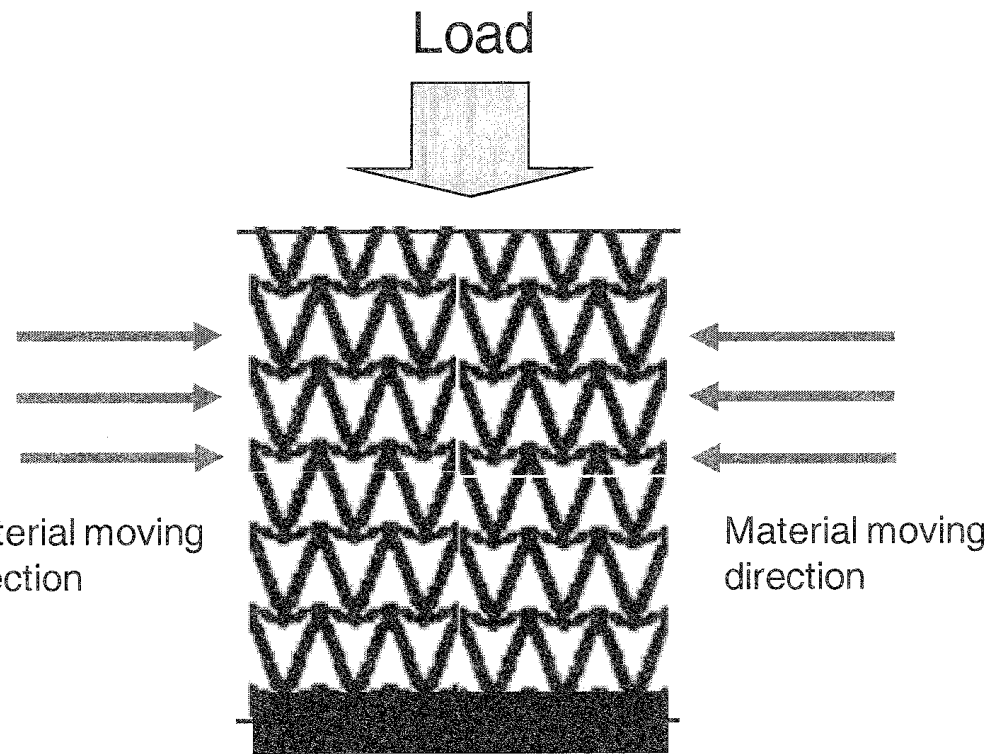


Figure 3.1: Auxetic structure from patent. (United States of America Patent No. 8544515 B2, 2013)

The idea of an auxetic mesh was very intriguing as it allows for a lightweight design where the geometry can be tuned for certain wheel characteristics, such as: deformation, maximum load, soil contact pressure, and wheel sinkage.

3.2.2. Terramechanics

The primary advantage of the auxetic wheel is that it allows for the wheel to be conformable while being lightweight and robust. This is different from many of the rigid wheel designs used by the other universities, but is however relatively common amongst the ground vehicles that have been or are planned to be deployed to the Moon or Mars, such as NASA's LRV (Vivake Asnani, 2009). This idea of having a compliant wheel is very important, but possibly required. This is shown through Bekker's empirical formulations for soil and wheel interactions where three cases are examined: a stiff wheel rolling on compliant ground, a compliant, possibly elastic, wheel rolling on stiff ground, and a compliant wheel rolling on a compliant ground. (Genta, 2012). Genta claims that the case in which a stiff wheel is used on compliant ground is the worst case since the wheel causes great deformation to the

soil and has large resistances to motion. This is then shown through the derivation and analysis of the soil resistance equations. Along with this, it is also shown that a compliant wheel also improves the tangential forces in longitudinal and traversal directions.

Further study of terramechanics led to the implementation of grousers to the design of a wheel to increase the drawbar pull of the wheel. This is shown not to be due to an increase in thrust but due to the decrease in motion resistance, more specifically the compaction resistance (Scott Moreland, 2012).

The same group at Carnegie Mellon later developed an equation for grouser spacing (Krzysztof Skonieczny, 2012). This equation gives the minimum angle of grouser displacement around the wheel:

$$\phi < \frac{1}{1-i} \left[\sqrt{(1+\hat{h})^2 - (1-\hat{z})^2} - \sqrt{1 - (1-\hat{z})^2} \right] \quad 3.1$$

Where ϕ is the displacement angle, i is the wheel slip, \hat{h} is the normalized grouser height, and \hat{z} is the normalized wheel sinkage. \hat{h} and \hat{z} are normalized by diving the grouser height and wheel sinkage by the wheel's radius.

3.3. Design Concepts

3.3.1. Inner Rings Concept based on DLR's MOVE

The first wheel designed was based on the spring concept developed by DLR, called MOVE. It consists of a rim with a pattern of inner rings that act as support and can be easily deflected (DLR develops wheels for the ExoMars mission rover, 2006). The teams concept design for this wheel, as shown in Figure 3.2, was quickly replaced by the auxetic mesh wheel due its favorable properties.

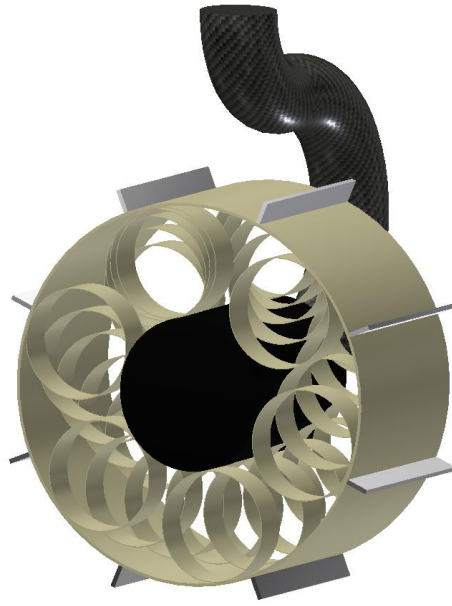


Figure 3.2: Wheel design concept based on DLR's MOVE wheel.

3.3.2. Auxetic Mesh

Using the Quasi-3D N-tire design presented in patent No. US 8544515 B2 the first iteration of the auxetic wheel was developed. An image of this wheel design is shown in Figure 3.3.

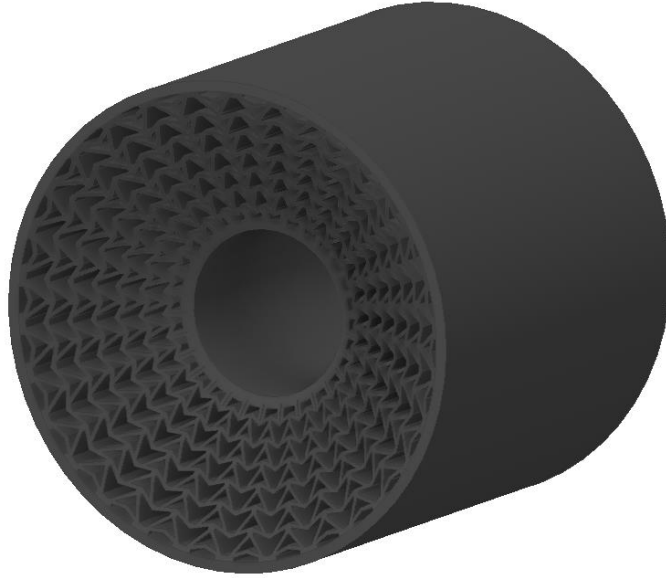


Figure 3.3: First iteration design of the auxetic wheel.

The wheel was designed to be printed on a Formlabs SLA printer using their proprietary, flexible resin. The properties of this resin can be found in the appendix.

This limited the diameter of the wheel to 135mm plus the size of the grousers. However, even with the limitation in place, a large enough diameter was able to be used that allows for good trafficability.

This wheel features a radial periodicity of seven and an angular periodicity of thirty. The wheel is also concaved on the sides to allow better conformity to smaller size obstacles that may lay in its path.

After fabricating the wheel, a view of which can be found in Figure 3.4, a compression test was conducted (figure 3.5). This led to a reduction in the radial periodicity of the triangular pattern. It is important to note that this design had no way of mounting to a motor, nor did it have any grousers. The reason for this was to study the geometry and make changes to it based on the observations and tests.



Figure 3.4: First iteration print of the auxetic wheel.

After an unknown number of compressions of varying forces by the designers, cracks started to propagate from the outer edges of the wheel within the outer post period of the geometry, which can be seen in Figure 3.5. It is hypothesized that this was due to the stress concentrators in the corners of triangles and due to the concavity of the wheel's design.



Figure 3.5: Cracks forming at the edges of the auxetic wheel.

Even with these cracks forming from fatigue the wheel was still capable of operating without trouble. Regardless, the issue was addressed in the next design iteration.

3.4. Calculations

To determine certain geometries of the wheel and to determine how much torque a motor would need to supply to the wheel to have it move through the BP-1, Bekker's empirical model was utilized to determine the different soil-wheel interactions. Note that in the following calculations, the soil parameters used were found in the Lunar Handbook, provided to the teams participating in the competition by NASA and are also found below in table 3.1.

Table 3.1. List of soil properties for lunar soil.

Name	Symbol	Value
Coefficient of Cohesion	c	$0.017 \frac{N}{cm^2}$
Angle of Repose	ϕ	35°
Friction Modulus of Soil Deformation	K_c	$0.14 \frac{N}{cm^2}$
Cohesive Modulus of Soil Deformation	K_ϕ	$0.82 \frac{N}{cm^3}$
Exponent of Soil Deformation	n	1

The first thing to determine is how far the wheel will sink into the ground. This is determined utilizing the following equation:

$$z = \frac{(bP)^{\frac{1}{n}}}{k_c + bk_\phi} \quad 3.2$$

Where, b is the smallest dimension of the wheel's contact patch, and P is the contact pressure for the wheel.

From there, the slippage, i can be conservatively estimated utilizing the following relationship suggested by Krzysztof Skonieczny (Krzysztof Skonieczny, 2012).

$$\hat{z} \leq \frac{1}{2}i \quad 3.3$$

Where the wheel sinkage, z is normalized to be \hat{z} by dividing by the wheel's radius.

The next thing to determine is the Compaction Resistance from the soil. This is determined utilizing the following equation:

$$R_c = \frac{(bP)^{n+\frac{1}{n}}}{(n+1)(k_c + bk_\phi)^{\frac{1}{n}}} \quad 3.4$$

This resistance to motion is due to the anelastic deformation of the soil, which ultimately acts as a point where energy is lost.

To determine if this wheel will move forward there must be forces to counter the physical elements that are preventing the wheel from moving. This is given by the following equation for tractive effort for a wheel with grousers (Gerhart, 2004).

$$H = blk_c \ (1 + 2h)/b + W * \tan(\phi) [1 + 0.64 h/b \ \cot^(-1)(h/b)] \quad 3.5$$

Where b is the wheel width, h is the grouser height, W is the wheel load, and l is the arc length of the soil and wheel contact, which is defined by the equation:

$$l = \pi r / 90 [\cos^(-1)((r - z)/r) - \sin^(-1)(b_l/zr)] + b_l \quad 3.6$$

Where r is the wheel radius, z is the wheel sinkage, and b_l is the contact patch length.

To determine if this wheel will move forward or simply rotate in place the drawbar pull must be calculated. This is simply done by taking the difference of the tractive effort and the total resistance to motion.

$$DP = H - R_c \quad 3.7$$

Knowing that gravity is also something that can resist the wheel's motion, the following equation can be used to determine the max incline this wheel can traverse.

$$\theta_{max} = \sin^{-1}(DP) \quad 3.8$$

However, there is a limiting factor to this equation. The angle of repose for a soil is the point at which the soil will start to flow at a certain angle of inclination. When the soil starts to flow the system has then changed and the above equation is no longer valid. Knowing that the angle of repose for this soil is about 35 ° this equation is limited to this point.

It is important to note that drawbar pull is typically normalized against the load on the wheel for the sake of comparison to other system.

$$\widehat{DP} = \frac{DP}{W} \quad 3.9$$

The final equation to be used in the design of this wheel is one that is derived from a free body diagram of the wheel. This equation will be used to determine how much torque is required for this wheel to accelerate forward.

$$\tau = I_G \alpha + r \left[\frac{m}{N} a_x + R_c + W \sin(\theta) \right] \quad 3.10$$

Where m is the mass of the robot, N is the number of wheels, a_x is the linear acceleration, r is the wheel radius, W is the load of the wheel, θ is the angle of accent, I_G is the wheel's moment of inertia, and α is the angular acceleration of the wheel.

3.5. Preliminary Analysis and Simulation

Utilizing MATLAB and the equations found in section 3.4 the ideal geometries and characteristics of the wheel can be determined. Plots for all the major wheel characteristics were generated to be used in the final design of the wheel.

It is important to note that the following plots are the ones from a series of geometric iterations to balance the required torque and drawbar pull of the wheel. During the process of reading these charts, they should be viewed as arbitrary units as the y-axis values can be easily manipulated based on different wheel parameters. The plots found below use the same wheel parameters found in the final design of the wheel.

With that being said, the first characteristic of the wheel to investigate was the height of a basic grouser (figure 3.6).

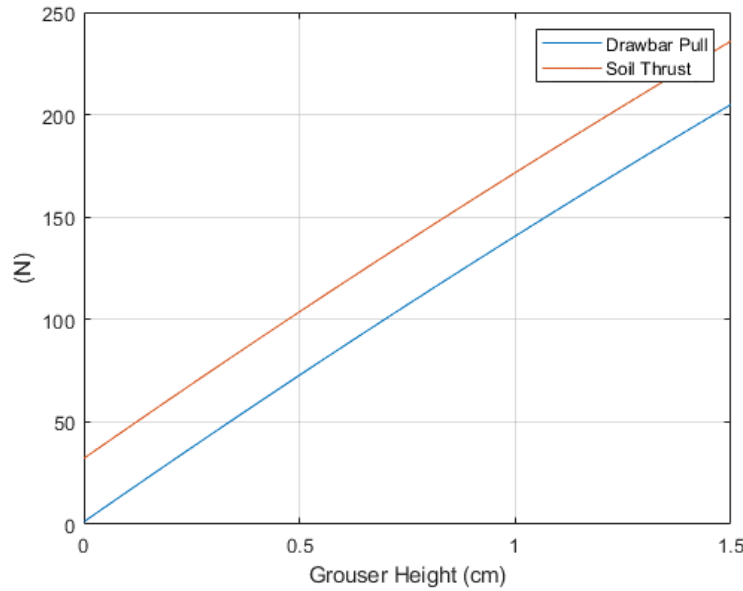


Figure 3.6: Grouser height vs. soil thrust (tractive effort) and drawbar pull.

It is easily seen in Figure 3.6 that the increase in the height of the grouser also increases the tractive effort and drawbar pull of the wheel.

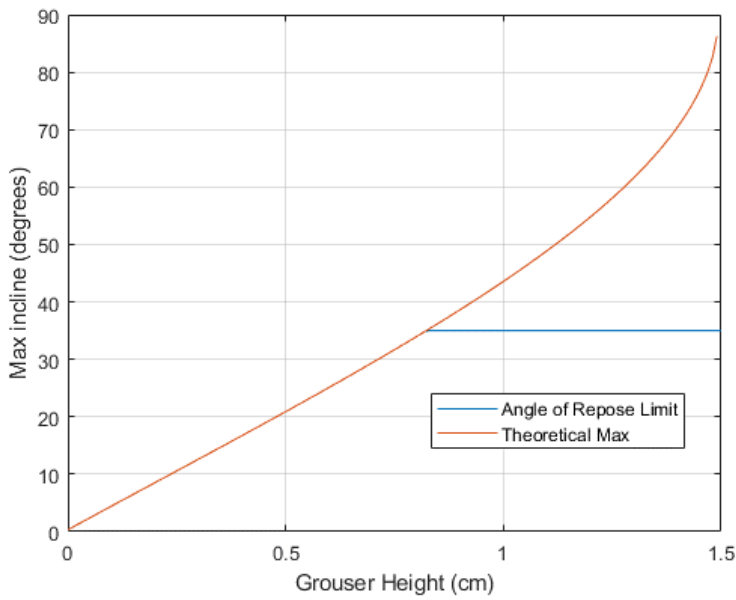


Figure 3.7: Grouser height vs. max incline.

In Figure 3.7, one can see that a grouser height larger than 0.9cm is not necessary for this wheel, given that anything greater than it would put it over the angle of repose limit.

The next aspect of the wheel to analyze is the width. This part was found to be very critical to the design and had significant effects when changed.

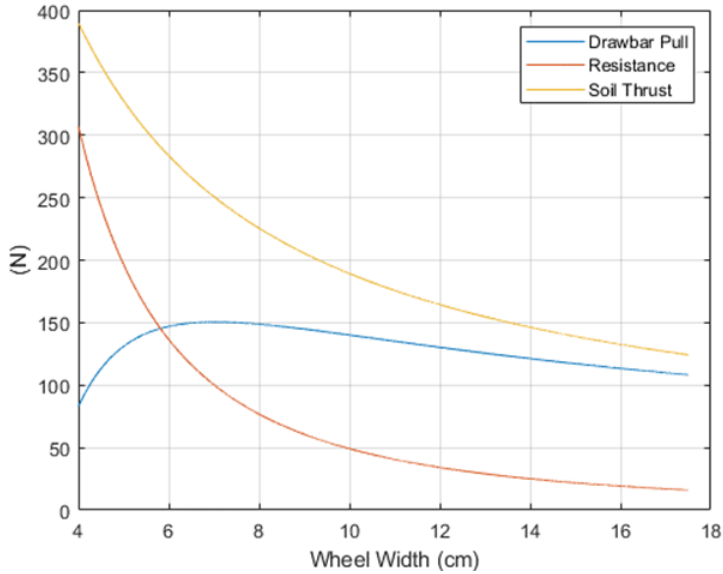


Figure 3.8: Wheel width vs. drawbar pull.

In Figure 3.8, it is seen here that the drawbar pull is maximized at a width of 6.5cm. This may seem like a good width to choose but when we look at Figure 3.9 for torque, some engineering judgement must be used to help determine what width should be used.

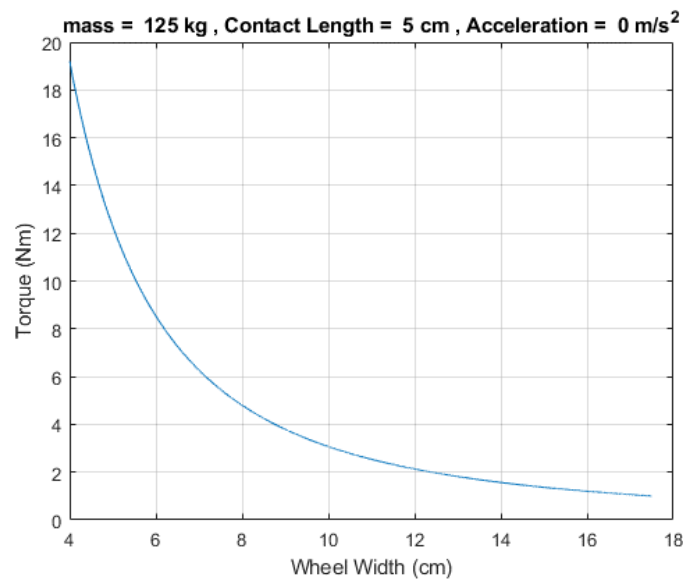


Figure 3.9: Wheel width vs. torque.

To help with the selection of the wheel's width a plot against was also generated in Figure 3.10.

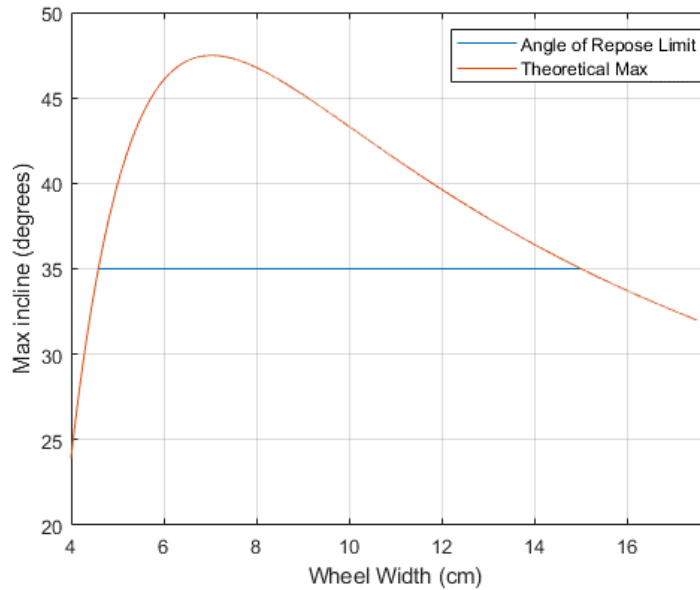


Figure 3.10: Wheel width vs. max incline.

This plot gives an ideal boundary range for the wheel's width. Using the intersection points for the theoretical max and incline and angle of repose limit the ideal width of the wheel should fall somewhere between 4.5cm and 14.5cm.

3.6. Final Design and Conclusions

Utilizing the plots generated in section 3.5 the wheel parameters used in the final design were chosen. These can be seen in Table 3.2.

Table 3.2. Final wheel geometry.

Geometric Parameter	Value (cm)
Grouser Height	0.9
Diameter	12.5
Width	11.4

Using these values, the overall performance of the wheel can be predicted for the chosen motor, as listed in Table 3.3.

Table 3.3. Predicted wheel performance.

Max Incline at motor's peak torque	35° (Angle of repose limit)
Max Incline at motor's rated torque	2.45°
Max acceleration at motor's peak torque	$6.54 \frac{m}{s^2}$
Linear Velocity at motor's rated torque	$0.25 \frac{m}{s}$
Normalized Drawbar Pull	0.69

In this final design iteration, a view of which can be seen in Figure 3.11, along with a comparison to the initial test design in Figure 3.12, several changes were made. The most notable were the adjustments made to the auxetic mesh based on the experimental observations from the first design.

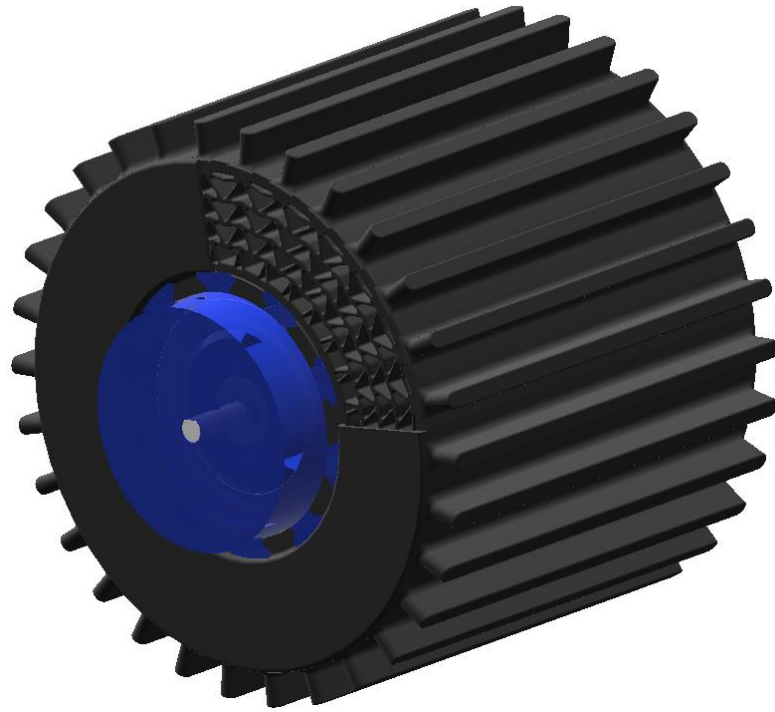


Figure 3.11: Final design iteration for the auxetic wheel, with cut away for internal geometry.

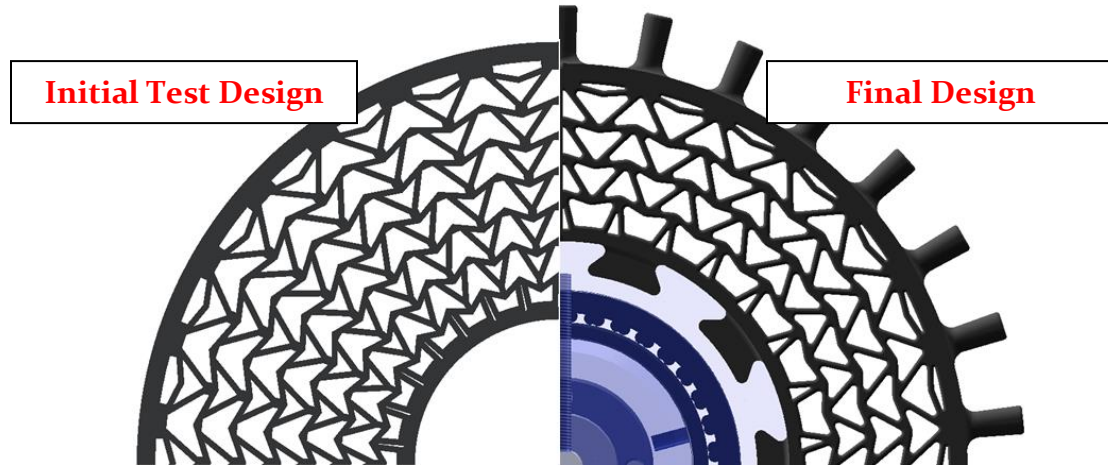


Figure 3.12: Comparison of auxetic meshes and other wheel features.

The first thing to note is the reduction in radial periodicity of the triangular pattern. The radial periodicity was reduced from seven to four due to the observations of the wheel when put under compression. It was observed that the majority of the deformation took place in the first four radial periods. Along with this, it was also observed that large stress concentrators were discovered in the initial test design as

seen in Figure 3.5. This led to the corners of each triangle being rounded to reduce this concentrated stress.

Along with this, a dovetail pattern was introduced for the interfacing of the non-pneumatic tire to the wheel and integrated motor system. This pattern allows for a tight press fit between the two parts and for a smooth torque transfer.

Another addition was the mesh guards, which is seen in Figure 3.6. The guard's purpose is to keep dirt out of the inner geometry which would prevent the wheel from properly deforming. The mesh guard is lifted 2mm off the surface of the wheel to allow for enough space for the malleable guard to buckle and not interfere with the internal geometry's deformation. Due to printing constraints, the mesh guards must be printed separately and then adhered to the wheel's surface using a syringe full of Formlabs' Flex resin. The resin is then hardened by a 415nm laser pointer. This method acts as a surface weld between the two parts.

This method of adhering two parts together also opens doors for the possibility of a healing/repair procedure to be utilized on Mars or the Moon where these wheels may be used. This possibility will require further investigations to determine its feasibility.

CHAPTER IV

AUTONOMOUS SYSTEMS

4.1. Overview

4.1.1. Design Considerations

Autonomously functioning robots are an important step towards extraterrestrial exploration and may be crucial to the success of planetary colonization. A large distance between the robot operator and the robot can induce many complications such as signal and feedback delay. Robots capable of completing repetitive tasks such as on-site resource utilization by use of on-board systems will be much more efficient for future missions. The addition of autonomous operation poses some potential challenges in the design and programming of such robots. A robot may either be semi-autonomous, or fully autonomous depending on how much input data is supplied to the robot from the user during its operation. Ideally, a user would only need to supply some mission parameters to the robot before it begins to operate. The robustness of the autonomous systems is key; if the robot consistently runs into issues while autonomously operating, the mission may be compromised. The three main programming considerations for the resource recovering robot are as follows: path planning, localization, and obstacle detection.

4.2. Initial Design

4.2.1. Path Planning

Path planning is used to find the shortest distance between the robot's starting location, and the robot's intended destination. When planning a path, the robot must consider set of potential waypoints between the start and end location. The A* algorithm is a path planning algorithm most commonly used to find the shortest distance between the waypoints while also implementing a heuristic to consider the overall shortest distance of potential paths. For these reasons, a modified A*

algorithm was tested for motion planning. See Figure 4.1 for a flow chart of the codes' logic.

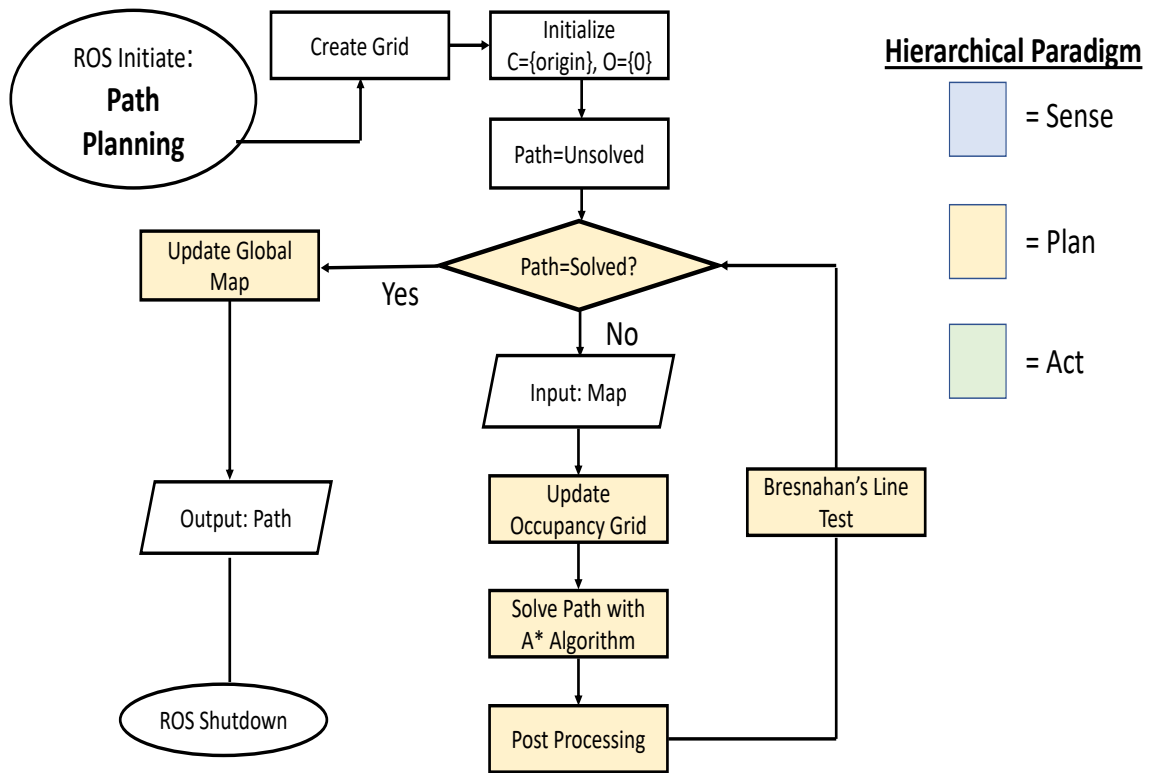


Figure 4.1: Flow chart of initial path planning algorithm.

The ROS-MATLAB interfacing functionality was utilized by setting up MATLAB as ROS node, this means that ROS will communicate with MATLAB much in the same way the ROS retrieves information from various sensors on the robot. After the program is started, an initial grid with the dimensions of the mission area is created. Two sets are initialized, a closed set, $C=\{\}$, and an open set, $O=\{\}$, the open set contains points in the mission domain that need to be evaluated. A binary occupancy grid is created from an input LiDAR scan. The program evaluates the input grid at points, also called nodes, and then calculates the shortest distance to the goal location in terms of an array of open points called way points. Bresnahan's Line algorithm is implemented to test the accuracy of the path. By calculating whether there is a shorter distance between waypoints, the potential path is

evaluated. If the path is in fact the shortest, the path will be updated in the robot's global map and output as the path the robot needs to follow. After the output is generated, ROS is shutdown, but can be reinitialized as many times as necessary. See Figure 4.2 for an example of a binary grid generated from a picture of a lunar surface.

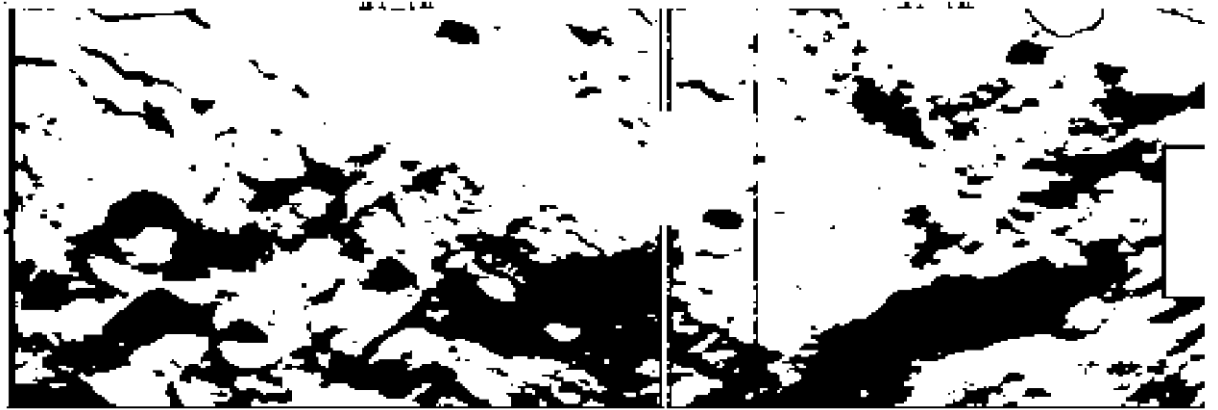


Figure 4.2: Binary occupancy grid.

See Figure 4.3 for an example of a path planned through various nodes generated on the example landscape of Figure 4.2.

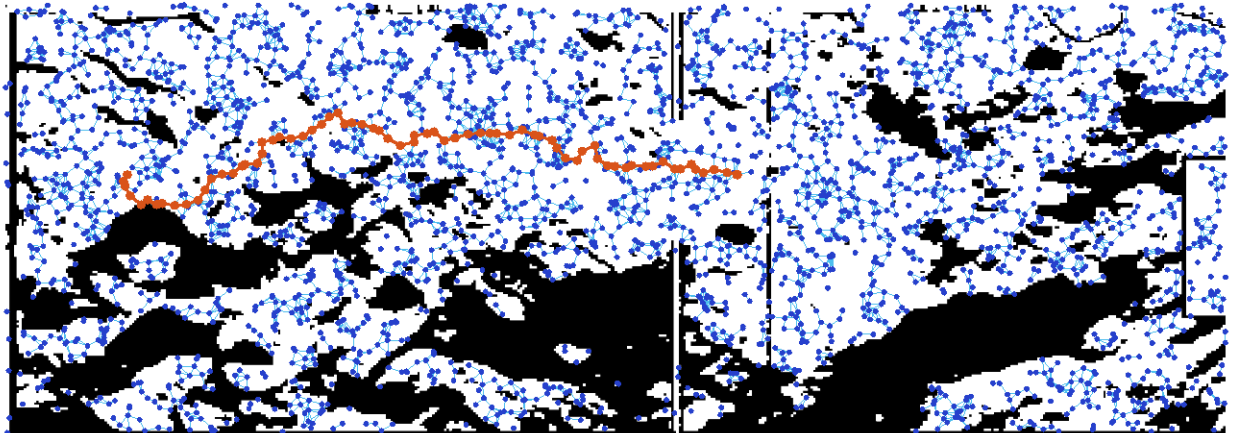


Figure 4.3: Probabilistic roadmap.

After the probabilistic roadmap shown above is generated, the grid is post-processed to get rid of nodes not used in the path. A big drawback of this current iteration of the motion path planning program include long calculation time since the entire domain is generated rather than a discrete radius immediately around the robot.

CHAPTER V

SUSPENSION AND CHASSIS

5.1. Overview

A vehicle required to operate on rough terrain requires an efficient and sturdy suspension system. Over the past few years, multiple rover suspension systems have been proposed by various researchers to meet the needs of an off-world NASA mission. The broad term for the rover suspension system configuration used by NASA is the rocker-bogie system. A rocker-bogie system is a type of suspension that maintains the chassis' pitch and roll while the wheels drive over rough terrain. The term 'rocker' refers to linkages on the suspension that are able to move relative to one another. The advantage of having rockers on rough terrain is that the rover will be able to maneuver over uneven ground more efficiently. The rockers are connected to each other by a differential to ensure the chassis does not flip or change orientation at any point during operation. A wheel on a suspension system can be actively driven, meaning that the wheel has its own motor and controller, and thereby can operate independently of the other wheels. The term 'bogie' refers to the arms of the suspension that are connected to the wheels that are not driven. If a suspension system is completely actively driven, it may still be referred to as a rocker-bogie system, or simply be called a rocker suspension system. Suspension systems such as the Mars Exploration Rover by NASA (MER), the CRAB by Autonomous Systems Laboratory (ASL), and the Concept-E by RCL (RCL-E) are widely regarded as the base by which future rover suspensions systems will be modeled after (Thueer, 2006). See Figure 5.1 for pictures of each of the aforementioned designs. Each suspension system has advantages and drawbacks and the choice of one over the other should be based on the application.

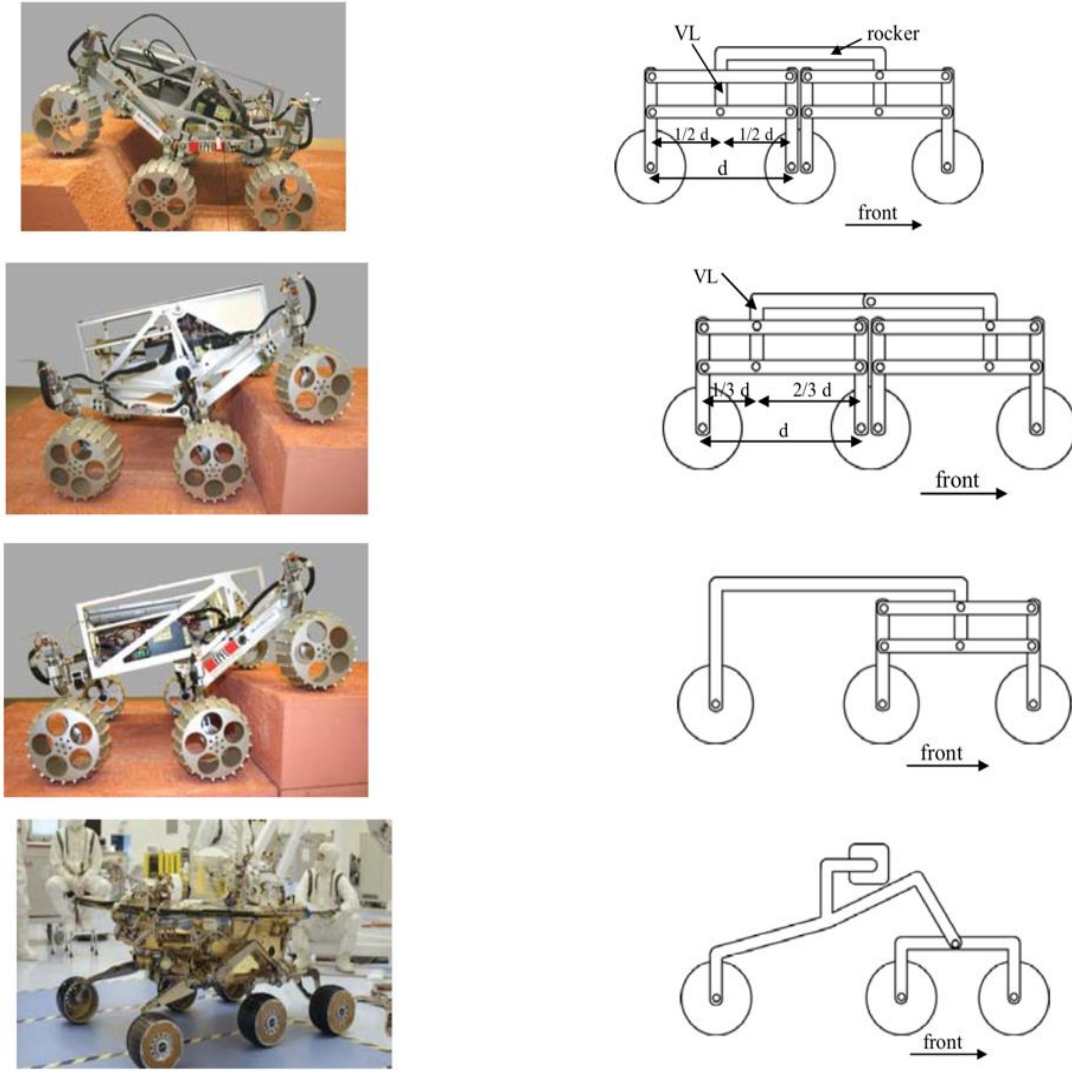


Figure 5.1: (From top down) CRAB 1, CRAB 2, RCL-E, MER.

The CRAB suspension by ASL has gone through multiple iterations as shown in the above picture. The rocker-bogie systems don't have any shocks or springs, the motion of the chassis comes from the rocking motion of the suspension arms. This allows the main body, or chassis, to remain relatively still while the robot climbs obstacles that are up to twice the diameter of the wheel with ease. The chassis should be kept level for multiple reasons: reduce jostling of electronics, to keep the center of gravity in a safe location so that the robot doesn't flip, and to maintain operation orientation for whatever tools may be running on the body.

The main factors in considering a design for the mining robot are simplicity, and high performance. Simplicity is important because we are working on a short time scale to finish this project. Additionally, a simple suspension with the least amount

of moving parts is less likely to need to be repaired. This is critical due to the rigorous testing phase before the competition. A high performance of the suspension is equally important, because the competition has a large obstacle course. Rather than relying on navigating around the obstacles, it is important the robot be able to climb over a rock or crater if need be. Another consideration is the amount of clearance between the bottom of the main body, and the ground. Bottoming out on obstacles could make the robot get stuck, or even ruin the more delicate components.

5.2. Final Design

The suspension type chosen for this year's NASA Robotic Mining competition was the Concept E by RCL, commonly referred to as the RCL-E. The reason for choosing this design as opposed to the others, is that the RCL-E is relatively simple compared to the other mechanisms. For example, both the MER and CRAB both incorporate a differential in the design, while the RCL-E does not require a dedicated differential. The rear rocker of the RCL-E serves as the differential, so if the right side of the vehicle is going over a rock, the movement of the right-side rocker is translated to the left side rocker by the rear rocker's change in orientation. A picture of the drive base and suspension is shown in Figure 5.2.



Figure 5.2: Drive base and suspension.

The suspension arms are connected by a 2 in. diameter piece of aluminum tubing with a pin connection to a 1 in. pillow block bearing (not self-adjusting). This connection allows the rocker to rotate about the pin. A bottom to ground clearance of 6 in. was determined to be enough, because the maximum height of objects in the competition is about 5.9 inches.

The suspension arms are made up of bent circular aluminum tubing with a 1 in. diameter, and a wall thickness of 0.125 in. A finite element analysis (FEA) was ran on the suspension arm with an element size of 0.1 in. to ensure that the arm could hold up under the applied load when the rover is at max payload. The load on one wheel was calculated to be 45 lbf when the robot is carrying the maximum amount of regolith. See Figure 5.3 for the FEA results for induced stress in the rocker.

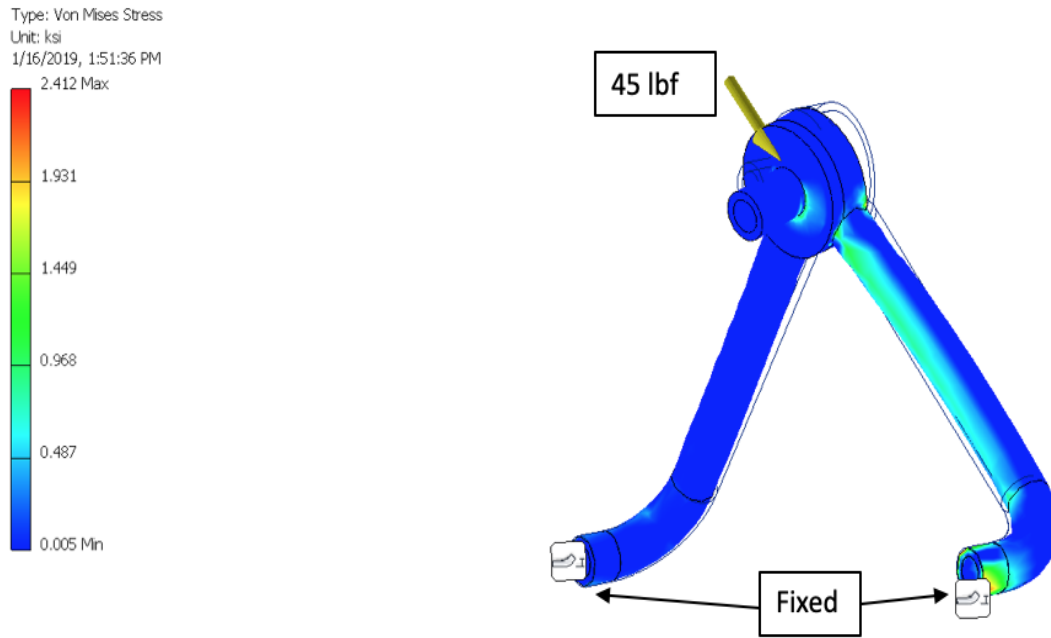


Figure 5.3: FEA analysis of rocker.

The stresses in the rocker are acceptable, and the factor of safety of about 14 is found from the static FEA. The worst stress is found at the bottom end of the arm in the fixed location where the wheel would be pinned.

CHAPTER VI

ASSEMBLY AND CONTROLS

6.1. Full Mechanical Assembly

The full mechanical assembly of the robot can be seen in Figure 6.1. All subsystems were attached to a basic box frame made of aluminum square tubing. Suspension arms were mounted to the frame on the inside such that the maximum width limit of 0.75 m for the robot could be respected. Additional trussed risers of the same tubing were to the box frame base for the mounting of the mining system. These risers were necessary in mounting the mining system high enough such that it would not attempt to intersect with other parts of the robot while performing its necessary motions. A large printed box was added to the front of the robot as well. Its primary function was to contain the exposed ends of the augers during travel, reducing the amount of material lost between completion of mining and dumping. Additionally, it also served as an effective mounting location for the Velodyne LiDAR vision system and the Nvidia Jetson central computer. Full mechanical drawings of all machined parts can be found in Appendix A.



Figure 6.1: Full assembly of robot.

6.2. Electrical Controls

To achieve manual control of the robot while complying with the NASA RMC rules the following electrical system is to be utilized.

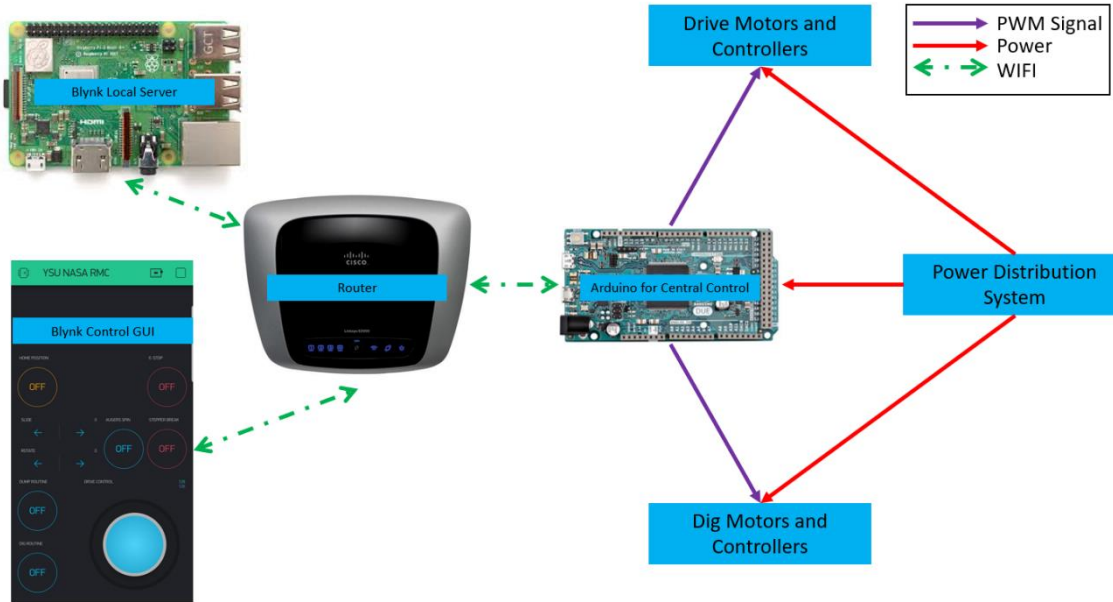


Figure 6.2: Simplified diagram of the electrical and communication system to be used in the control of the robot.

An Arduino is used in the robot to control the motors and handle the operation routines of the system. The Arduino will output PWM signals to the motor controllers based on the inputs it receives from the graphical user interface that was developed using the Blynk system (figure 6.3). To allow the Blynk system to properly work, a Raspberry Pi was used as a local server to facilitate the communications between the user's phone and the Arduino on the robot.



Figure 6.3: Blynk control, graphical user interface used by the operator.

The Blynk GUI has buttons that allows the user to either manually control the motion of each motor or to give the robot the command to carry out a series of commands in a routine.

CHAPTER VII

CONCLUSION

7.1. Project Scope Review

7.1.1. Project Timeline

The project timeline was defined early in the span of the project as seen in Table 1.7. The team was able to remain mostly on schedule for the majority of the Fall semester, with only December's goal of completing the mechanical design being delayed into early January. The team however fell much further behind over the course of the Spring semester. Due to delays in grant approval from NASA, and complacency in the team in being able to complete the project on time, component purchasing was significantly delayed into late February and early March, and the majority of the construction did not begin until late March, continuing through the end of April, eliminating the possibility of performing more extensive testing of the robot's performance. Work on automation algorithms also needed to be set aside in order to complete the project on time.

7.1.2. Scope Creep

The team experienced no scope creep over the duration of the project. The team extensively defined all necessary aspects for the robot to perform at the beginning of the project, and as such saw no new requirements appear in the following months. The team did however, experience a large amount of work creep, as the team was unable to recruit other capstone teams from Electrical Engineering and Computer Science disciplines to collaborate on for the project and were forced to undertake those responsibilities themselves.

7.2. Engineering Characteristic Targets

Early on in the lifetime of the project, during the problem definition stage, a set of engineering characteristics were established, based on the requirements of build

and performance for the robot. From there, a set of targets, minimum and ideal, were set for each characteristic to give the team goals to aim for with regards to each while designing the robot, as seen in Table 1.4. In Table 7.1, the final values achieved for each characteristic are listed, along with the target met for each.

Table 7.1. Final engineering characteristic performance.

Engineering Characteristic	Measurement	Unit	Final Performance	Target Met
Robot Speed	Time to Start Mining	s	23	Minimum
Trafficability	Size of Obstacles Maneuvered Around/Over	cm	±15	Minimum
Slip	Difference between Distance Traveled and Expected	m	0.092	Ideal
Weight	Weight	kg	60	Minimum
Mining Speed	Amount Mined During Run	kg	40	Ideal
Power Consumed	Power Consumed	Watt Hour	81	None
Operability in Dusty Conditions	Protection of Electrical Components	P/F*	Vital Components Protected	Minimum
Dust Produced During Run	Amount of Dust Kicked Up	P/F*	Minimal Dust	Ideal
Bandwidth**	Bandwidth	kb/s	Not measured	N/A

*Indicates Pass/Fail Criterion. No applicable unit of measurement.

**Bandwidth usage unable to be measured prior to competition trials.

7.2.1. Robot Speed

The speed at which the robot can traverse the pit is a critical parameter of the robot's performance. With a 10 minute time limit on the competition trial, the faster that the robot can traverse from one end of the pit to the other, the more time that is able to spend on mining. The team set their initial minimum target at 60 s from competition start to the start of mining. This was chosen keeping in mind the robot's need to orient itself before it can begin driving. The autonomy was unable to be fully

implemented prior to competition, meaning manual control would be used for orientation of the robot. Knowing the speed at which the robot will drive, 0.25 m/s, as well as the length of the competition arena, 5.76 m, the amount of time that the robot takes to traverse the pit can be calculated at 23 s, meeting the minimum target set and falling just short of the ideal target at 20s. This time does not include the time taken for orientation prior to driving, as the initial placement of the robot is random, but it is assumed that the time taken will be much less than the remaining 37 s to meet the minimum target.

7.2.2. Trafficability

The team was able to achieve a suspension design capable of overcoming obstacles of 15 cm in size, meeting the minimum target set at 10 cm, the size set by NASA to be smallest size of designated obstacles in the competition. The maximum size, which the team was unable to achieve was 30 cm. Due to height restrictions of the robot (0.75 m initial, up to 1.5 m fully extended), a suspension large enough to accommodate these obstacles was unable to be achieved. Designing a higher suspension also has the negative effect of raising the robot's center of gravity, making it more prone to tipping, so the team opted for the current design as a worthy compromise, especially when the larger obstacles can just as easily be driven around rather than over.

7.2.3. Slip

The efficiency of motion transformation from the wheels' rotation to the robot's linear motion is 99.6%. This means that in each wheel rotation 0.4% of the rotation is lost in wheel slippage. This means that for each meter the robot travels, the odometry from the wheel's encoders will think that the robot has traveled an additional 0.4 cm. If one assumes that the robot completes two full trips down and back across the pit, a total distance of 23.04 m, that would mean that the total slip differential would be approximately 0.092 m, less than one-third of the initial minimum target. The initially set ideal target of 0 was an unreasonable target as

7.2.4. Weight

The competition has a maximum mass limit placed on competing robots of 80 kg. The team set a goal for the robot of 40 kg, a mass that very few teams are able to achieve, giving the team a significant leg up in the competition. The team was unable to achieve this ideal goal, with the final design weighing in at approximately

60 kg. The goal of improving redundancy in the design (having each wheel driven independently, 4 augers, etc.) required many more motors and other motion drivers, which were the heaviest of all the individual components, and thus significantly added to the total mass. Even with all of the additional weight, the robot still falls neatly in the average among competing teams, with the vast majority of the robots, falling in the 50-70 kg range.

7.2.5. Mining Speed

The team set an arbitrary goal for the robot's performance of being able to mine 40 kg of gravel over the duration of the competition. As stated above, as no full scale test was able to be performed prior to competition, a definitive result was unable to be determined. Potential results can be inferred through the design of the robot however. Based on the available storage volume inside of the robot and combining it with an estimate of the density of the mined material, the robot is capable of holding 40 kg of material, meaning that it can meet the ideal target. Not all of the material mined is score-able however, as only the mass of the gravel counts for the competition. With this, even assuming that only half of the mass of material contained within the robot is attributed to the gravel, only 2 successful runs, the standard performance of competing robots, need to be completed to meet this goal.

7.2.6. Power Consumed

Individual power consumption for each component of the system is listed in table 7.2. This data was used to determine the theoretical power consumption of the robot.

Table 7.2. Total Power Consumption.

Usage	Item Name	Current (A)	Voltage (V)	Wattage	Number of units	Total Wattage	Total Current (A)	Time Running (min)	Watt-Hour
Drive	Anaheim Automation BLDC	2.83	24	42	6	252	16.98	10	42
Auger Spin	SuperDroid IG42 Brushed DC Motor	2.1	24	34.7	4	138.8	8.4	7	16.19
Auger Rotation	Progressive Automation Linear Actuator	7.6	12	91.2	2	182.4	15.2	0.7	2.128
Auger Translation	Moon Industries ML34HD3 L4500 Stepper	5	24	120	1	120	5	7	14
Computer	Nvidia Jetson	1.5	12	15	1	15	1.5	10	2.5
LiDAR	Velodyne Puck	2	12	24	1	24	2	10	4

This gives a total power consumption of about 81 watt-hours. However, this calculation is based on very conservative estimates. It is assumed that all the motors are operating at maximum rated load and are running for a longer duration of time than would be abnormal for operation. This estimate is more than twice the minimum target, failing the desired power usage. While in an actual test scenario, the total output would be a fraction of this estimate, almost certainly meeting the minimum target and possibly even the ideal, a full test was unable to be performed and so the appropriate result was unable to be determined.

7.2.7. Operability in Dusty Conditions

During operation of the robot, large amounts of dust can be kicked up due to the loose and lightweight nature of the BP-1 simulant and lunar and martian soil. The dust can have extremely negative impacts on performance of the robot, clogging gears, causing motor or other electrical failures, and so important components must be protected at all costs. The was able in the design of the robot to enclose all of the wheel and auger motors, as well as the central computer, Arduinos, and other vulnerable electrical components, meeting the minimum requirement for effective operation of the robot. Some components that were not able to be contained though included the stepper motor, rack and pinion drive, and the linear actuators. While

these components were designed with harsher conditions in mind than the previously mentioned components, the team could assure better prolonged operation of the robot should these components have been shielded from the dust as well, thus the team decided that their ideal target of protecting all components was not met.

7.2.8. Dust Produced During Run

Another important factor when considering the impacts of dust on robot performance is how much dust the robot produces in the first place. As again, the resources were lacking to perform a full-scale test, the team expects that the robot's design will significantly limit the dust produced during operation. All mining with the augers aside from initial ground penetration where dust production is inevitable will be performed in a subsurface environment. As the auger shell of the will penetrate into the ground behind the augers, material will be contained as it moves upwards past the surface. From there, the material is only once again exposed to the atmosphere upon expulsion at the collection trough, where dust again will inevitably be produced. By limiting major dust production to the two points during operation when it cannot be avoided, the team is satisfied that it has met its target for this characteristic.

7.2.9. Bandwidth

During operation of these robots in their intended environment, many miles away from Earth, communication between the robot and a human controller will take a lengthy amount of time and should be limited as much as possible. In this case, full autonomy is desired such that no communication is necessary. Full autonomy was unable to be completed for the robot, failing the ideal target set, however no resulting amount of bandwidth was able to be measured for the resulting necessary communication. Bandwidth was to be measured at competition and the team possessed no method of measuring the usage during testing of the robot, thus no result can be obtained to determine if the minimum target was met. Efforts to reduce the bandwidth were made however, such as setting up a digging or dumping set of motions as a defined subroutine in the central computer, thus requiring only the press of a button by the controller to initiate these functions, rather than controlling a complex set of variables all at once.

7.2.10. Overall Performance

Of the nine characteristics determined for the project, seven were able to meet the targets set for performance, three of which met the ideal target, the remaining four met the minimum target. One target was unable to be measured, and only one target was failed to be met, though the measurement determined for that characteristic was an extremely conservative estimate.

The team did not meet as many ideal targets as would have been preferred, although each set of targets were set assuming a system designed to optimize that characteristic. In reality, there are necessary compromises to be made when designing such a robot that will hinder optimization in any one category. One such example would be the implementation of a suspension system to meet the trafficability characteristic. In doing so, each wheel will be required to be individually driven. This leads to an increase in mass due to additional motors, and subsequently an increase in power usage to run them and increase to bandwidth to control them. With this in mind, that of the eight measured characteristics only one was determined by the team to have been failed, the design of the robot has been considered successful, though future optimizations can and should most certainly be made.

7.3. Suggestions / Recommendations

The team writes their suggestions and recommendations for the project with future Robotic Mining Competition teams from the University in mind. Teams should look to begin work on the project over the course of the summer months preceding the Fall semester. The extra few months of time will allow more time for the team to troubleshoot any problems or setbacks that will appear as well as allowing more time for extensive testing and optimization to occur. Teams as well should also look to improve on weight reduction of the robot while not sacrificing performance in other areas. The team recommends that future teams look to perform more thorough FEA simulations to minimize and optimize frame designs, as well as limiting moving components, as the numerous amount of motors necessary for this robot's operation increased the overall weight of the robot by a significant amount.

7.4. Further Considerations

7.4.1. External Factors

As with any project, engineering or otherwise, one must consider the greater effects of the project on the world around it. This includes such considerations as the health, safety, and welfare of the public, as well any global, cultural, social, environmental and economic implications the project may have.

With regards to public health, safety, and welfare, the team did not have many considerations to make. As the robot is intended for operation on the Moon and Mars, many miles away from the nearest human, such contexts are out of the scope of the project. However, for the terrestrial testing of the robot, for which humans will be present, safety considerations do need to be made. Firstly, the robot is equipped with an emergency stop switch in the event that robot operation requires immediate termination. The robot was also designed with the goal in mind of minimizing production of dust during operation. While a more minimal concern while off-planet, hence the category's lower weighting in the overall score, the dust can be harmful to humans under excessive exposure. Competition operators and team members inside the pit during performance are equipped with protective full-body suits to negate these dangers. The team however, still looked to mitigate as much of that risk as possible through the design of the robot by performing all mining in a subsurface environment through the use of augers. Mined material is contained on the augers and only again exposed to the environment upon expulsion at the collection trough, thus minimizing opportunities for dust to be produced.

With regards to global, cultural, social, environmental, and economic factors, the team made several considerations to design of the robot. The largest consideration made that affected all aspects of the design was the minimization of the robot's weight. Weight is everything when launching rockets, and reduction of this characteristic both saves on the cost of fuel required to launch the robot, as well as reduces the emissions produced by burning said fuel. The team used aluminum as the metal of choice for construction due to its high strength-to-weight ratio. Other metals could be used to further serve this goal, but aluminum was the most cost efficient within the budget available for the project. The use of additive manufacturing where applicable also served to accomplish these goals. The material used was very lightweight compared to aluminum, further reducing the weight. Additive manufacturing also has the additional benefit of reducing material waste. The other consideration made was more in regards to the overall objective of the

project, in which the robot is intended to provide the resources necessary for more permanent operations on the Moon and Mars, and eventually pave the way for human settlement.

7.4.2. Team Dynamics

Tuckman Team Maturity Test. The team took the Tuckman Team Maturity Test to determine an objective view of the team's strength and cohesion. The model upon which the test is based establishes four stages of team growth: Forming, Storming, Norming, and Performing. Each category is given a score based on the team's responses, ranging from a maximum score of 40, indicating a strong association of team performance with that stage, to a minimum score of 8, indicating a weak association. A score of 32 or higher typically indicates a team's primary stage of function.

The team scored as one would expect for a team that has been working together for approximately 9 months. The highest score of 34 was achieved in the Performing stage, indicating that the team has clear shared goals and members are working towards completion of the project with minimal personal conflicts. The next highest score was achieved in the Norming stage at 29, where the team looks to clarify communal goals and develop trust among one another. The remaining stages: Forming and Storming, scored much lower at 19 and 18, respectively. These stages focus on developing goals and learning team members' personalities and strengths and weaknesses. The lower scores show that the team has largely moved away from these stages of performance, which should be expected for a strong team by the time completion of the project is being reached.

Team Functionality. The team results of the Tuckman test suggested that the team was working strongly together by the end of the project timeline. The team actual functioning supports this conclusion. All members contributed collectively to leading the project. Sage typically led team discussions, but with regards to design and work on the project each member provided guidance and direction to the others when working on their assigned subsystems. While each member was assigned specific subsystems of the robot to work on, there was much collaborative discussion that the team participated in among one another. As all subsystems of the robot are required to be able to work with each of the others, collaborative work is required to an extent, but members very often shared suggestions with regards to others' work and just as often asked for guidance or advice on their own work. The team formally met at least once a week to share work from the previous week and to plan

ahead for the next. Members often met in more impromptu meetings outside of specified meeting times to work together on the project. The team looked to accommodate for all members' schedules for these meetings, though sometimes settled for meetings of just two members when this could not be achieved. Outside of meetings, the team frequently shared messages between each other, consistently updating on the day-to-day progress of the project.

REFERENCES

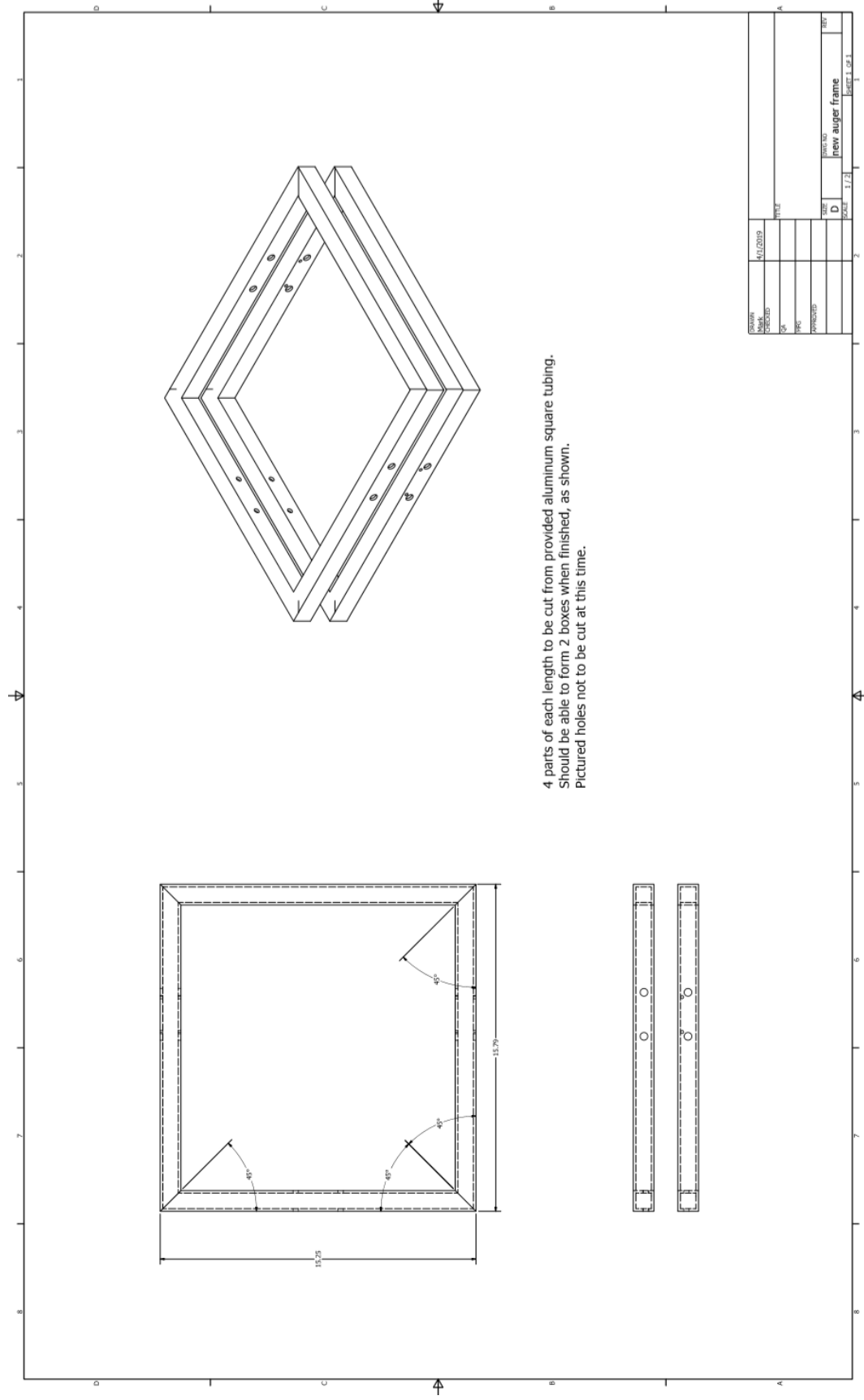
- Anderson, G. (2015, September 28). MRO. Retrieved from NASA: <https://www.nasa.gov/press-release/nasa-confirms-evidence-that-liquid-water-flows-on-today-s-mars>
- Anderson, G. (2015, September 28). MRO. Retrieved from NASA: <https://www.nasa.gov/press-release/nasa-confirms-evidence-that-liquid-water-flows-on-today-s-mars>
- DLR develops wheels for the ExoMars mission rover.* (2006). Retrieved from DLR: https://www.dlr.de/en/desktopdefault.aspx/tabid-4531/1157_read-2669/1157_page-1/
- Genta, G. (2012). Mobility on Planetary Surfaces. In G. Genta, *Introduction to the Mechanics of Space Robotics* (pp. 153-234). Springer.
- Gerhart, G. R. (2004). The Bekker Model Analysis for Small Robotic Vehicles. *SAE International.*
- Hustad, K. (2015, June 18). *Check Out The Robot That College of DuPage Engineering Students Showed Off To NASA.* Retrieved from ChicagoINNO: <https://www.americaninno.com/chicago/nasa-robotics-competition-invites-college-of-dupage-engineers/>
- Krzysztof Skonieczny, S. J. (2012). A Grouser Spacing Equation for Determining Appropriate Geometry of Planetary Rover Wheels. *IEEE.*
- RMC Archive.* (2017). Retrieved from NASA: <https://www.nasa.gov/content/rmc-archive>
- Scott Moreland, K. S. (2012). Soil Behavior of Wheels with Grousers for Planetary Rovers. *IEEE.*
- Siewart, T. T. (n.d.). Kinematic Analysis and Comparison of Wheeled Locomotion Performance.
- Thueer, T. & (2006). CRAB- Exploration Rover with Advanced Obstacle Negotiation Capabilities.

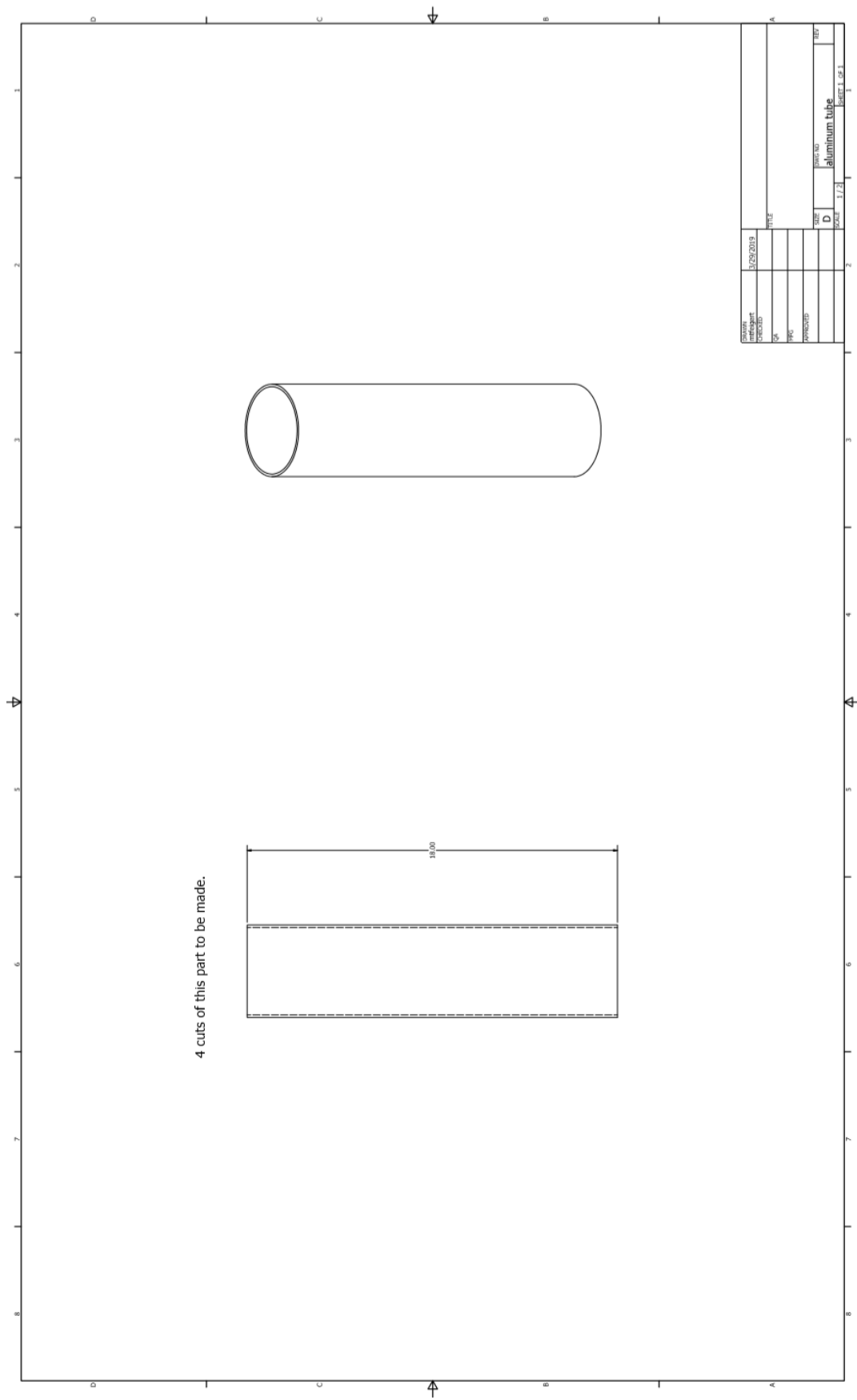
University of Alabama Astrorobotics. (2015). *NASA RMC Systems Engineering Report*.

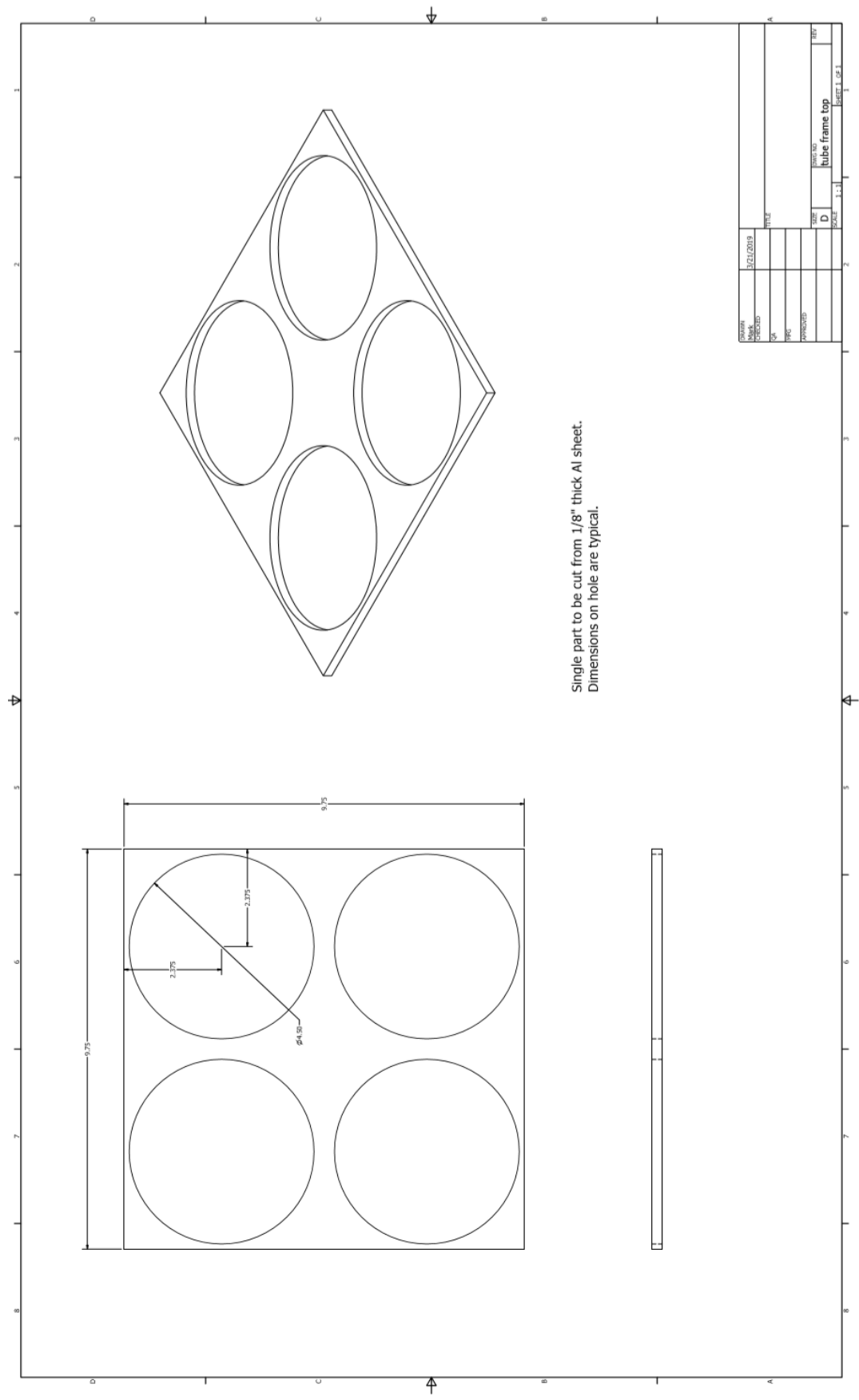
Vivake Asnani, D. D. (2009). *The Development of Wheels for the Lunar Roving Vehicle*. Cleveland: NASA Glenn Research Center.

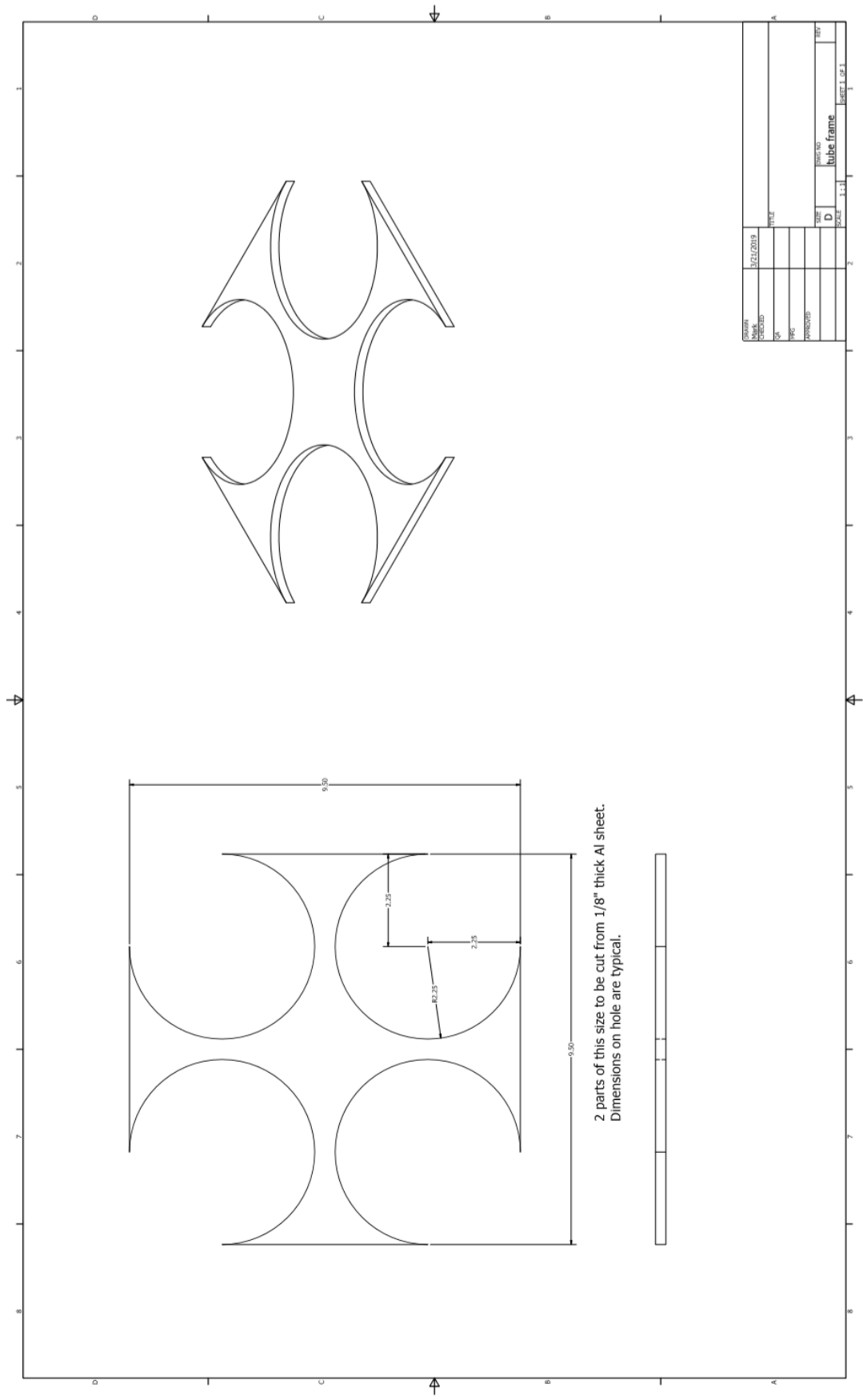
Zheng-Dong Ma, Y. L. (2013). *United States of America Patent No. 8544515 B2*.

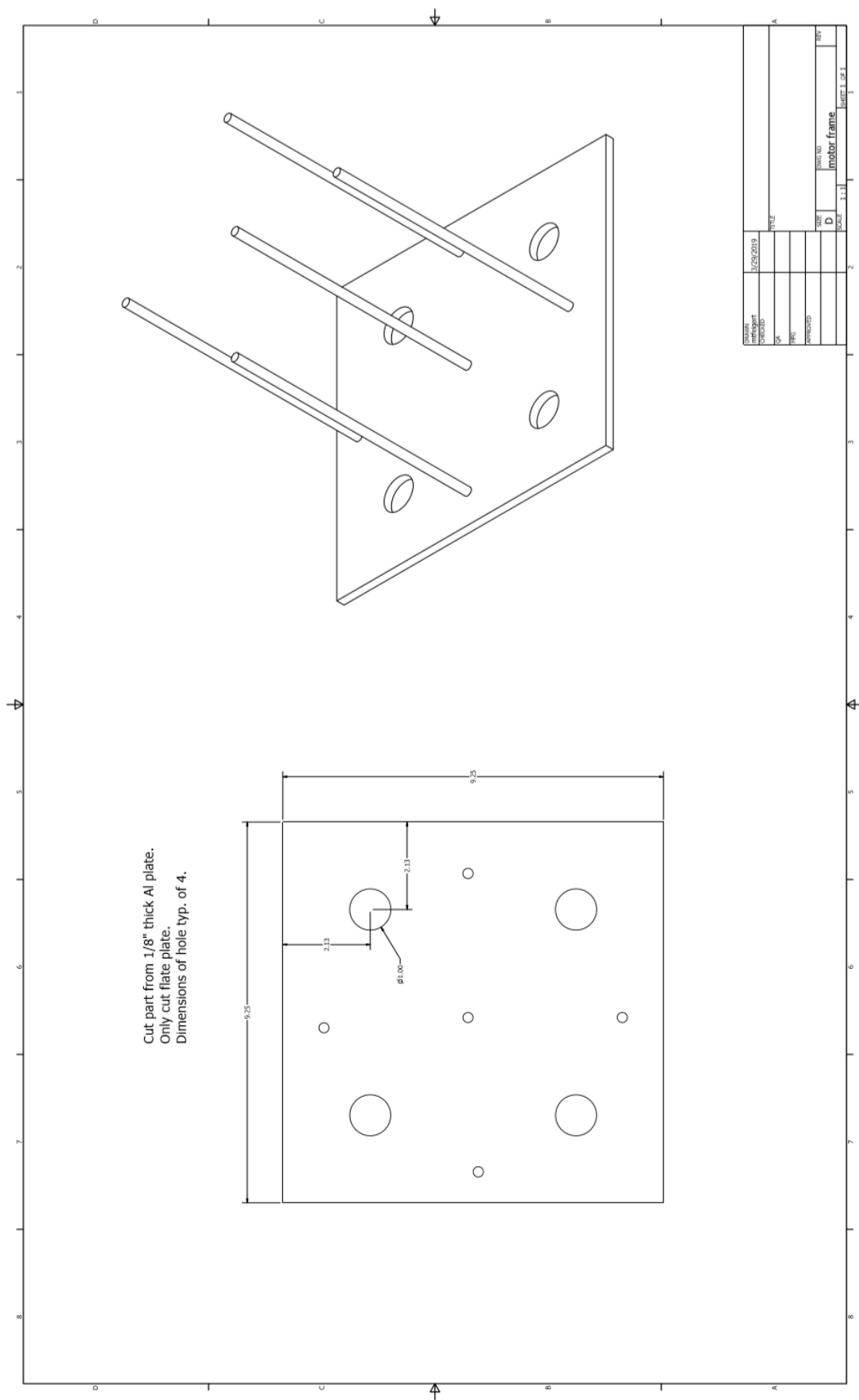
Appendix A: Mechanical Drawings of Machined Components

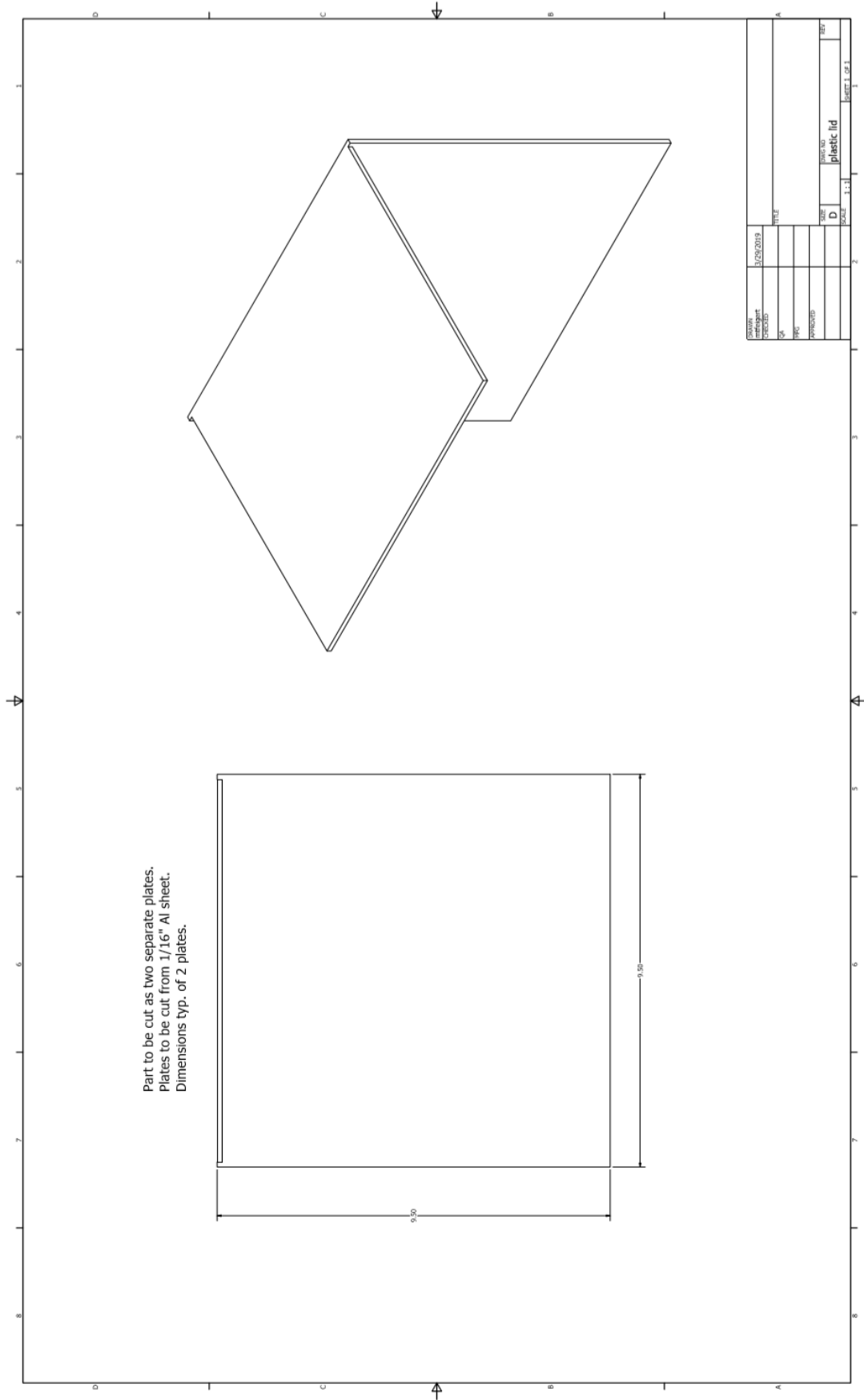


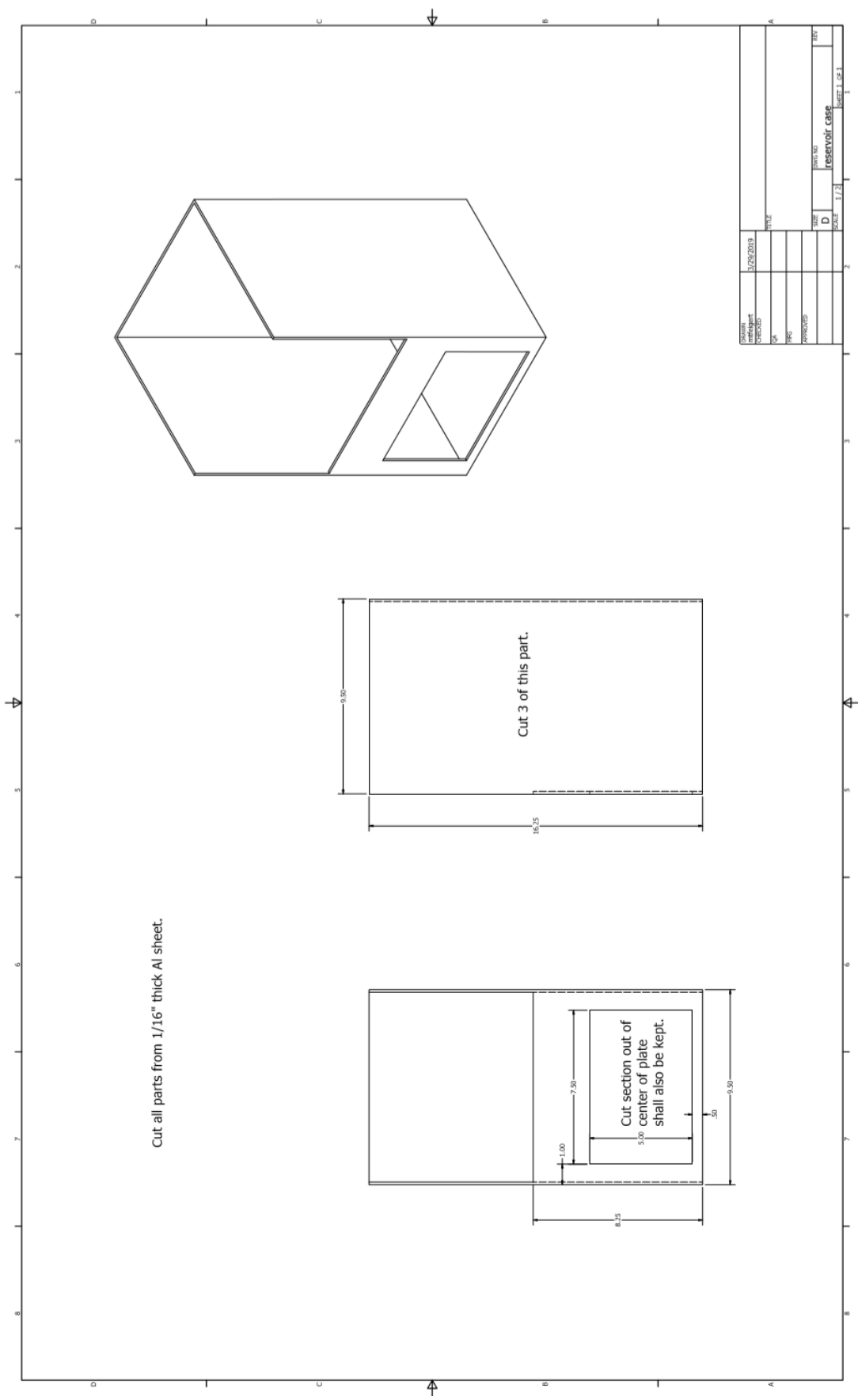


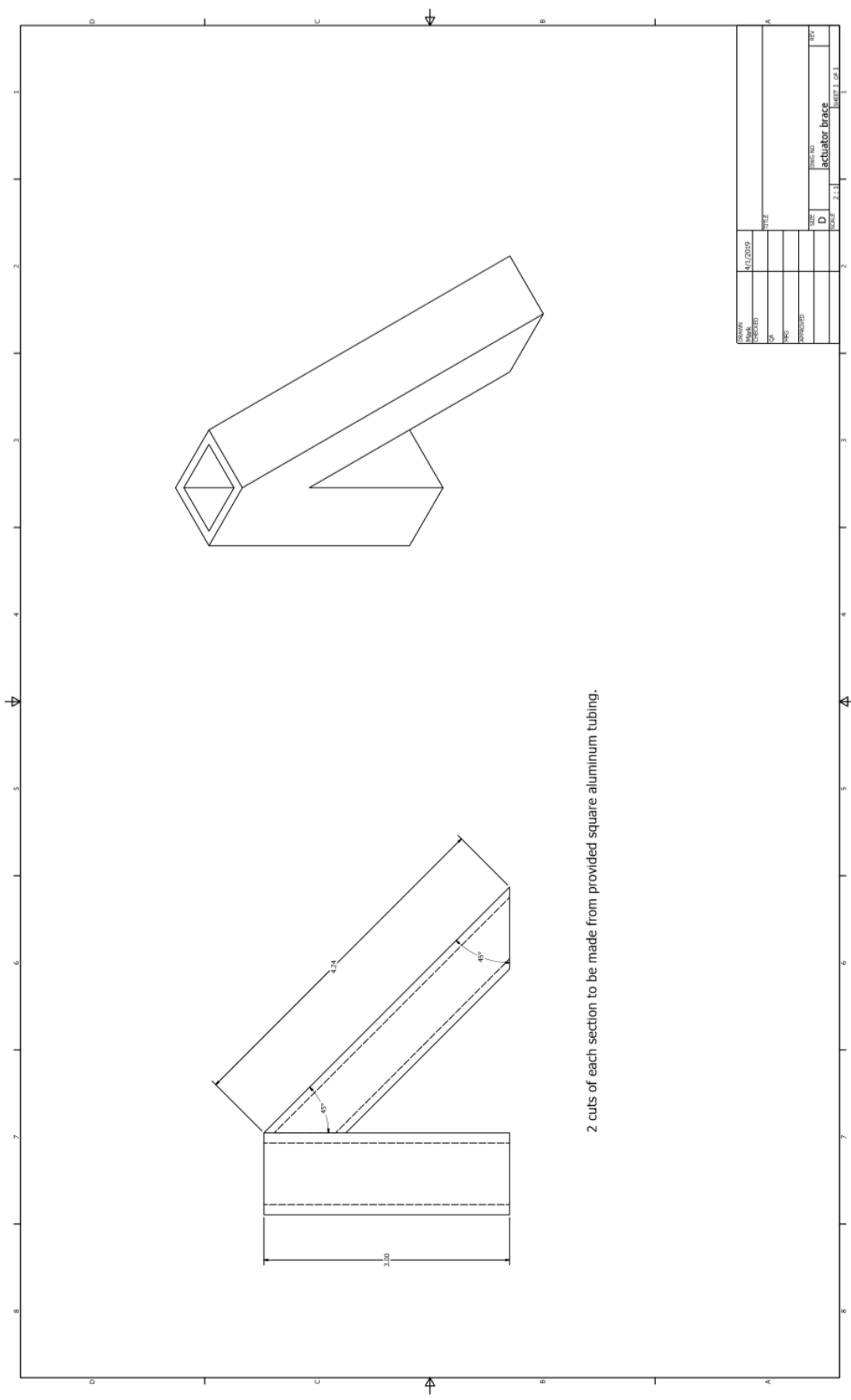


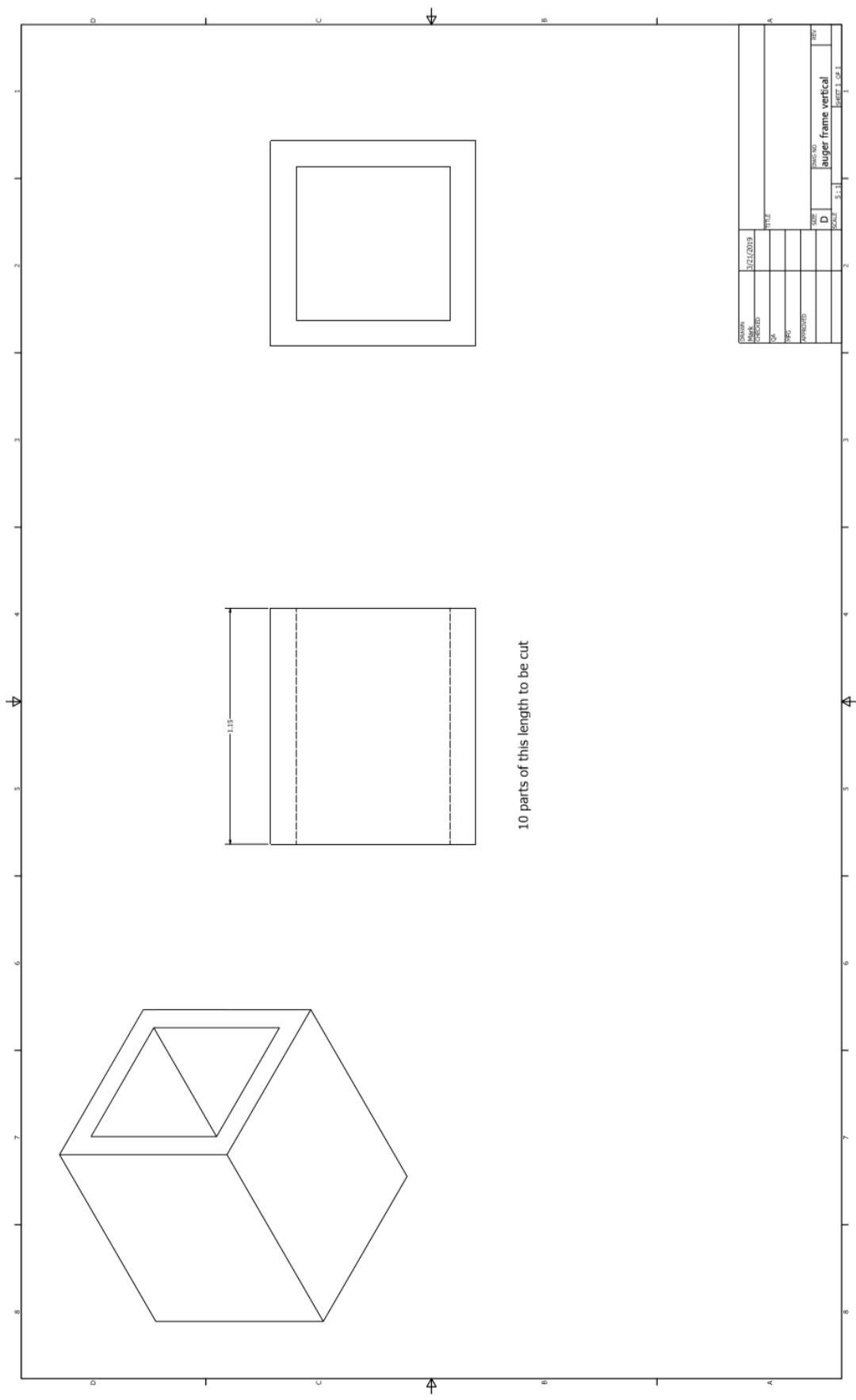


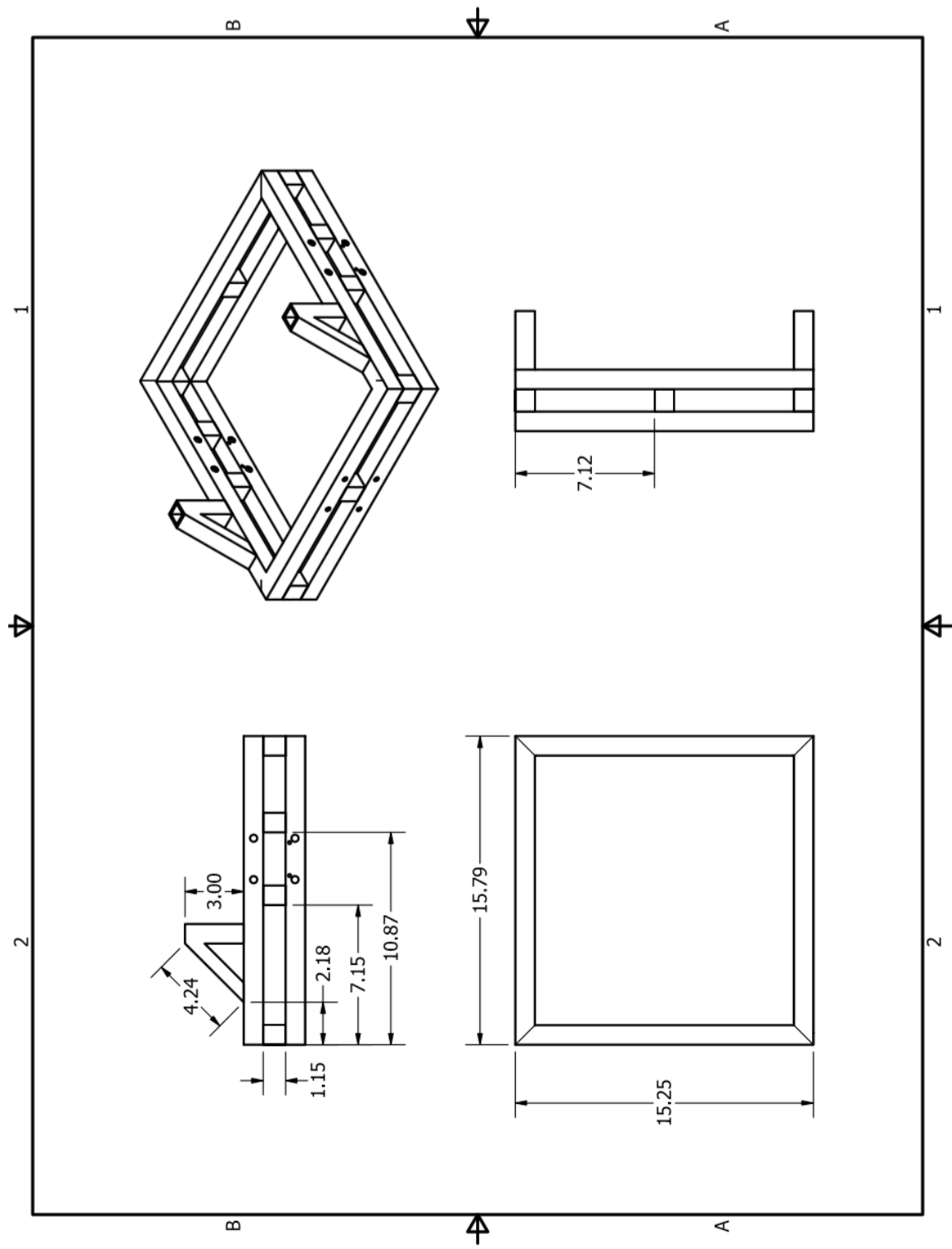


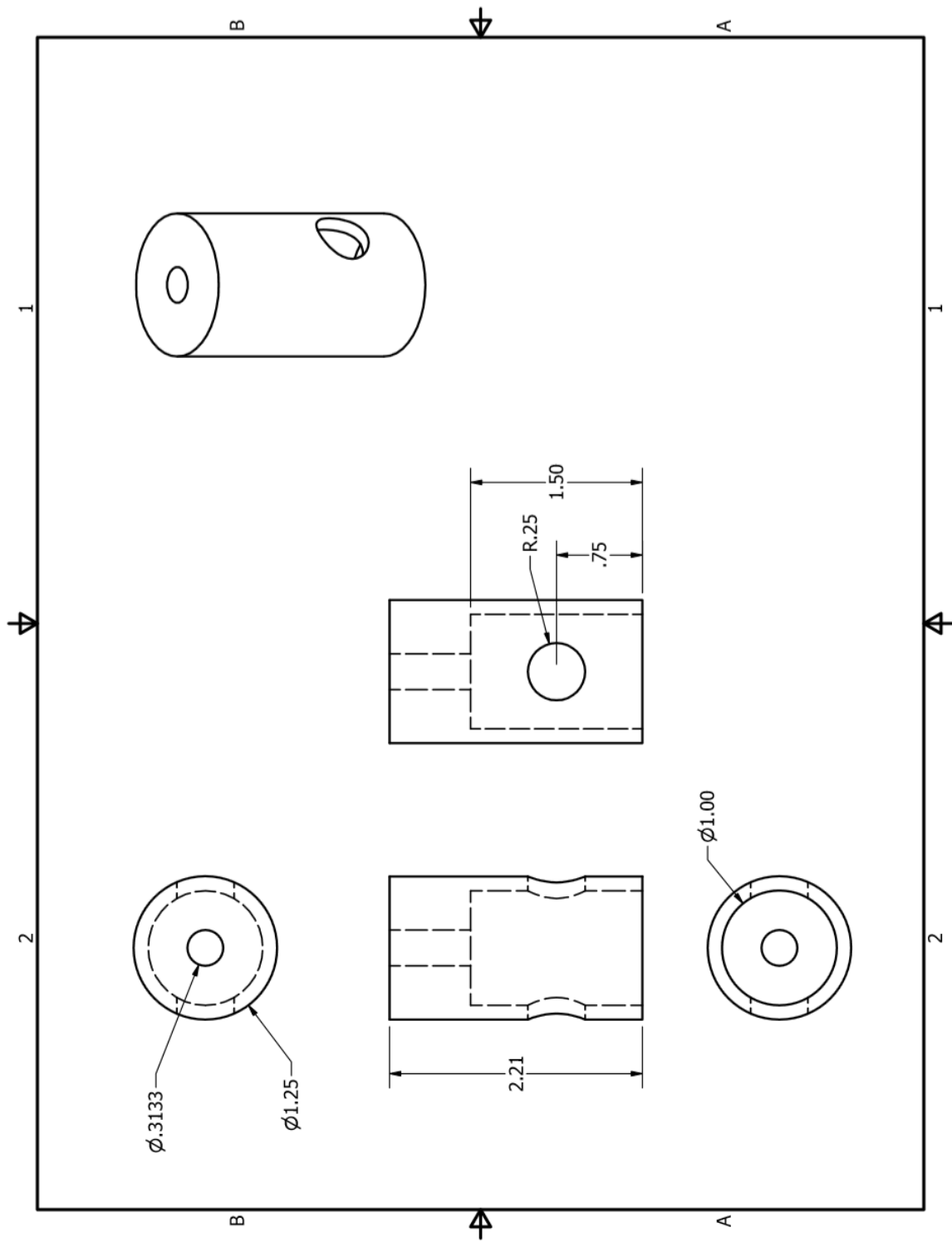


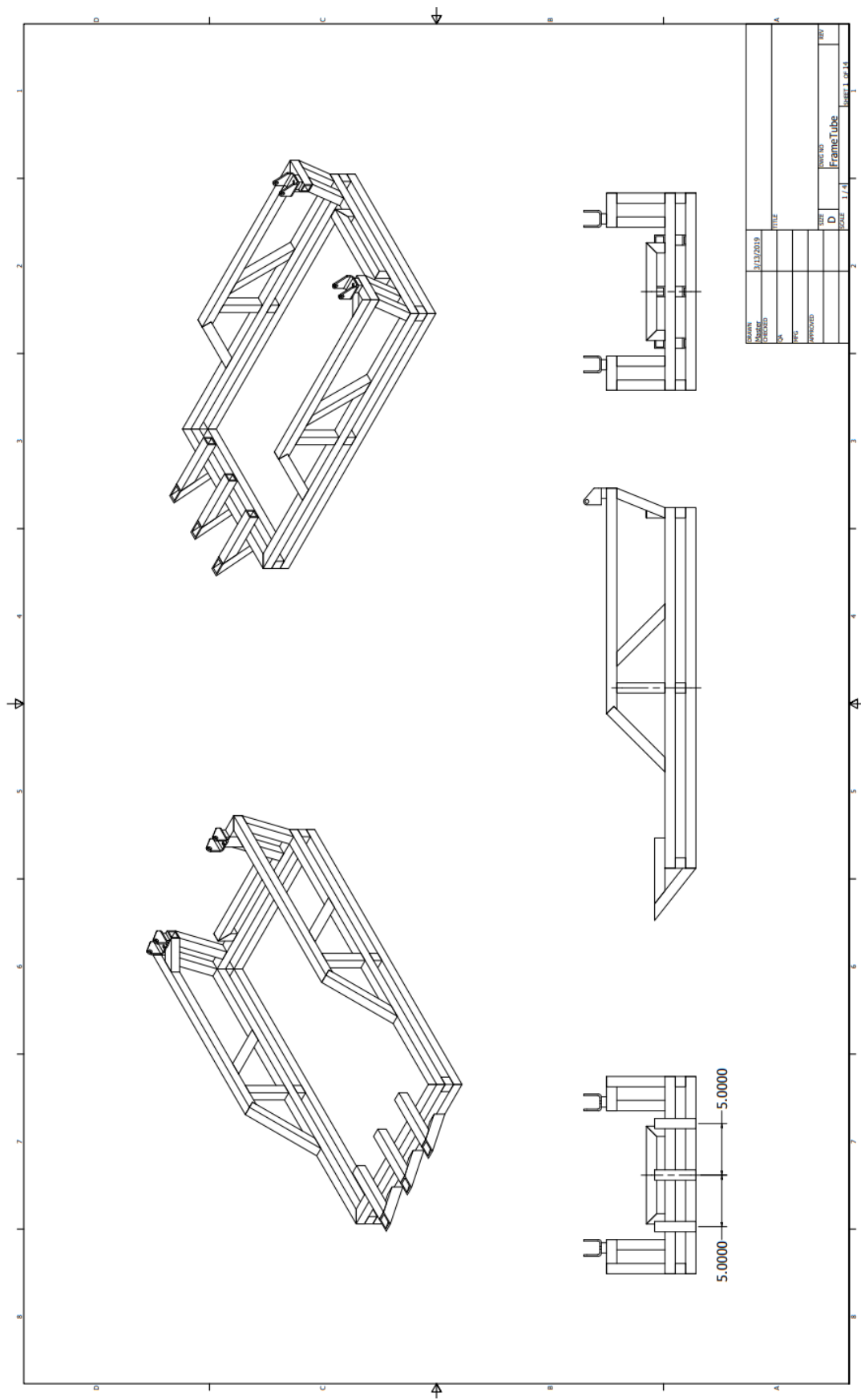


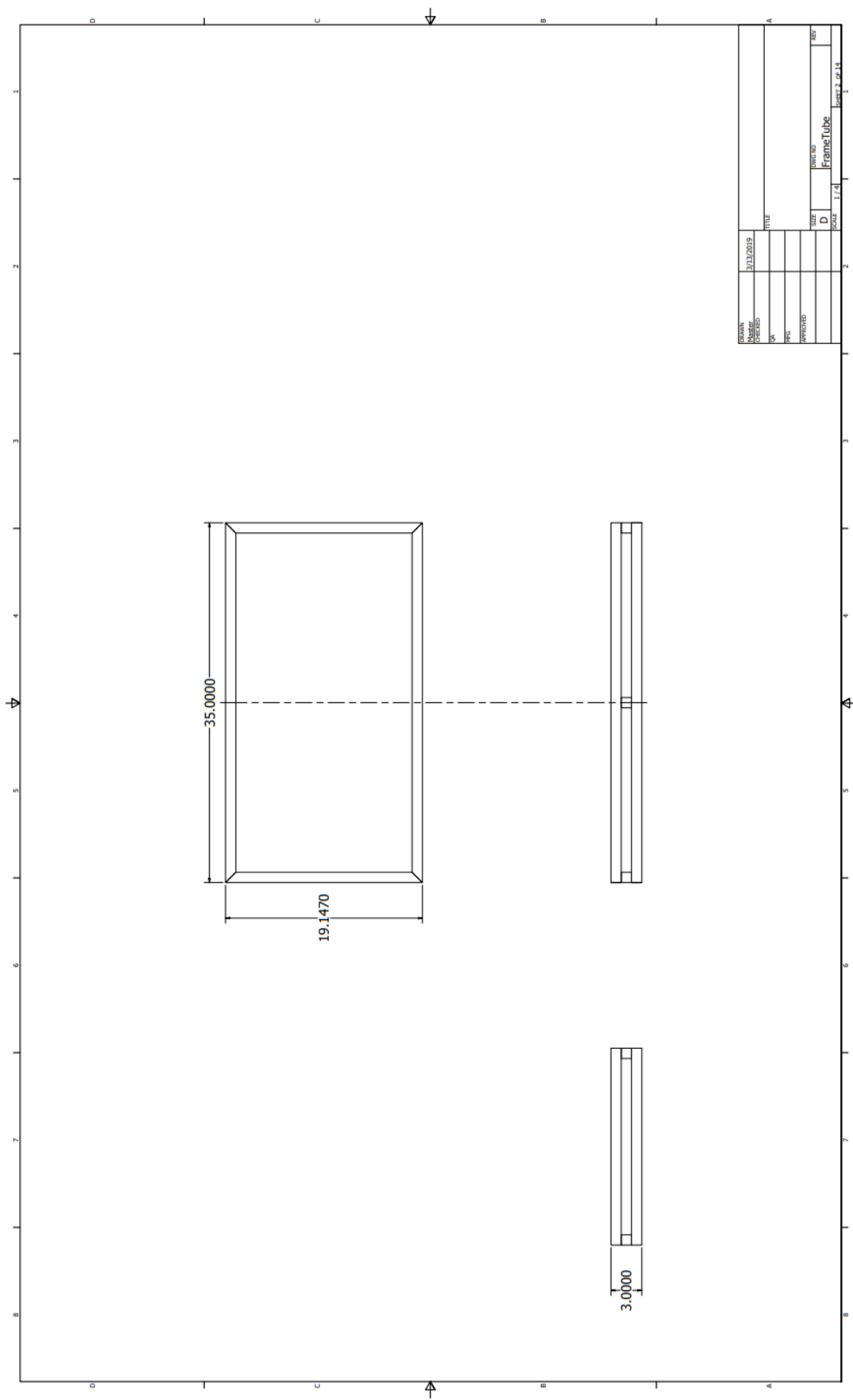


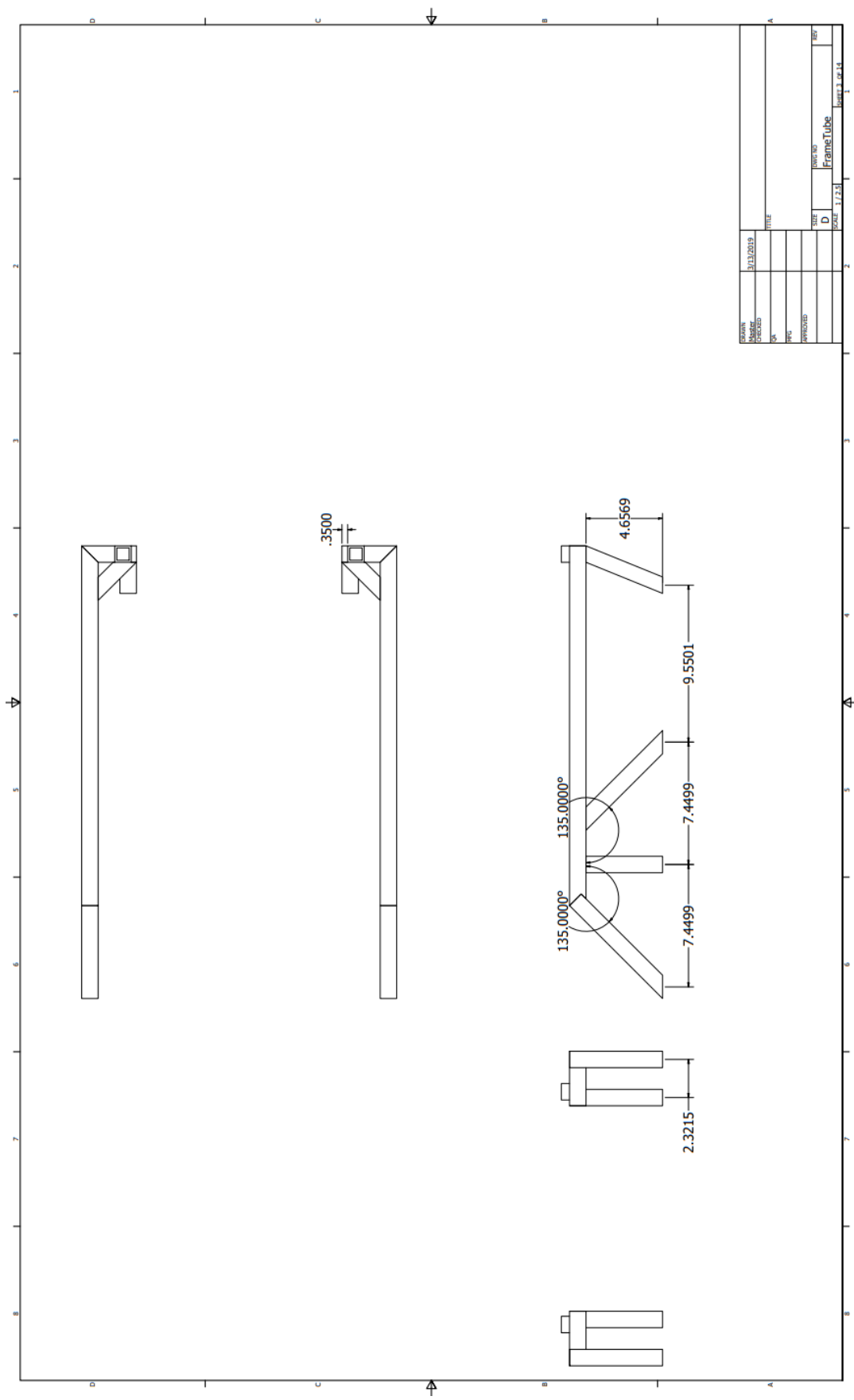


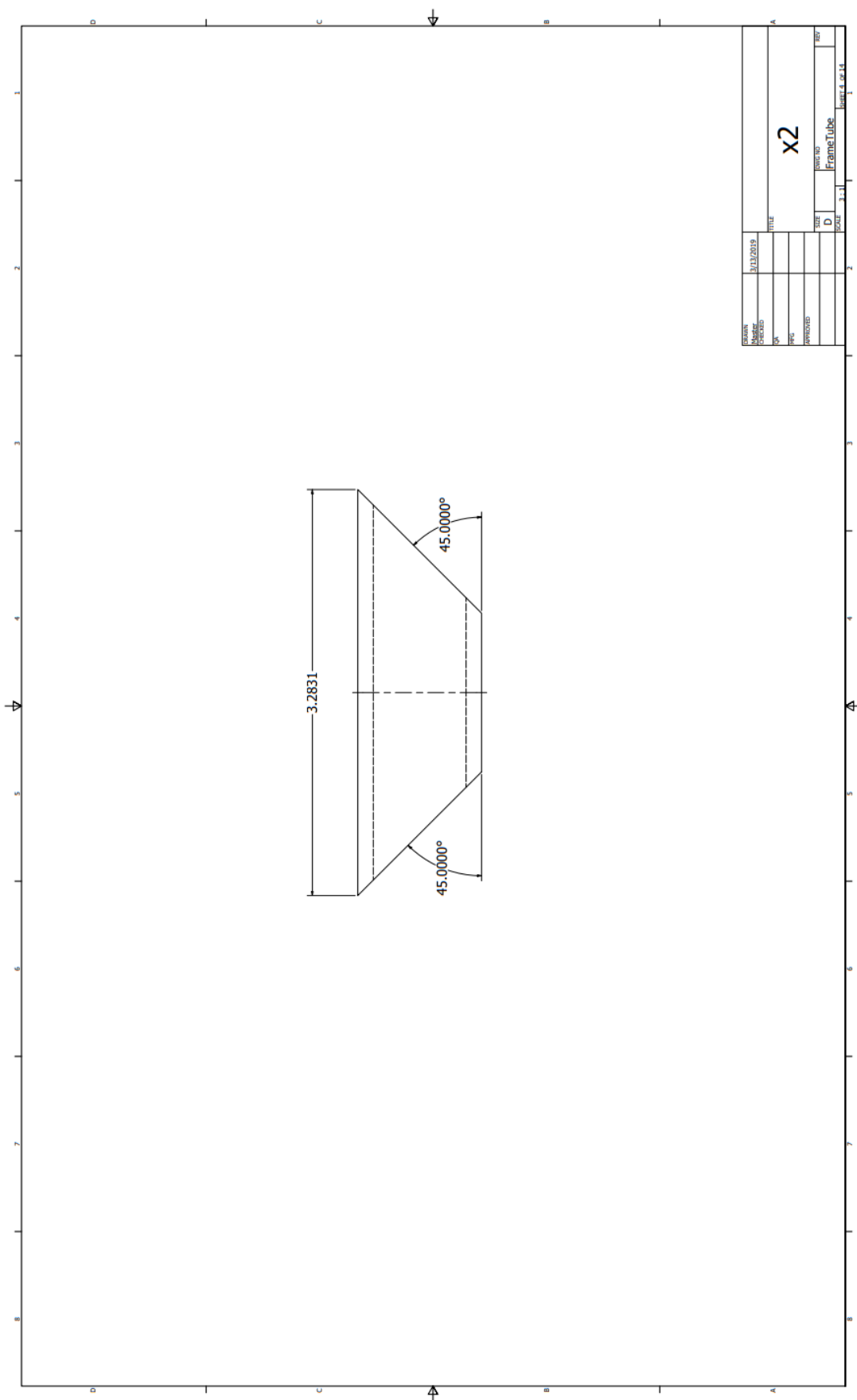


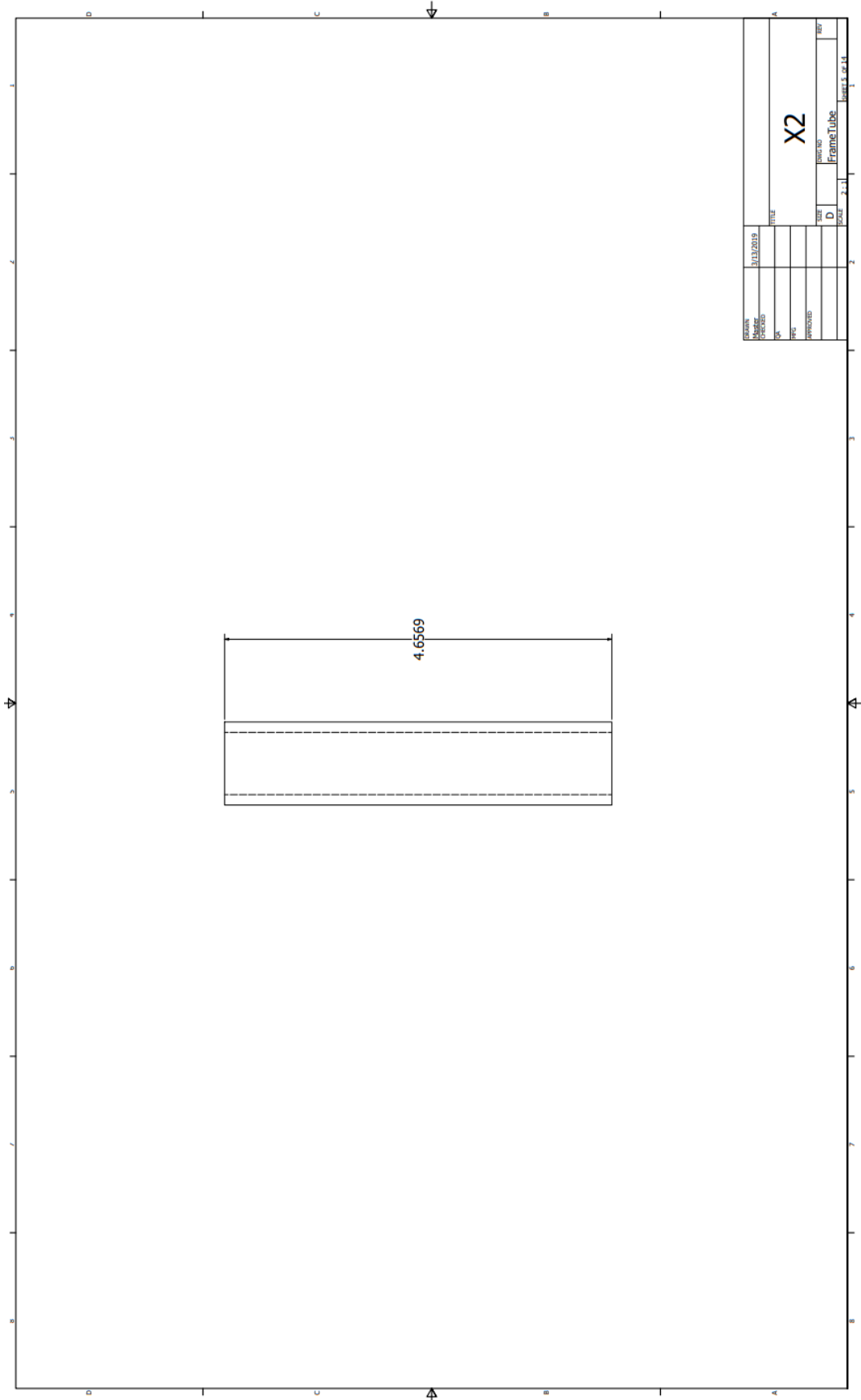


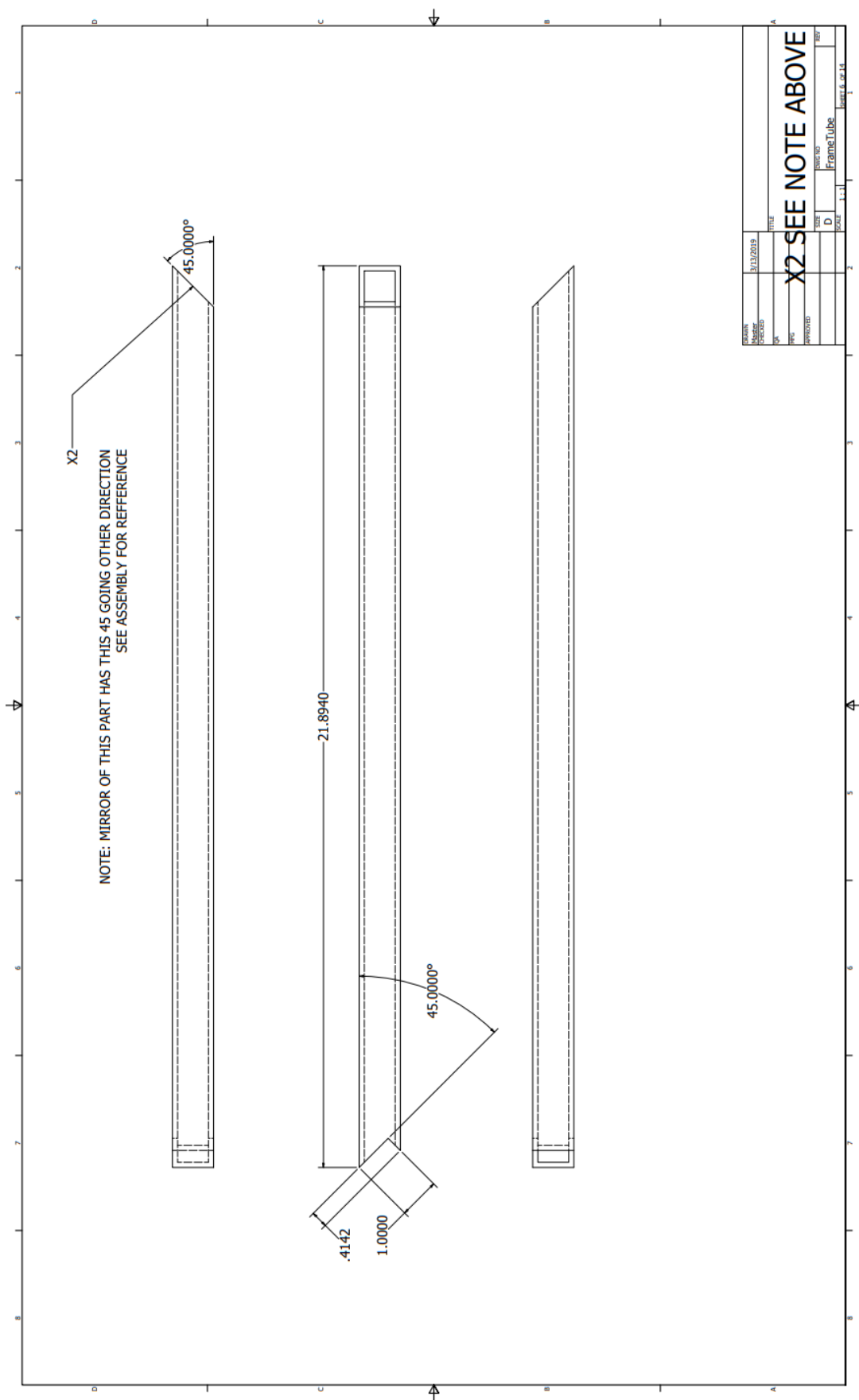


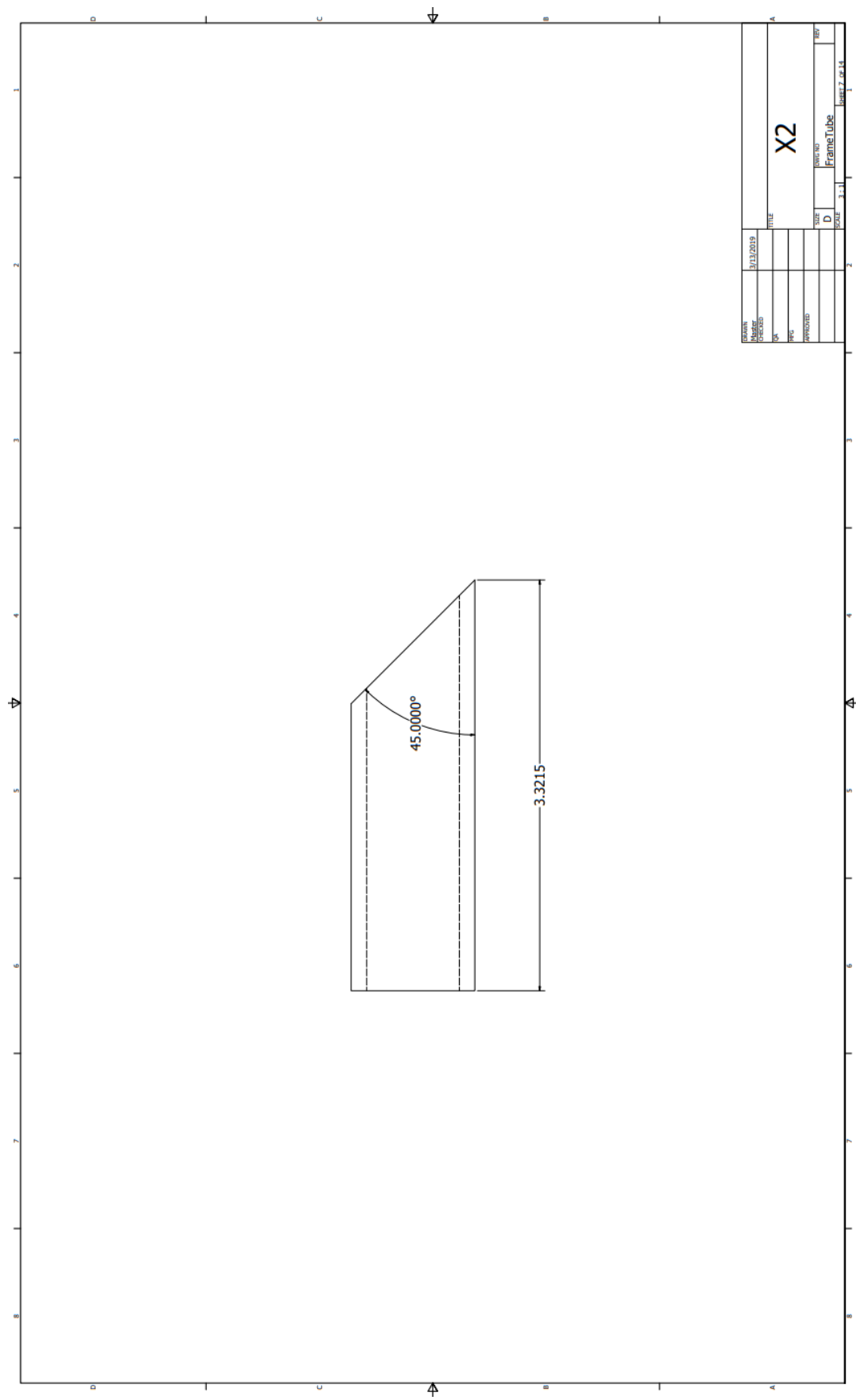


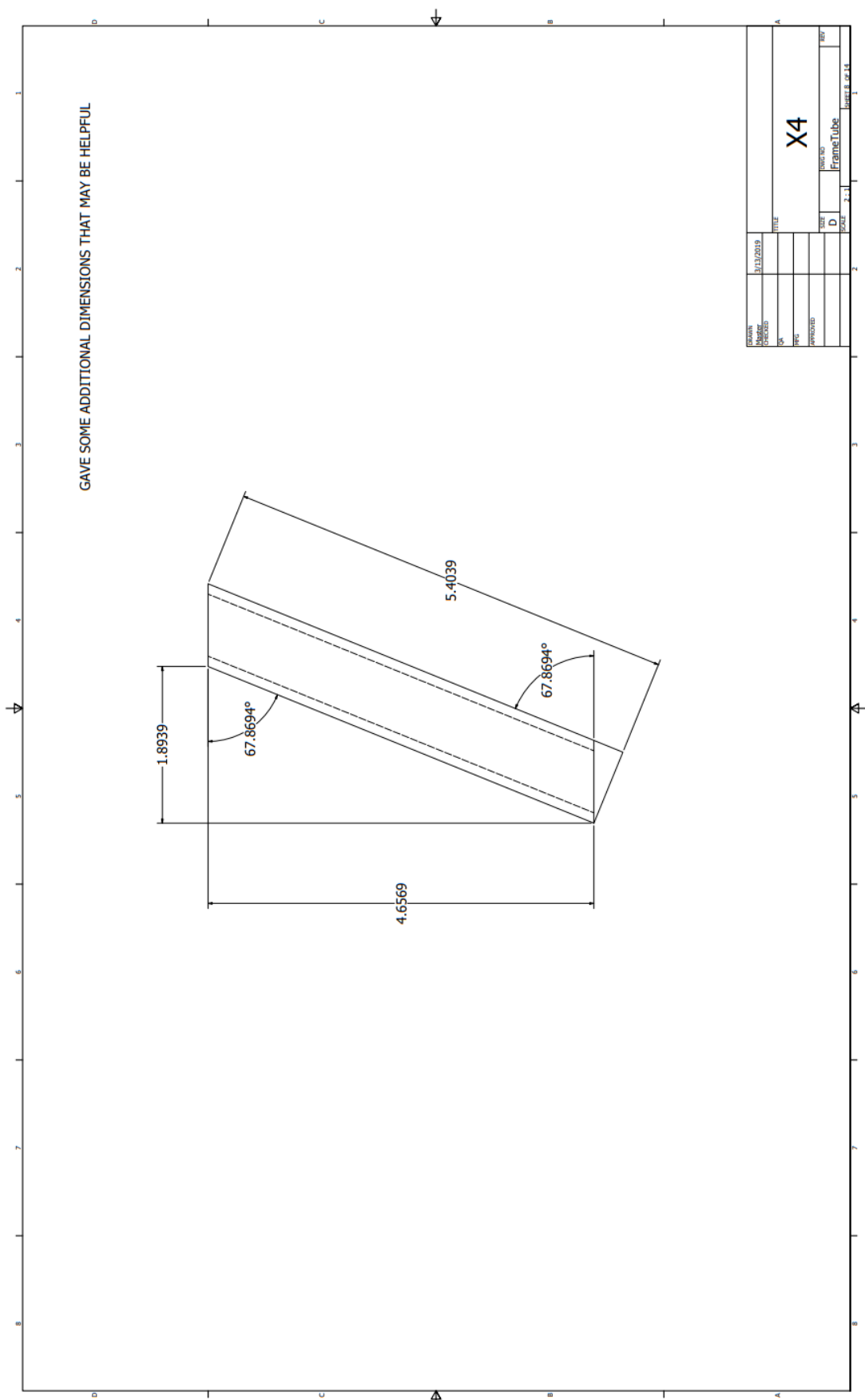


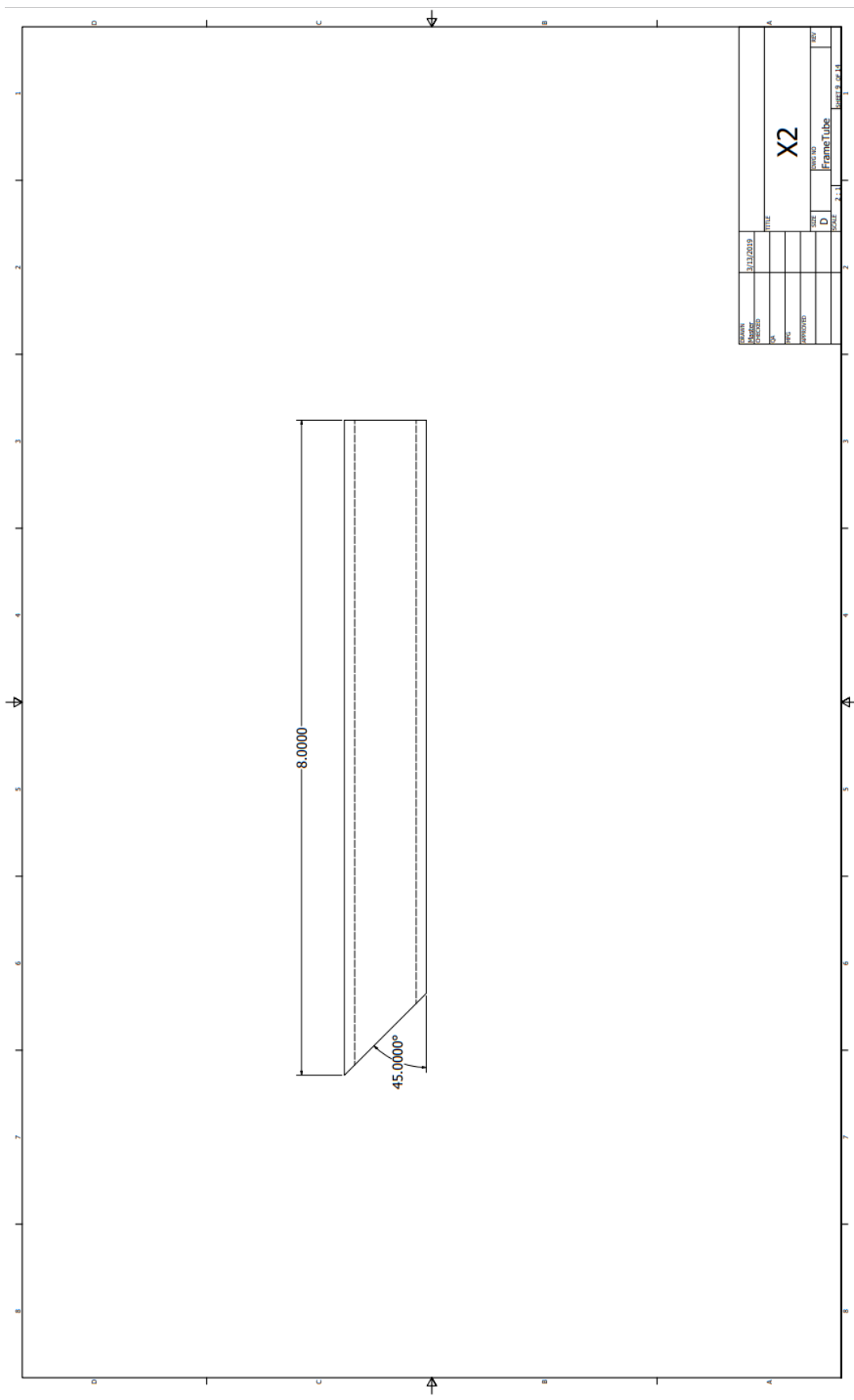


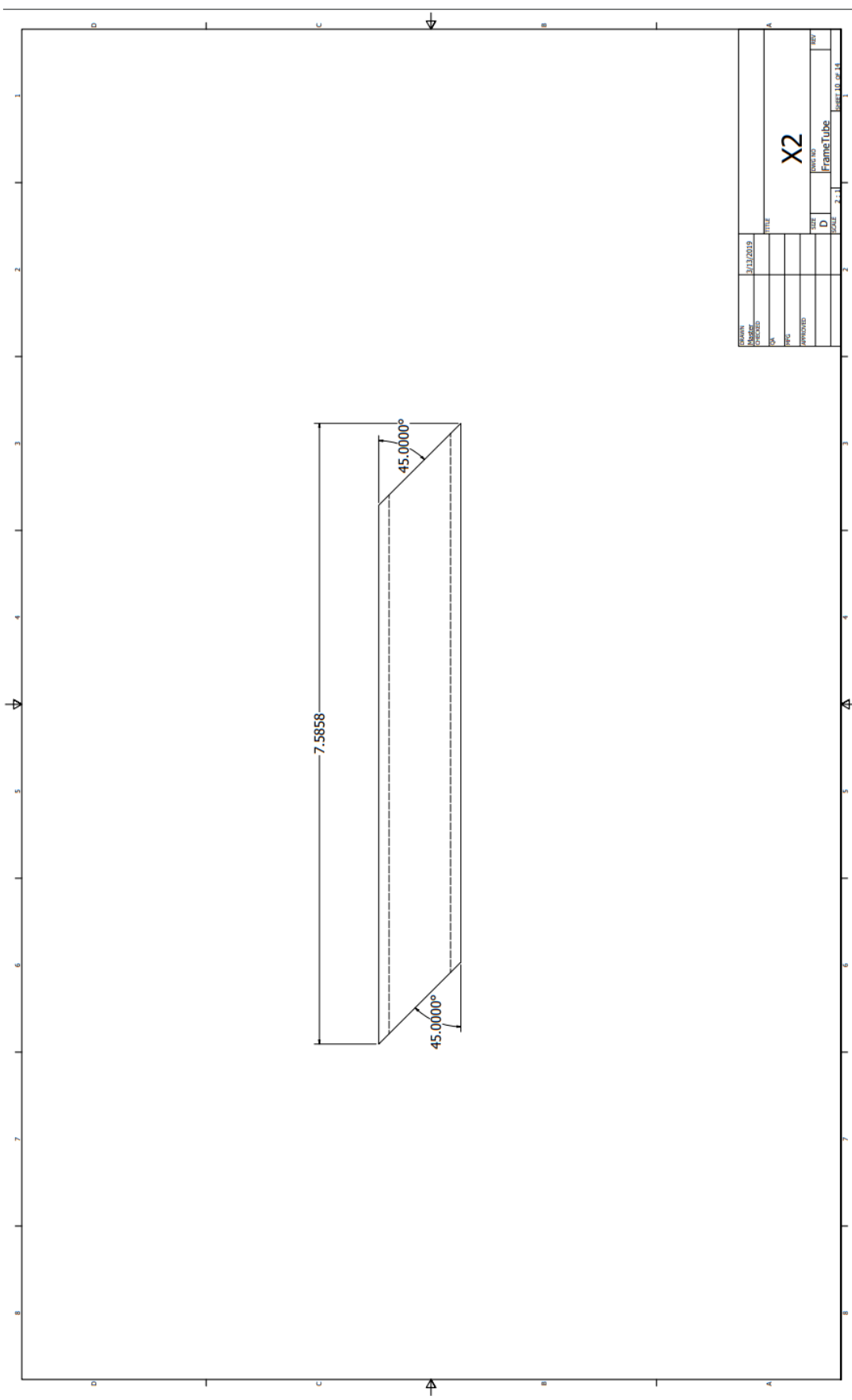


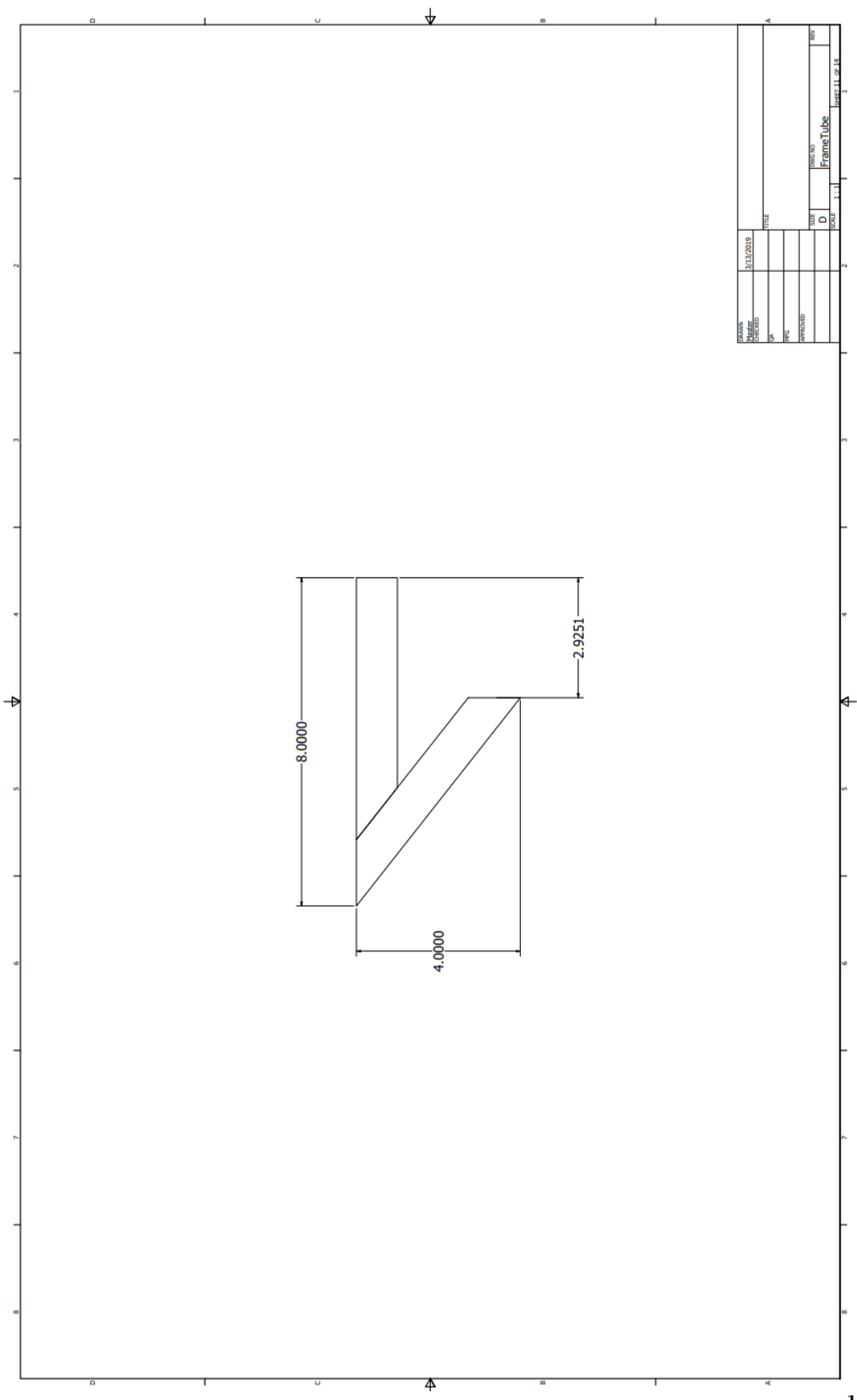




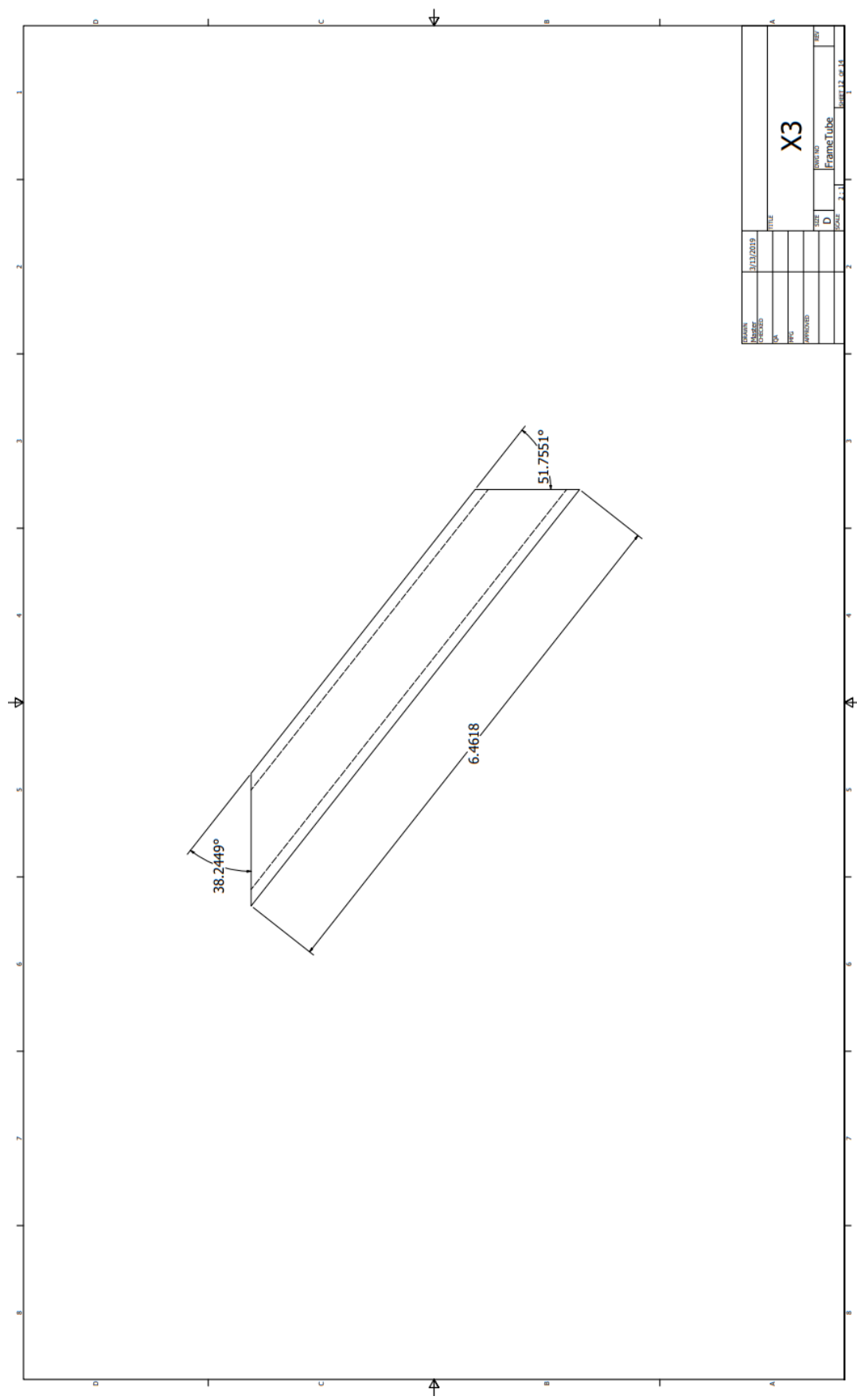


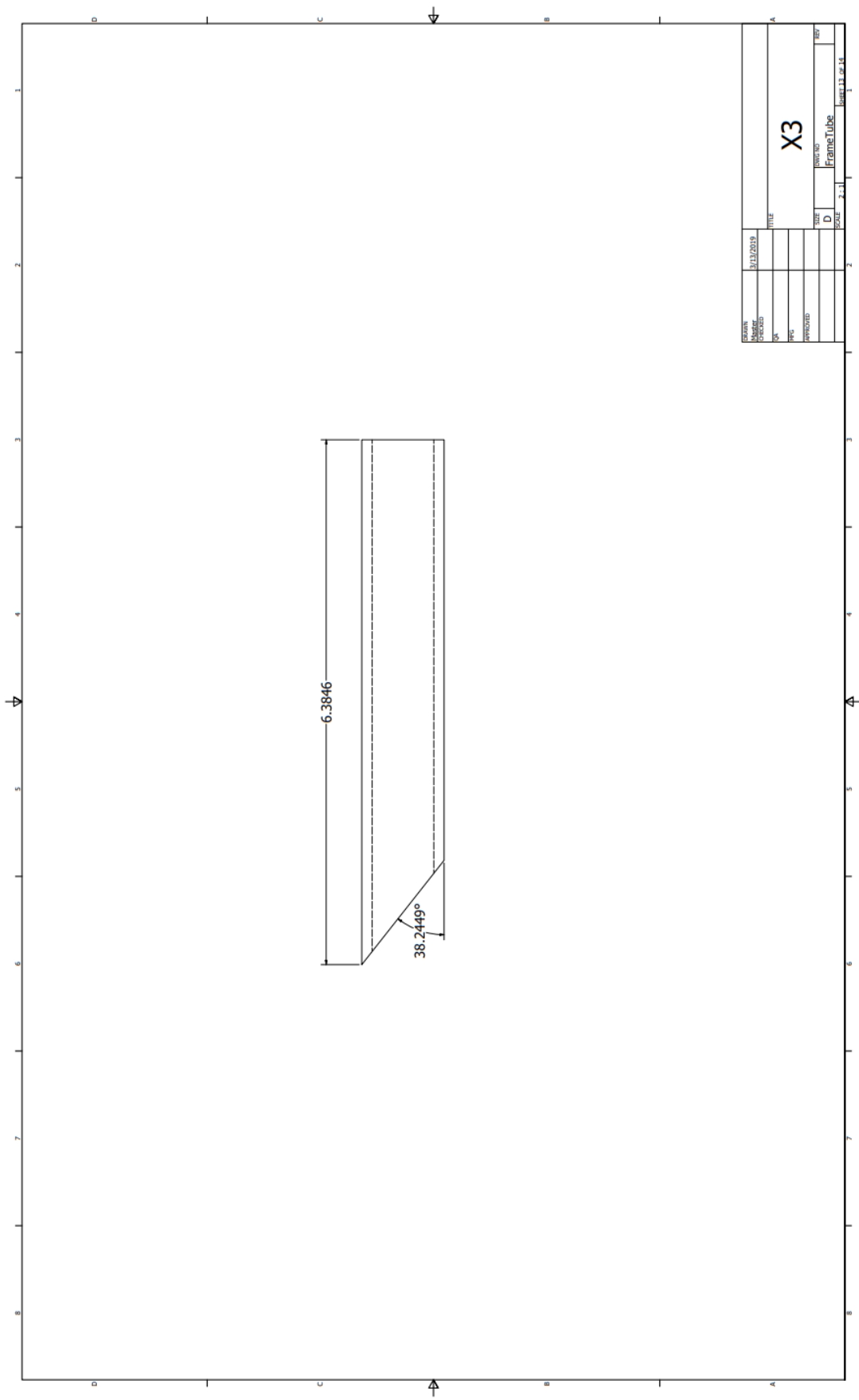


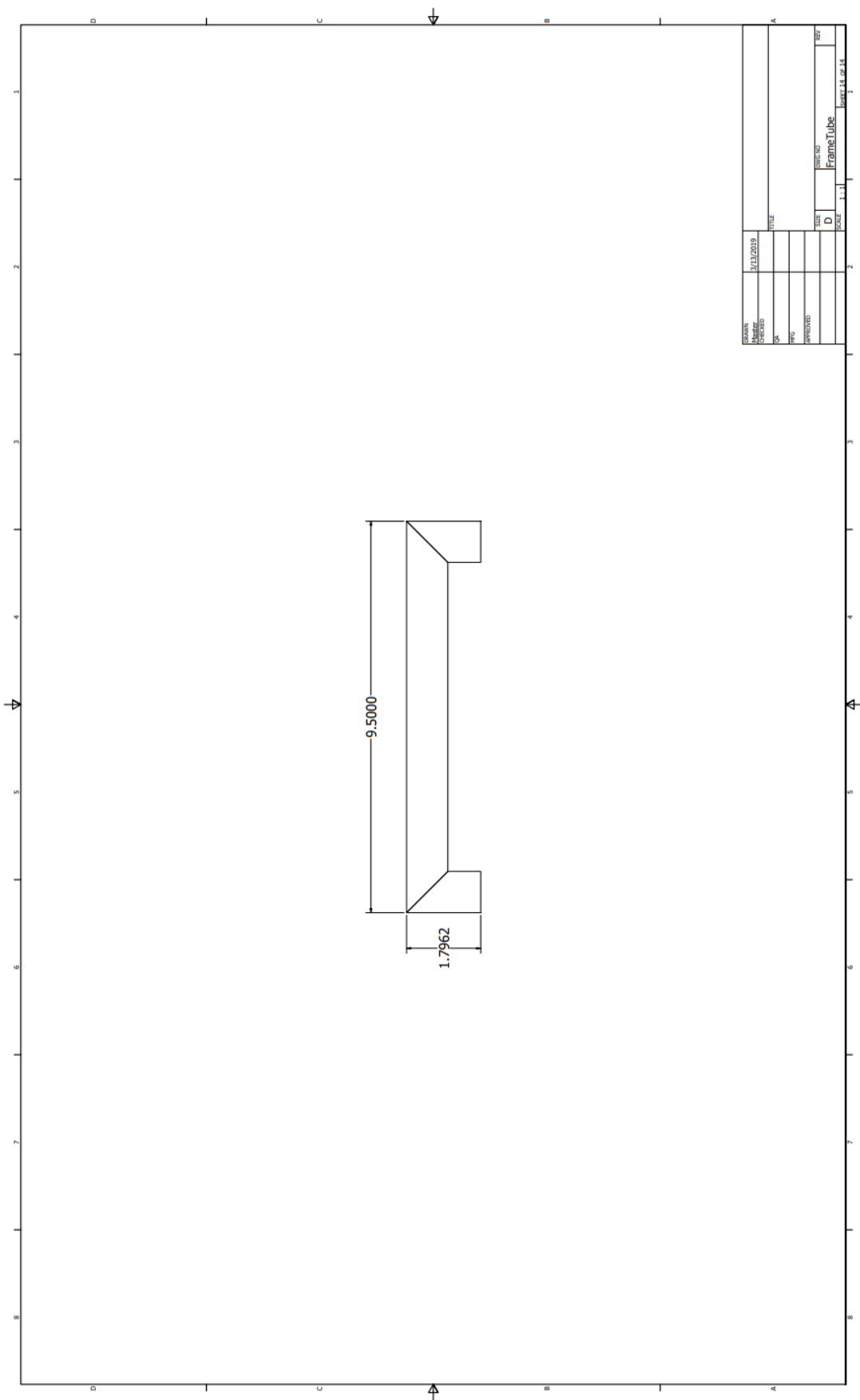




100







Appendix B: Gantt Chart

